Downloaded from orbit.dtu.dk on: Dec 20, 2017

Technical University of Denmark

Eigenbeamforming array systems for sound source localization

Tiana Roig, Elisabet; Jacobsen, Finn; Jeong, Cheol-Ho; Agerkvist, Finn T.

Publication date:
2014

Document Version
Publisher's PDF, also known as Version of record

Link back to DTU Orbit

Citation (APA):
Tiana Roig, E., Jacobsen, F., Jeong, C-H., & Agerkvist, F. T. (2014). Eigenbeamforming array systems for sound source localization. Technical University of Denmark, Department of Electrical Engineering.

DTU Library
Technical Information Center of Denmark

General rights
Copyright and moral rights for the publications made accessible in the public portal are retained by the authors and/or other copyright owners and it is a condition of accessing publications that users recognise and abide by the legal requirements associated with these rights.

- Users may download and print one copy of any publication from the public portal for the purpose of private study or research.
- You may not further distribute the material or use it for any profit-making activity or commercial gain
- You may freely distribute the URL identifying the publication in the public portal

If you believe that this document breaches copyright please contact us providing details, and we will remove access to the work immediately and investigate your claim.

Technical University of Denmark

Elisabet Tiana Roig

Eigenbeamforming array systems for sound source localization

PhD thesis, November 2014

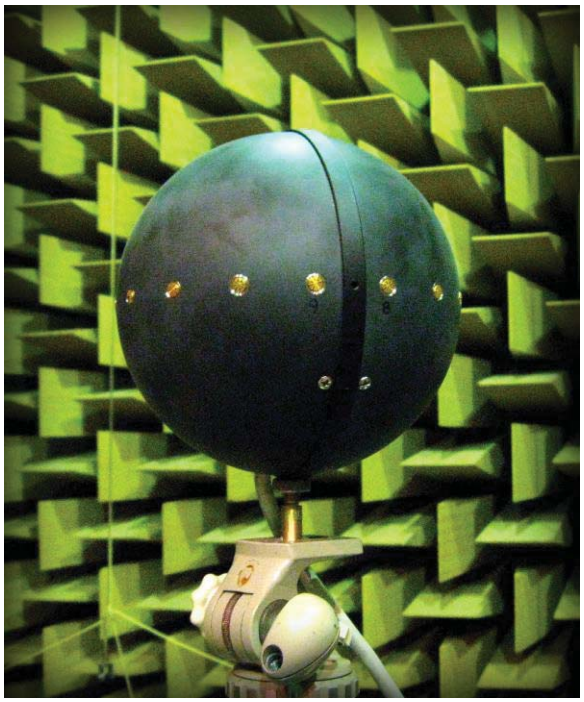

DTU Electrical Engineering
Department of Electrical Engineering

Eigenbeamforming array systems for sound source localization

PhD thesis by

Elisabet Tiana Roig

Technical University of Denmark

2014

This thesis was submitted to the Technical University of Denmark (DTU) as partial fulfillment of the requirements for the degree of Doctor of Philosophy (PhD) in Electronics and Communication. The work presented in this thesis was completed between October 1, 2010 and August 1, 2014 at Acoustic Technology, Department of Electrical Engineering, DTU, under the supervision of Associate Professor Finn Jacobsen, until June of 2013, and Associate Professors Cheol-Ho Jeong and Finn T. Agerkvist, from March of 2013 to the end. The project was funded by the Department of Electrical Engineering at DTU.

Cover illustration: Circular microphone array mounted on
a rigid sphere, by Elisabet Tiana-Roig

Department of Electrical Engineering
Technical University of Denmark
DK-2800 KONGENS LYNGBY, Denmark

Printed in Denmark by Rosendahls - Schultz Grafisk a/s

© 2014 Elisabet Tiana Roig

No part of this publication may be reproduced or transmitted in any form or by any means, electronic or mechanical, including photocopy, recording, or any information storage and retrieval system, without permission in writing from the author.

In memory of Finn Jacobsen.

I al Toni, el meu far,
i al Quim, la meva llum.

Abstract

Microphone array technology has been widely used for the localization of sound sources. In particular, beamforming is a well-established signal processing method that maps the position of acoustic sources by steering the array transducers toward different directions electronically.

The present PhD study aims at enhancing the performance of uniform circular arrays, and to a lesser extent, spherical arrays, for two- and three-dimensional localization problems, respectively. These array geometries allow to perform eigenbeamforming, beamforming based on the decomposition of the sound field in a series of orthogonal functions. In this work, eigenbeamforming is particularly developed to improve the performance of circular arrays at low frequencies. Compared to conventional delay-and-sum beamforming, the proposed technique, named circular harmonics beamforming, provides a better resolution at the expense of being more vulnerable to noise. A simple way to further improve the array performance is to flush-mount the transducers on a rigid scatterer. For a circular array, an ideal solution is a rigid cylindrical scatterer of infinite length. Due to its impracticality, the use of a rigid spherical scatterer is recommended instead.

A better visualization in the entire frequency range can be achieved with deconvolution methods, as they allow the recovery of the sound source distribution from a given beamformed map. Three efficient methods based on spectral procedures, originally conceived for planar-sparse arrays, are adapted to circular arrays. They rely on the fact that uniform circular arrays present an azimuthal response that is rather independent on the focusing direction.

Finally, a method based on the combination of beamforming and acoustic holography is introduced for both circular and spherical arrays. This new approach, also expressible in terms of eigenbeamforming, extends the frequency range of operation of conventional delay-and-sum beamforming toward the low frequencies.

Keywords: uniform circular arrays, spherical arrays, circular harmonics beamforming, deconvolution methods, spherical harmonics beamforming, holographic virtual arrays

Resumé

Mikrofon-array-teknologi har været meget anvendt til lokalisering af lydkilder. Navnlig beamforming er en veletableret signalbehandlingsmetode, som kortlægger placeringen af akustiske kilder ved elektronisk at styre array transducere mod forskellige retninger.

Dette Ph.d.-projekt stræber efter at forbedre præstationen af ensartede cirkulære array-systemer, og i mindre grad sfæriske arrays, for hhv. to- og tredimensionale lokaliseringsproblemer. Disse array-geometrier giver mulighed for at udføre eigenbeamforming, dvs. beamforming baseret på dekompositionen af lydfeltet i en række ortogonale funktioner. I dette arbejde er eigenbeamforming specielt udviklet for at forbedre præstationen af cirkulære arrays ved lave frekvenser. Sammenlignet med konventionel delay-and-sum beamforming giver den foreslåede teknik, kaldet circular harmonics beamformning, en bedre opløsning på bekostning af at være mere sårbar over for støj. En enkel måde til yderligere at forbedre array-præstationen er at placering mikrofonerne på overfladen af en hård scatterer. For et cirkulært array er en ideel løsning en hård cylindrisk scatterer af uendelig længde. På grund af vanskeligheder ved implementeringen anbefales en hård sfærisk scatterer i stedet for.

En bedre visualisering i hele frekvensområdet kan opnås med deconvolution-metoder, da de tillader gendannelse af lydkilders distribution fra et givet beamformed kort. Tre effektive metoder, baseret på spektrale procedurer, der oprindeligt er udtænkt til plane, sparse arrays, er tilpasset cirkulære arrays. De er afhængige af det faktum, at ensartede cirkulære arrays viser et azimut respons, der er temmelig uafhængig af fokuseringen retning.

Endelig indføres en metode, der bygger på en kombination af beamforming og akustisk holografi, for både cirkulære og sfæriske arrays. Denne nye fremgangsmåde, som også kan udtrykkes i form af eigenbeamforming, udvider frekvensområdet for brugen af konventionel delay-and-sum beamforming mod de lave frekvenser.

Nøgleord: ensartede cirkulære arrays, sfæriske arrays, circular harmonics beamforming, spherical harmonics beamforming, deconvolution-metoder, holografiske virtuelle arrays

Acknowledgments

I would like to dedicate these first lines to pay my deepest homage to my supervisor, Finn Jacobsen. This work would have not been possible without his teachings, his generous dedication, and his wise advice. I will always admire him for being committed to his work and to his students until the very end of his life. Moving the project forward without him has been extremely tough. However, his legacy has given me strength and has accompanied me every single day until the end of the project. His memory will always live within me.

I will never forget the support of the other professors of the group, Cheol-Ho Jeong, Finn T. Agerkvist, and Jonas Brunskog, when Finn Jacobsen was forced to step aside a year and a half ago. In particular, I would like to thank Cheol-Ho for taking over the main supervision, and for doing it with motivation and efficiency. I am also extremely grateful to Efrén Fernández-Grande for his great support, guidance, and help, all the way through.

All my colleagues, former colleagues, and friends, at the 'House of Acoustics' have contributed immensely to my personal and professional time at DTU. In particular, I would like to express my gratitude to Jørgen Rasmussen and Tom A. Petersen for their help with the equipment and the experimental work, and to Nadia J. Larsen for her help with administrative tasks and for her empathy. I am very grateful to Aggeliki Xenaki, Oliver Lylloff, and Marco Ottink for letting me participate in their Master's theses; I have really learned a lot from you. Many thanks to Salvador Barrera Figueroa for his advice and also for his subtle way of cheering me up. Thanks to Marton Marschall for his Matlab code and for the fruitful discussions regarding spherical arrays. I am also very grateful to Torsten Dau for his experienced advice during a complicated peer-review process of one of the articles. Special thanks to my wonderful office mates, Joe Jensen, Gerd Marbjerg, and Alba Granados, for creating a fantastic working atmosphere. Joe, thanks for your permanent good mood, and your (almost perfect) musical taste. Gerd, Alba, I have really enjoyed this short, but intense, time together in our particular fortress. Without your support in the last months, this would have been a lot harder.

I am very grateful to Karim Haddad and Jørgen Hald from Brüel & Kjær for lending me equipment for the experiments, and for very inspiring discussions.

Thanks to Daniel Fernández-Comesaña from Microflown Technologies for inviting me to participate in one of his articles.

I would also like to thank an anonymous reviewer of the Journal of the Acoustical Society of America, whose valuable comments became the basis of one of the appendices of this dissertation.

I am indebted to my family and friends for encouraging me countless times, especially when I needed it most. I deeply thank my mom, my brother Eduard, my dad, Piluca, my sister Vicky, my grandma Carme, in short, all my closest family, for their love and support in all my pursuits. This PhD degree is an accomplishment that belongs to all of them. It also belongs to my dear grandpa Guillem, who left us a few months after the beginning of the project, and to my son Quim, who, born in the course of this project, has been a great source of happiness. Finally, my most sincere gratitude to Toni Torras Rosell. Without your precious and enthusiastic contribution to the papers, your guidance on the dissertation, and your faith in me, this would have simply been impossible. Thanks for being always there, for the dedication to our family, and for your love.

Contents

List of acronyms

CMF	Covariance matrix fitting
DAMAS	Deconvolution approach for the mapping of acoustic sources
DI	Directivity index
ESPRIT	Estimation of signal parameters via rotational invariance techniques
FFT	Fast Fourier transform
FFT-NNLS	Fourier-based non-negative least squares
FISTA	Fast iterative shrinkage-thresholding algorithm
GSC	Generalized sidelobe canceler
ISCA	Iterative sidelobe cleaner algorithm
MACS	Mapping of acoustic sources
MEMS	Microelectromechanical systems
MSL	Maximum sidelobe level
MUSIC	Multiple signal classification
NAH	Near-field acoustic holography
SHARP	Spherical harmonics angularly resolved pressure
SNR	Signal-to-noise ratio
SONAH	Statistical optimized near-field acoustic holography
WNG	White noise gain
2D	Two-dimensional
3D	Three-dimensional

List of symbols

A	Amplitude of the acoustic wave
A_n	Expansion coefficient of order n
b	Beamformer output
$\mathbf{b}$	Beamformer power response expressed as a vector
$\mathbf{C}$	Cross-spectral matrix
C_n	nth Fourier coefficient obtained with a continuous circular aperture
$\tilde{C}_n$	nth Fourier coefficient estimated with a circular array
C_{mn}	mnth Fourier coefficient obtained with a continuous spherical aperture
$\tilde{C}_{mn}$	mnth Fourier coefficient estimated with a spherical array
c	Speed of sound in the medium of propagation
c_{mn}	mnth element of the cross-spectral matrix $\mathbf{C}$
d	Sensor spacing of a linear array
d_n	Constant associated to the nth order in eigenbeamforming
$\mathcal{F}$	Direct FFT
$\mathcal{F}^{-1}$	Inverse FFT
f	Frequency
G	Grid
H	Point-spread function
$\mathbf{H}$	Point-spread function matrix
$H_n^{(1)}$	Hankel function of the first kind and order n
$h_n^{(1)}$	Spherical Hankel function of the first kind and order n
J_n	Bessel function of the first kind and order n
j	Imaginary number $\left(\sqrt{-1}\right)$
j_n	Spherical Bessel function of the first kind and order n
k	Wavenumber

$\mathbf{k}$	Wavenumber vector
$\mathbf{k_i}$	Wavenumber vector of an incident wave
M	Number of array sensors
N	Number of orders in eigenbeamforming
N_v	Number of orders in eigenbeamforming with a holographic virtual array
P_n^m	Associated Legendre function of order m and degree n
p_m	Sound pressure captured at the mth array sensor
p	Sound pressure
Q_n	Baffle condition function
R	Radius of a circular/spherical array of sensors
R_v	Radius of a holographic virtual array
$\mathbf{r}$	Position vector
$\mathbf{r}_m$	Position of the mth array sensor
s	Spatial source power distribution
$\mathbf{s}$	Spatial source power distribution vector
t	Time
U_n	Chebyshev polynomial of the second kind of degree n
W	Array pattern
w_m	Weighting of the mth array sensor
w_n	Weighting of the nth harmonic order
Y_n^m	Spherical harmonic of order n and degree m
α_m	Integration factor of the mth sensor of a circular/spherical array
δ	Delta function
$\delta_{n\nu}$	Kronecker delta function
φ	Azimuth angle, from 0 to 2π
φ_l	Azimuth angle of the array looking direction, from 0 to 2π
φ_m	Azimuth angle of the mth array sensor, from 0 to 2π
φ_s	Azimuth angle of a sound source, from 0 to 2π
$\hat{\boldsymbol{\kappa}}$	Array's steering vector
λ	Wavelength
θ	Polar angle, from 0 to π
θ_m	Polar angle of the mth array sensor, from 0 to π
θ_s	Polar angle of a sound source, from 0 to π
ϑ	Polar angle, from $-\pi$ to π

ϑ_s	Polar angle of a sound source, from $-\pi$ to π
τ_m	Delay applied to the mth array sensor
ω	Angular frequency

Notations and conventions

Conventions

- The convention $e^{-j\omega t}$ is considered in the entire manuscript. Hence, a progressive plane wave is of the form $e^{j(\mathbf{k}\cdot\mathbf{r}-\omega t)}$.
- Vectors are denoted by boldface lowercase characters, e.g., $\mathbf{a}$.
- Matrices are denoted by boldface uppercase characters, e.g., $\mathbf{A}$.
- Unit vectors are denoted by boldface lowercase characters with a hat, e.g., $\hat{\mathbf{a}}$.

Mathematical operations

$(\cdot)^*$	Complex conjugate of the argument
$\lvert\cdot\rvert$	Absolute value of the argument
$\lceil\cdot\rceil$	Ceiling function of the argument
$\lVert\cdot\rVert_2$	2-norm of the argument

Chapter 1

Introduction

A problem of practical importance when dealing with acoustic measurements is to estimate the directions from which sound waves arrive to the measurement point. While a single microphone cannot provide this information, as microphones are only capable of measuring the sound pressure at that specific point, combination of simultaneous signals from an array of microphones makes it possible to filter the sound in space and, thus, achieve directionality. With proper signal processing, array systems can focus into a particular direction, to enhance the signals arriving from there, and attenuate those from other directions. This idea was explored for the first time in 1976, when Billingsley and Kinns introduced the acoustic telescope, a system that was able to localize the main contributions of jet engines in real-time [1]. This work laid the foundations of beamforming, which soon became popular among the acoustic community, giving rise to numerous studies not only for sound source localization purposes, but also for signal enhancement and spatial filtering. Nowadays beamforming is an essential tool widely used in the industry for all sorts of applications, such as vehicle assessment, computer games and surveillance, among others. Depending on the application, the most adequate processing techniques and array geometries vary. Generally, beamforming is based on measurements in the far field of the sources so that the waves have become planar at the array position. However, it should be noticed that near-field beamforming is also possible. Readers interested in the history of beamforming are addressed to the concise monograph by Michel, Ref. [2].

An ideal sound source localization system should present a delta function on the focusing direction and nulls elsewhere. However, beamforming presents two inherent limitations; firstly, an imperfect resolution on the focusing direction, due to a main

beam instead of a delta function, and secondly, the appearance of sidelobes in directions other than the focusing direction. Moreover, the array response is frequency dependent. The frequency range of operation of an array is determined, at low frequencies, by the dimensions of the array, and by the microphone spacing, at high frequencies. The larger the array, the better the performance at low frequencies, whereas the closer the microphones, the better at high frequencies. However, the dimensions of the array and the number of microphones are usually limited by practical issues, such as the maneuverability of the array and the overall cost of the equipment. Therefore, dealing with broadband sources poses some challenges. In the almost 40 years of development of acoustic array technology, numerous beamforming algorithms, as well as array geometries, have been suggested to improve the overall performance of array systems.

1.1 Scope of the thesis

The present thesis deals with circular and spherical arrays of microphones, to a lesser extent, for localization of sound sources in 2-dimensional (2D) and 3-dimensional (3D) sound fields, respectively. While spherical arrays have been examined widely in the last decade for speech enhancement and sound source localization purposes, less literature has been devoted to circular arrays. This geometry is particularly interesting for scenarios where sources placed in the far field are distributed 360° around the array. That is, for instance, the case of many outdoor measurements for environmental noise identification, in which reflections from the ground are sufficiently attenuated, and also the case of measurements in rooms where floors and ceilings are acoustically treated to reduce reflections. One of the main applications involving rooms is conferencing, a scenario that requires beamforming in real-time; see, e.g., Ref. [3]. By contrast, for environmental noise purposes, measurements can be often post-processed at a later stage, which allows the application of more sophisticated algorithms that require a high computational load. The primary goal of the present thesis is to suggest and examine alternatives to the traditional methods for enhancing the performance of these array geometries for sound source localization purposes.

It should be noticed that, throughout this dissertation, it is assumed that the acoustic sources are static, placed in the far field of the array, and not coherent. It is also assumed that all the array transducers have the same characteristics and are omnidirectional.

1.2 A brief overview on acoustic array systems

1.2.1 Beamforming techniques

Beamforming techniques are generally classified in two groups: fixed beamforming and adaptive beamforming. Fixed beamforming algorithms are data-independent, that is, all signals are treated in the same manner without taking into account their individual properties. The simplest method is delay-and-sum beamforming, which is addressed in Chapter 2. Another example is filter-and-sum beamforming, based on linearly filtering the signals prior to applying delay-and-sum; see, e.g., Ref. [4]. Filtering helps removing disturbances, such as out-of-band noise. A new and specially attractive technique for its simplicity is functional beamforming [5]. This method that results from modifying delay-and-sum beamforming in the frequency domain offers a much higher dynamic range than other beamforming techniques. However, it is very sensitive to microphone positioning errors.

On the other hand, adaptive beamforming methods are data-dependent, that is, their parameters follow from statistical observations in the captured signals. As a result, their performance exceeds that of fixed beamforming techniques, at the expense of being more complex to implement and more sensitive to sensor calibration errors [4]. Furthermore, in the presence of coherent sources, most methods fail dramatically. Usually, adaptive techniques rely on narrow-band signals. Several methods are based on solving a constrained mean-squared optimization problem. That is, for instance, the case of the generalized sidelobe canceler (GSC) [6], which basically consists of a fixed beamformer, a blocking matrix, and an interference canceler. The fixed beamformer is steered to the desired direction, while the blocking matrix blocks any signal coming from that direction so that only noise signals from undesired directions pass through. By means of an adaptive algorithm the unwanted signals are emphasized and finally they are subtracted from the fixed beamformer output. Another type of adaptive techniques, the so-called high-resolution spectral estimation techniques, are derived from parameter estimation theory. One such method is the multiple signal classification (MUSIC), which, based on eigenanalysis, relies on the orthogonality between the signals subspace and the noise subspace to improve the quality of the signals [7]. Adaptive methods are out of the scope in this dissertation. Readers interested in adaptive beamforming are, for instance, referred to Chapter 7 in Ref. [4] and Chapter 5 in Ref. [8].

Although most beamforming techniques are in essence independent of the array

geometry, there is a group of methods conceived for 'closed' arrays, such as circular and spherical arrays, known as eigenbeamforming. Eignebeamforming relies on the decomposition of the sound field captured with the array in a series of harmonics, which adds more features compared to traditional beamforming. Fixed eigenbeamforming methods are addressed in Chapter 3.

In the last decade, a group of inverse methods, generally referred to as deconvolution methods, has become of interest, as they allow to visualize sound sources with more accuracy than beamforming methods, and even determine their levels. However, the main limitation is that they are computationally expensive, as they are based on iterative algorithms. An overview of these methods is given in Chapter 4.

It should be noted that beamforming can be applied also to moving sources. Since in the present study only static sources are considered, the reader is addressed to, e.g., Chapter 8 in Ref. [4] for a basic introduction to tracking problems.

1.2.2 Other array techniques

Besides beamforming, there are other sound visualization techniques that rely on array measurements. The most relevant one is acoustic holography, a well-established method that aims at reconstructing sound fields quantitatively. By means of measurements in a 2D surface (the array), the entire sound field, sound pressure, particle velocity, and sound intensity, can be reconstructed in a 3D space. Acoustic holography and beamforming are complementary techniques, as acoustic holography is generally preferred for near-field measurements, such as in near-field acoustic holography (NAH) [9, 10], whereas beamforming is more adequate for the far-field case. Moreover, acoustic holography handles better coherent than incoherent sources, which contrasts with the opposite behavior of beamforming. In most applications, acoustic holography serves to describe the radiation characteristics of the source under analysis.

Array technology is also used for blind source separation, although an array layout is not strictly necessary. As the name suggests, blind source separation is a sound source identification method that intends to simultaneously recover signals from independent sources without requiring any information on their locations. The main limitation of the method is that it fails when there are more sources than sensors. Blind source separation is not addressed in this thesis. Readers interested in a thorough comparison between

blind source separation and beamforming in the time-domain (for speech purposes) are referred to Ref. [11].

1.2.3 Array layouts

Traditionally, beamforming has been carried out mostly with planar-sparse arrays. The simplest configuration is the rectangular grid of elements. However, due to the periodical placement of the sensors, severe sampling error, in the form of aliasing, occurs above the frequency where the spatial Nyquist sampling criterion is not fulfilled. This causes a sudden increase in level of the sidelobes, which become replicas of the main lobe in unwanted directions in the worst case. This is addressed in Chapter 2. This characteristic prevents this geometry from being generally used for beamforming purposes. Contrarily, rectangular arrays, with one or two parallel layers, are typically used for NAH.

Planar irregular arrays are usually preferred for beamforming over regular arrays, because they do not exhibit an abrupt aliasing pattern. The effect of an aperiodical spatial sampling is a smooth increase in the level of the sidelobes, which leads to a wider frequency range of operation toward high frequencies [12]. Typical irregular arrays used for aeroacoustic purposes are based on spirals, such as the equiangular or logarithmic spiral array with one or more arms [13, 14]. Some other irregular layouts result from optimization processes that determine the position of the sensors that ensures the best possible level of the sidelobes for the frequency range of interest [12]. For some applications, such as wind tunnel measurements, it is convenient to flush-mount the array microphones on a wall or a baffle so that the array structure does not alter the aerodynamic environment. References [12] and [15] examine various planar irregular arrays in detail.

Spherical arrays are also widely used for beamforming [16], as well as for acoustic holography [17], whereas circular arrays are less common [18], especially for holography. Generally, spherical and circular arrays used for sound source localization are shift-invariant, that is, the output pattern is independent of the focusing direction so that the system is equally fair in all directions. One way to achieve this characteristic is by keeping a constant microphone spacing all over the array. That is, for instance, the case of a uniform circular array [19]. This interesting feature cannot be achieved with linear or planar-sparse arrays.

On the other hand, spherical arrays with non-uniform spacing have also been investigated, e.g., in Ref. [20]. That is, for instance, the case of a rigid spherical array with the sensors placed in horizontal rings with a higher density of sensors on the equator of the sphere suggested in Refs. [21–23] to enhance the horizontal spatial resolution over other directions. This array is suitable for 3D recordings that can afterwards be used to create virtual environments for hearing instrument testing and psychoacoustic purposes via a high-order or a mixed-order Ambisonics loudspeaker system [24]. Circular arrays with a non-uniform spacing are rather unusual. An example can though be found in Ref. [25], where the angular position of the array sensors is determined by the golden-ratio.

Variations of the circular and spherical geometries are also found in the literature. For example, Refs. [26, 27] suggest a dual-radius spherical array for beamforming and for NAH that consists of an open spherical array with a smaller spherical array mounted on a baffle in its interior, whereas Ref. [28] introduces an open dual-radius spherical array. Similarly, Refs. [29, 30] examine systems that consist of concentric uniform circular arrays of different radius. For beamforming purposes on a half 3D acoustic scenario, Ref. [31] suggests a baffled hemispherical microphone array that makes use of the image source principle.

To achieve a rather constant pattern in the entire frequency range of interest, some arrays are conformed by subarrays, each being responsible for a certain frequency band. Usually, this is approached with planar-sparse arrays [8, 32], although other configurations are applicable to, such as the previous mentioned concentric circular and spherical arrays. A wise solution to reduce the overall cost of the system is to share, when possible, array elements between different subarrays, giving rise to the concept of nested arrays. The idea of using nested arrays, is, in fact, the essence of constant directivity beamforming, a fixed beamforming method based on applying filter-and-sum to the the different nested arrays [8, 32]. The main drawback of this technique is that it is impractical at low frequencies, as it requires extremely large arrays.

In the presence of stationary signals, ‘scanning arrays’ are alternatives to conventional arrays. The procedure only requires two transducers: while one is kept at a position that serves as a reference, the other is moved along a grid [33]. The main advantage is that the equipment required is obviously cheaper than a that of a conventional array system. Besides, the method offers more flexibility in the sense that the scanning area is not limited to a predefined grid of points. The main drawback, though, is that

measurements are more time consuming. Based on this principle, a scanning array consisting of a rotating microphone set-up is suggested to capture the acoustic behavior of auditoriums in Ref. [34]. The data measured with the array, a large set of impulse responses, is later used for creating virtual acoustic scenes with a 2D or 3D Ambisonics loudspeaker system.

Most array systems assume that the sensors are completely omnidirectional. However, microphones with well-defined directivity patterns can also be used, provided that all of them are of the same type and are oriented identically. In such a case, the transfer function of the directive microphones must be taken into account for the beamforming procedure [32]. Besides conventional microphones, pressure-velocity transducers, e.g., Microflown PU probes [35], are progressively attracting interest. These transducers provide simultaneous measurements of pressure and particle velocity, which make them particularly suitable for acoustic holography [36]. In fact, some NAH methods rely on the combination of the two quantities to achieve an enhanced performance [37–39].

Recently, a completely new approach for beamforming based on the acousto-optic effect, i.e., the interaction between sound and light, has been introduced in Ref. [40]. Instead of using a discrete number of sensors as in conventional arrays, the proposed acousto-optic beamformer senses the sound field with a laser beam in a continuous manner so that spatial aliasing is totally avoided. So far, only an optical linear aperture has been examined [41]. At the moment, the main drawback of this technique is that the beamformer requires manual steering. However, this problem could be overcome by developing an optical array.

1.3 Structure of the thesis

The present PhD thesis follows a paper-based format, that is, the main findings of the PhD project are presented in a collection of articles elaborated in the course of the project. It is important to emphasize that the articles represent the core of the thesis.

The dissertation is structured as follows: Chapter 2, *Basic beamforming methods*, gives the basic concepts of beamforming required to follow the contributing papers. Readers familiar with the topic can skip this chapter. Chapter 3, *Eigenbeamforming*, Chapter 4, *Deconvolution methods*, and Chapter 5, *Beamforming with holographic virtual arrays*, are devoted to the findings of the contributing articles. These chapters share

the same structure: they begin with an introduction that intends to supplement, when possible, the articles, followed by a synopsis of the articles, a survey on related work, and a discussion of the findings. Unlike Chapter 2, Chapters 3 to 5 are kept deliberately concise to minimize the repetition in content with the contributing papers. Since these chapters are understood as a complement to the papers, the reader is advised to read the papers before proceeding to the final chapter, *Conclusions*, which concludes the work and suggests further investigations for the future. The thesis also includes two appendices that supplement Chapter 3 and 5, respectively.

The contributing papers, five in total, are appended at the end. Three of them are published in the Journal of the Acoustical Society of America, and the rest are published in the proceedings of two relevant congresses. They are listed in the following:

Paper A E. Tiana-Roig, F. Jacobsen, and E. Fernandez-Grande, "Beamforming with a circular microphone array for localization of environmental noise sources," *J. Acoust. Soc. Am.*, vol. 128, no. 6, pp. 3535–3542, 2010.*

Paper B E. Tiana-Roig, F. Jacobsen, and E. Fernandez-Grande, "Beamforming with a circular array of microphones mounted on a rigid sphere (L)," *J. Acoust. Soc. Am.*, vol. 130, no. 3, pp. 1095–1098, 2011.

Paper C E. Tiana-Roig and F. Jacobsen, "Deconvolution for the localization of sound sources using a circular microphone array", *J. Acoust. Soc. Am.*, vol. 134, no. 3, pp. 2078–2089, 2013.

Paper D E. Tiana-Roig, A. Torras-Rosell, E. Fernandez-Grande, C.-H. Jeong, and F. T. Agerkvist, "Towards an enhanced performance of uniform circular arrays at low frequencies," in *Proc. of Inter-Noise 2013, Innsbruck, Austria*, 2013.

Paper E E. Tiana-Roig, A. Torras-Rosell, E. Fernandez-Grande, C.-H. Jeong, and F. T. Agerkvist, "Enhancing the beamforming map of spherical arrays at low frequencies using acoustic holography," in *Proc. of BeBeC 2014, Berlin, Germany*, 2014.

*Paper A is based on the Master's thesis by Elisabet Tiana Roig "Beamforming Techniques for environmental noise", Technical University of Denmark, 2009. The paper, written in 2010 during the application process of the PhD project, is included as part of this PhD thesis as it led to the research topic of the project.

Besides the aforementioned articles, the following articles were also produced in the course of the PhD project:

1 E. Tiana-Roig and F. Jacobsen, "Acoustical source mapping based on deconvolution approaches for circular microphone arrays," in *Proc. of Inter-Noise 2011, Osaka, Japan*, 2011.

2 Fernandez-Comesaña, E. Fernandez-Grande, and E. Tiana-Roig, "A novel deconvolution beamforming algorithm for virtual phased arrays", in *Proc. of Inter-Noise 2013, Innsbruck, Austria*, 2013.

However, these articles are not explicitly mentioned in the thesis, as the contents of Paper 1 overlap with Paper C and Paper 2 does not directly relate to the work done in eigenbeamforming.

Chapter 2

Basic beamforming methods

This chapter provides the basic knowledge required to comprehend the main contributions of the PhD project. The chapter begins with an introduction to classical beamforming theory. Two array geometries are examined in detail, the uniform linear array, which serves to explain the basic concepts of beamforming, and the uniform circular array as most contributing papers (Papers A to D) elaborate on this array configuration. In addition, the case of a spherical array is touched upon, as paper E deals with this geometry. The chapter ends with a description of the measures of performance commonly used to evaluate beamforming systems.

2.1 Delay-and-sum beamforming

Delay-and-sum beamforming is the oldest and simplest array signal processing algorithm [4]. The principle behind this technique is shown in Fig. 2.1: in the presence of a propagating wave, the signals captured by the microphones are delayed by a proper amount before being added together, to strengthen the resulting signal with respect to noise or waves propagating in other directions. The delays required to reinforce the output signal correspond to the time it takes for the wave to propagate between microphones so that, after applying the delays, the microphone signals are *aligned* in time. Mathematically, delay-and-sum is formulated as

$$b(t, \hat{\boldsymbol{\kappa}}) = \sum_{m=0}^{M-1} w_m p_m(t - \tau_m(\hat{\boldsymbol{\kappa}})), \tag{2.1}$$

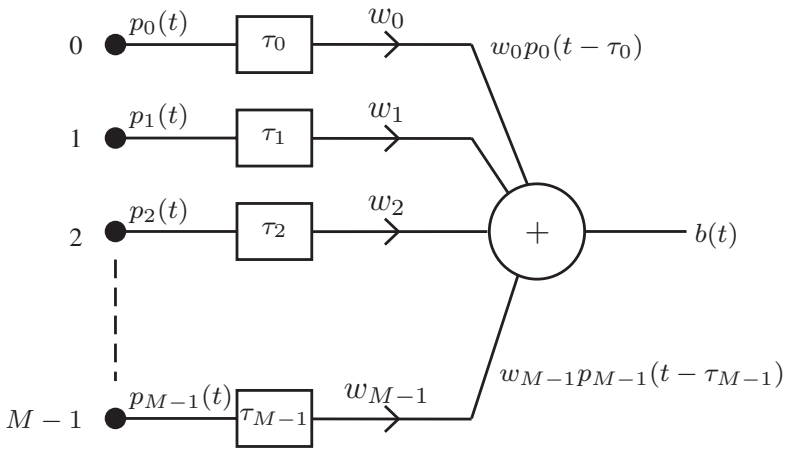

Figure 2.1: Sketch of a delay-and-sum beamformer. The signals captured by the sensors are delayed (and weighted) before adding them together.

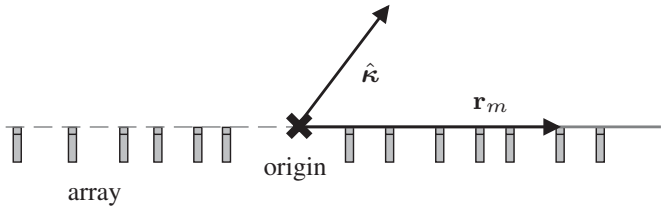

Figure 2.2: Array focused in the direction given by $\hat{\boldsymbol{\kappa}}$.

where M is the number of microphones, p_m is the pressure measured with the mth microphone, w_m is its associated amplitude weighting, and $\tau_m(\hat{\boldsymbol{\kappa}})$ is the delay applied to the mth microphone required to focus the array in the direction given by $\hat{\boldsymbol{\kappa}}$ depicted in Fig. 2.2. The delays are given by

$$\tau_m(\hat{\boldsymbol{\kappa}}) = \frac{\hat{\boldsymbol{\kappa}} \cdot \mathbf{r}_m}{c}, \tag{2.2}$$

where $\mathbf{r}_m$ is the position vector of the mth microphone and c is the speed of sound in the medium of propagation (approximately 343 m/s in air at 23°C).

Assuming a plane wave that impinges on the array, the pressure captured by the mth array microphone, expressed in complex notation, is

$$p_m(t) = A e^{j(\mathbf{k_i} \cdot \mathbf{r}_m - \omega t)}, \tag{2.3}$$

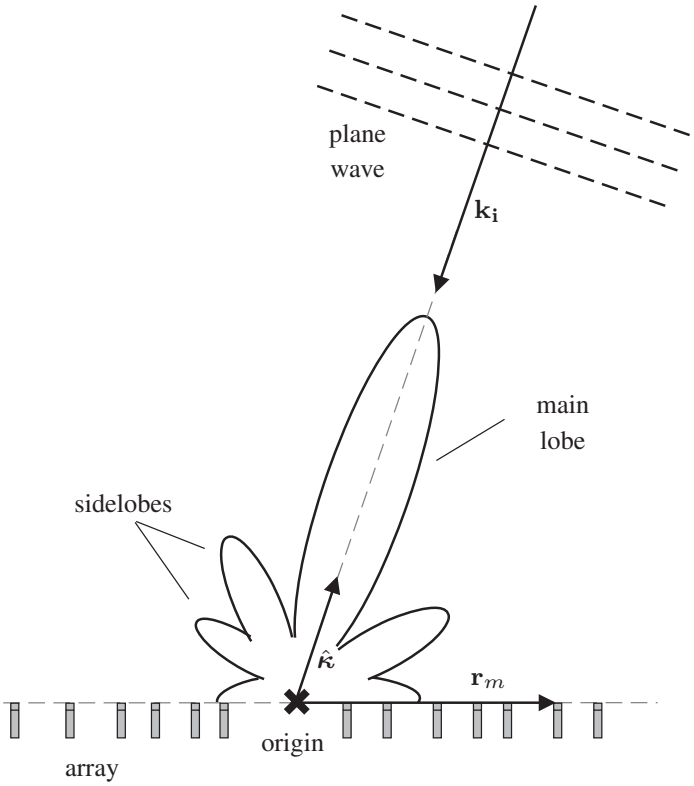

Figure 2.3: Plane wave impinging on an array. The beamformer response presents a main beam when steered in the direction of the impinging wave, whereas other directions are partially or totally attenuated.

where A is the amplitude, ω represents the angular frequency, related to the frequency f by $\omega = 2\pi f$, and $\mathbf{k_i}$ is the wavenumber vector, with magnitude $|\mathbf{k_i}| = k = \omega/c$. It can be shown that the beamformer output, Eq. (2.1), results in

$$b(t, \hat{\boldsymbol{\kappa}}) = Ae^{-j\omega t} \sum_{m=0}^{M-1} w_m e^{j(\mathbf{k_i} + k\hat{\boldsymbol{\kappa}}) \cdot \mathbf{r}_m}. \tag{2.4}$$

A close inspection of this equation reveals that when the array is steered in the precise direction $\hat{\boldsymbol{\kappa}}$ that satisfies $\mathbf{k_i} = -k\hat{\boldsymbol{\kappa}}$, the beamformer response presents its maximum value. When focused toward other directions, the response is partially or totally attenuated. If the array scans all possible directions with the appropriate associated delays, the resulting beamformed map will present a main lobe around its maximum and sidelobes elsewhere. This is illustrated in Fig. 2.3.

The weightings w_m, often referred to as *shading*, influence the shape of the main-

and sidelobes. They act as spatial windows and their effect is analogous to that observed with temporal windows in conventional signal processing. In fact, Eq. (2.4) can be rewritten as

$$b(t, \mathbf{k}) = Ae^{-j\omega t} W(\mathbf{k} - \mathbf{k_i}), \tag{2.5}$$

where $\mathbf{k} = -k\hat{\boldsymbol{\kappa}}$, and $W(\mathbf{k})$ is the spatial discrete Fourier Transform of the weightings

$$W(\mathbf{k}) = \sum_{m=0}^{M-1} w_m e^{-j\mathbf{k}\cdot\mathbf{r}_m}. \tag{2.6}$$

This function is usually known as *array pattern*. When the weightings follow a uniform distribution, the array pattern exhibits the narrowest possible main lobe, whereas tapered distributions, such as the triangular and the Hann windows, yield lower sidelobes at the expense of a wider main lobe [42]. Furthermore, the location of the nulls in the pattern also depends on the weightings.

In real case scenarios, the pressure captured by the microphones is contaminated by noise, e.g., background noise and electronic noise. In case of a single plane wave, the pressure is (cf. Eq. (2.3))

$$p_m(t) = Ae^{j(\mathbf{k_i}\cdot\mathbf{r}_m - \omega t)} + n_m(t), \tag{2.7}$$

where $n_m(t)$ is uncorrelated noise present at the mth microphone. Obviously, the presence of noise influences the response of beamforming systems. However, compared to a measurement with a single microphone, the combination of many measurements, as in the case of using a microphone array, leads to a better signal-to-noise ratio (SNR). Amongst all techniques, it can be shown that delay-and-sum is the most robust against noise and has, moreover, the ability to suppress uncorrelated noise equally at all frequencies [8].

For broadband signals, it is convenient to implement delay-and-sum beamforming in the frequency domain. The signal is decomposed in a set of monochromatic plane waves (i.e., single-frequency waves), each treated independently in the beamforming

procedure so that the applied phase shifts correspond to the desired delays. That is

$$b(\omega, \hat{\boldsymbol{\kappa}}) = \sum_{m=0}^{M-1} w_m p_m(\omega) e^{j\omega\tau_m(\hat{\boldsymbol{\kappa}})}, \tag{2.8}$$

where $p_m(\omega)$ is the discrete Fourier Transform of the signal measured with the mth sensor. The time domain version can be simply obtained with the inverse discrete Fourier Transform of $b(\omega, \hat{\boldsymbol{\kappa}})$.

A common practice when dealing with stationary sound fields is to formulate delay-and-sum beamforming in the frequency domain using the averaged cross-spectra of the input signals. From Eq. (2.8), the power output can be written as

$$|b(\omega, \boldsymbol{\kappa})|^2 = \sum_{m=0}^{M-1} \sum_{n=0}^{M-1} w_m w_n^* \overline{p_m(\omega) p_n^*(\omega)} e^{j\omega(\tau_m(\hat{\boldsymbol{\kappa}}) - \tau_n(\hat{\boldsymbol{\kappa}}))}, \tag{2.9}$$

where $(\,\cdot\,)^*$ denotes complex conjugation. For the sake of simplicity, the weightings are set to unity in the following. Let us now consider the averaged cross-spectral matrix*

$$\mathbf{C} = \begin{bmatrix} c_{00} & c_{01} & c_{02} & \cdots & c_{0(M-1)} \\ c_{11} & c_{11} & c_{12} & \cdots & c_{1(M-1)} \\ c_{20} & c_{21} & c_{22} & \cdots & c_{2(M-1)} \\ \vdots & \vdots & \vdots & \ddots & \vdots \\ c_{(M-1)0} & c_{(M-1)1} & c_{(M-1)2} & \cdots & c_{(M-1)(M-1)} \end{bmatrix}, \tag{2.10}$$

where

$$c_{mn}(\omega) = \overline{p_m(\omega) p_n^*(\omega)}, \tag{2.11}$$

is the averaged cross-spectrum between the signals captured at the mth and nth sensors, being

$$c_{mn}(\omega) = c_{nm}^*(\omega). \tag{2.12}$$

By using the cross-spectral matrix, the output power of the beamformer can be rewritten

*Note that the frequency dependence in the matrix is omitted.

as

$$|b(\omega,\hat{\boldsymbol{\kappa}})|^2 = \sum_{m=0}^{M-1} c_{mm}(\omega) + \sum_{m=0}^{M-1}\sum_{\substack{n=0\\n\neq m}}^{M-1} c_{mn}(\omega)e^{j\omega(\tau_m(\hat{\boldsymbol{\kappa}})-\tau_n(\hat{\boldsymbol{\kappa}}))}. \tag{2.13}$$

As can be seen, the first sum of this expression involves the diagonal elements, i.e., the auto-spectral terms, $c_{mm}(\omega)$, whereas the second sum accounts for off-diagonal terms, $c_{mn}(\omega)$. Note that the diagonal elements contain amplitude information plus self-noise. However, they do not carry phase information, and therefore, do not help in determining the source location. That is not the case for the cross-spectra elements; they contain the relative phase between each pair of sensors, and thus are essential for the beamforming process. Furthermore, self-noise is not present in these terms, as it is uncorrelated across channels. Therefore, it seems reasonable to remove the diagonal elements. This procedure, known as *diagonal removal*, decreases the level of the sidelobes, resulting in a clearer beamformed map [43]. However, the price to pay for this operation is that the resulting levels are biased.

The sound field at the array position can be generically described as the superposition of waves created by different sources so that waves arrive from different directions. When waves are incoherent, the beamformer output is equivalent to the superposition of outputs for each wave [12]. If the sources are sufficiently far from each other, they can be successfully identified. However, in the presence of coherent waves most beamformers fail. This problem, which appears, for instance, when dealing with (coherent) reflections, is often disregarded in the modern literature [2]. However, some studies have elaborated on this aspect, e.g., Refs.[44, 45].

Until now only sources in the far field, and thus, plane waves at the array position, have been assumed. In this situation only the (angular) direction of the sources can be identified. Their distance to the array cannot be determined, as, in fact, the beamformer is focused toward an infinite distance. In contrast, to localize sources in the near field, a finite focus distance has to be considered, together with spherical wavefronts. This is illustrated in Fig. 2.4, where the array is steered toward a point located at $\mathbf{r}$. Geometrical considerations show that, in order to align the signals at the sensor positions, the delays required for delay-and-sum beamforming are given by

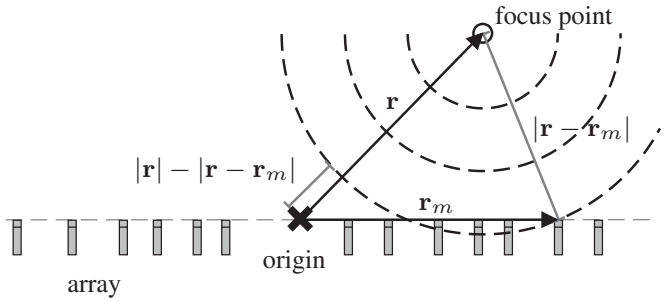

Figure 2.4: Beamformer focused toward a point in the near field. Spherical waves are expected at the array position.

$$\tau_m = \frac{|\mathbf{r}| - |\mathbf{r}-\mathbf{r}_m|}{c}. \tag{2.14}$$

Since the amplitude of spherical waves decays with the distance, it is possible to compensate for it by including amplitude corrections in the beamforming algorithm [46].

In what follows, only sources in the far field of the array, and thus, planar wavefronts at the array position, are considered.

2.1.1 Uniform linear array

A uniform linear array, the simplest array geometry, serves to illustrate the performance of a delay-and-sum beamformer. This array consists of a number of sensors placed in a line with uniform spacing, as shown in Fig. 2.5.

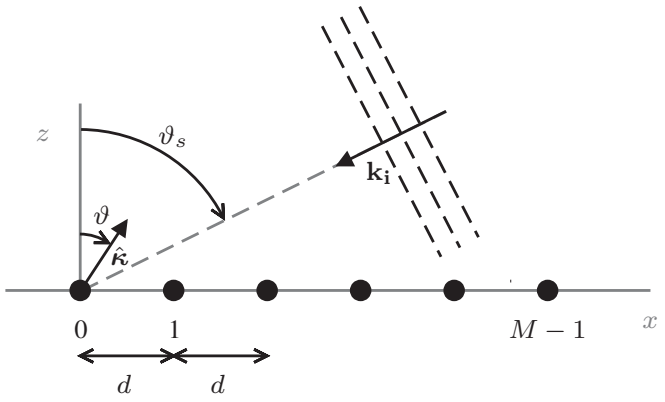

Figure 2.5: Plane wave impinging on a uniform linear array with M sensors.

From the geometrical considerations given in Fig. 2.5, the mth array sensor is located at

$$\mathbf{r}_m = \begin{bmatrix} md \\ 0 \\ 0 \end{bmatrix}, \qquad m = 0, \ldots, M-1, \tag{2.15}$$

where d is the spacing between sensors. Moreover, when the system is steered toward the direction given by the polar angle ϑ, here defined from $-180°$ to $180°$, the steering vector $\hat{\boldsymbol{\kappa}}$ becomes

$$\hat{\boldsymbol{\kappa}} = \begin{bmatrix} \sin\vartheta \\ 0 \\ \cos\vartheta \end{bmatrix}. \tag{2.16}$$

Let us assume that the array captures a plane wave with amplitude A and wavenumber vector

$$\mathbf{k_i} = -k \begin{bmatrix} \sin\vartheta_s \\ 0 \\ \cos\vartheta_s \end{bmatrix}, \tag{2.17}$$

where ϑ_s is the angular position of the source. Expressed in these terms, delay-and-sum beamforming, Eq. (2.4), becomes

$$b(t,\vartheta) = A\mathrm{e}^{-j\omega t} \sum_{m=0}^{M-1} w_m \mathrm{e}^{-jk(\sin\vartheta_s - \sin\vartheta)md}. \tag{2.18}$$

Notice that this expression does not depend on the azimuth angle φ, which implies that a linear array cannot discriminate between waves arriving from different azimuthal directions.

Considering a uniform amplitude weighting $w_m = 1$, the output reduces to

$$b(t,\vartheta) = A\mathrm{e}^{-j\omega t} \frac{1 - e^{-jk(\sin\vartheta_s - \sin\vartheta)Md}}{1 - e^{-jk(\sin\vartheta_s - \sin\vartheta)d}}. \tag{2.19}$$

After some rearrangement, the corresponding directivity pattern (or beam pattern) results in

$$|b(\vartheta)| = |A| \left| \frac{\sin(\pi(\sin\vartheta_s - \sin\vartheta)Md/\lambda)}{\sin(\pi(\sin\vartheta_s - \sin\vartheta)d/\lambda)} \right|, \tag{2.20}$$

where λ is the wavelength, $\lambda = c/f$. As an example, the directivity pattern of a uniform linear array with 10 microphones is shown in Fig. 2.6, when $A = 2$, $d/\lambda = 0.3$ and

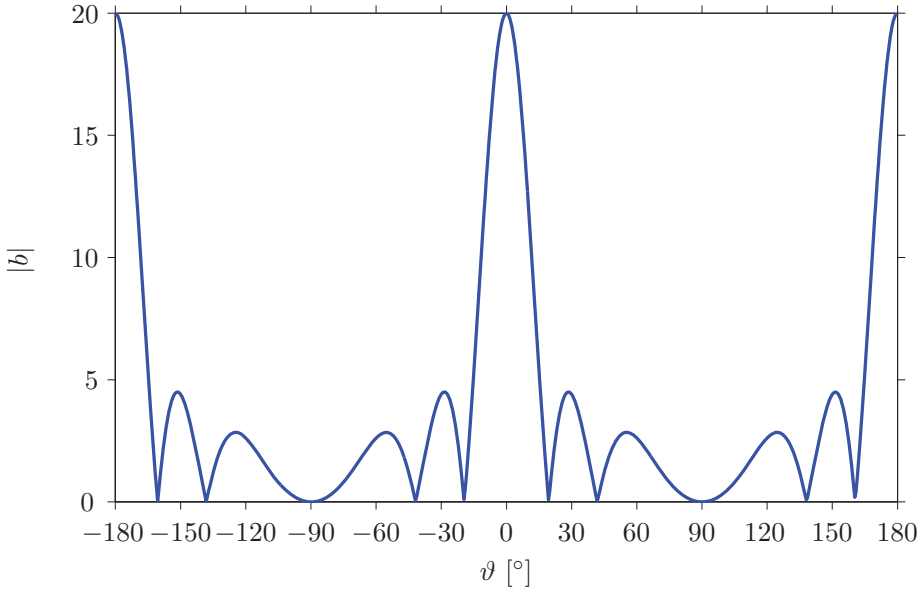

Figure 2.6: Directivity pattern of a uniform linear array with 10 sensors, when $d/\lambda = 0.3$ and a plane wave with amplitude 2 impinges on the array from $0°$.

the impinging wave comes from $\vartheta_s = 0°$. As can be seen the curve presents a main lobe around $0°$ as the present wave propagates in this direction. The value of the main beam peak is 20, which corresponds to $A \times M$. However, another main lobe appears around $180°$. This is a consequence of the line array geometry, as the delays applied at the microphones for both $0°$ and $180°$ are exactly the same. Hence, the uniform linear array presents a front-back ambiguity. This is inherent to all types of linear arrays. From this example, it is worth mentioning that the same directivity pattern can be achieved at all frequencies, as long as d varies according to the frequency to keep the ratio d/λ constant. This implies that at low frequencies, larger inter-spacings, and thus larger array dimensions, are needed in order to keep d/λ constant. In fact, this is a very important property as it suggests that the lowest frequencies that a beamformer can resolve properly are determined by the total size of the array.

Besides the two main lobes, the pattern also presents sidelobes with significantly lower amplitudes in the other directions. By adding more transducers and keeping d/λ constant, the main lobes become narrower and the number of sidelobes increases, but their overall amplitude decreases. This is illustrated in Fig. 2.7, where the patterns for three different number of sensors are shown in polar plots. This feature has two possible interpretations: 1) considering a fixed array length, having more sensors results in a smaller inter-spacing, which implies that the pattern becomes more directive toward

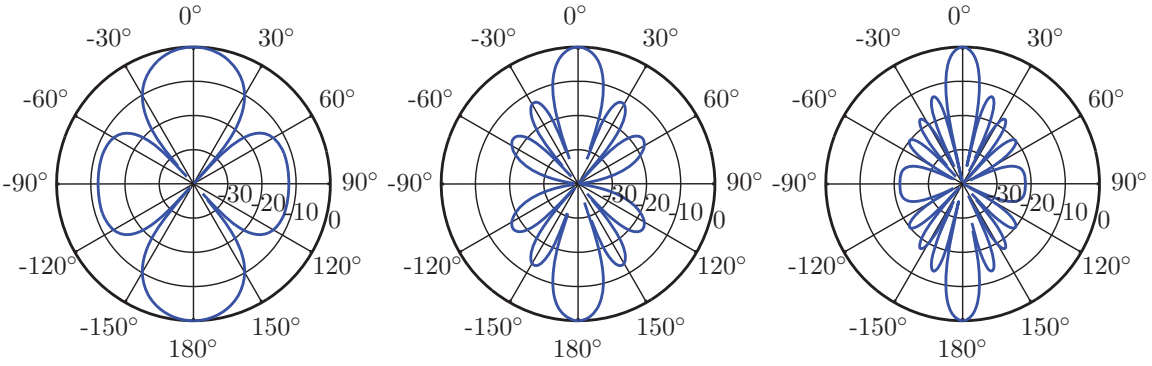

(a) $M = 5$ (b) $M = 10$ (c) $M = 20$

Figure 2.7: Influence of the number of transducers on the beamforming pattern of a uniform linear array. The magnitude is expressed in dB and normalized to $A \times M$. A plane wave approaches the array from $0°$. In all cases $d/\lambda = 0.3$

high frequencies (a smaller wavelength is needed in order to keep d/λ constant.) And 2) assuming a constant space between sensors, increasing the number of sensors is equivalent to extending the array, which implies that for a given frequency, the larger the array, the more directive the pattern. This agrees with the previous discussion regarding array size and low frequencies.

Similarly to the effect of increasing the number of sensors, the pattern becomes more directive with increasing the ratio d/λ, as can be seen in Fig. 2.8. However, the case $d/\lambda = 1.2$ shows replicas of the main lobe in unexpected directions. These replicas, usually called *grating lobes*, are caused by the aliasing effect, which is a consequence of undersampling the space with a finite number of transducers. The aliased replicas occur when $d/\lambda > 0.5$, which corresponds to the Nyquist sampling criterion in space. In fact, this criterion determines the highest frequency the array can capture without sampling error. The aliasing effect can be pushed beyond the Nyquist criterion, and thus, toward higher frequencies, by using irregular arrays. With an irregular layout, the level of the sidelobes is kept relatively low for a wider frequency range, and aliasing occurs at those frequencies where the average element spacing is several wavelengths; up to about 4λ according to Ref. [47], which is significantly above the Nyquist criterion ($\lambda/2$). Ideally, aliasing can only be totally avoided in the hypothetical case of using an array of sensors placed infinitely close to each other, or alternatively, by means of scanning the sound field in a continuous manner. Recent studies have shown that this is possible with a laser beam, as in the acousto-optic beamformer [40].

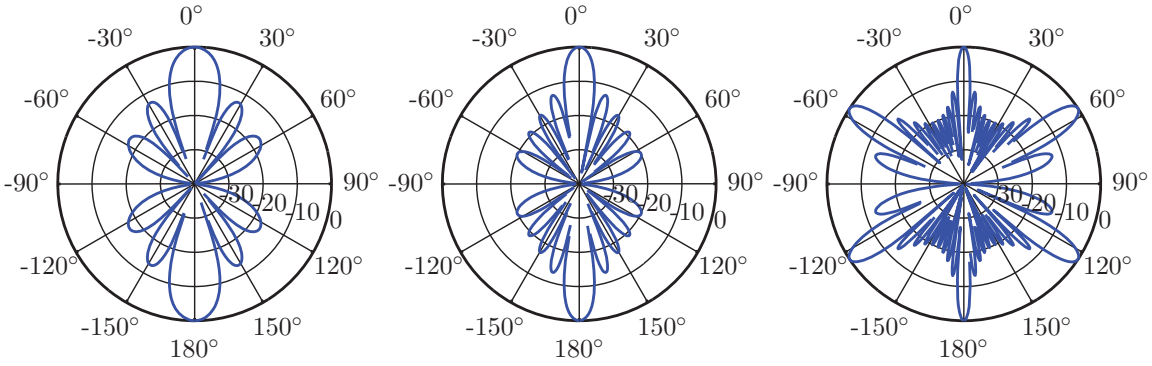

(a) $d/\lambda = 0.3$ (b) $d/\lambda = 0.5$ (c) $d/\lambda = 1.2$

Figure 2.8: Influence of the ratio d/λ on the beamforming pattern of a uniform linear array with 10 sensors. The magnitude is expressed in dB and normalized to $A \times M$. A plane wave approaches the array from $0°$.

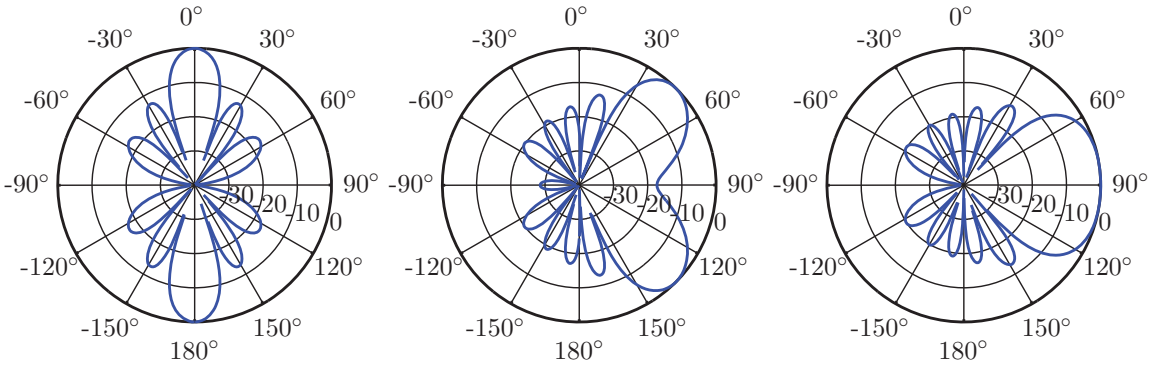

(a) $\vartheta_s = 0°$ (b) $\vartheta_s = 45°$ (c) $\vartheta_s = 90°$

Figure 2.9: Influence of the direction of an incident plane wave on the beamforming pattern of a uniform linear array with 10 sensors. The magnitude is expressed in dB and normalized to $A \times M$. In all cases $d/\lambda = 0.3$

When an incident wave comes from directions other than $0°$ and $180°$, the resulting main lobe becomes progressively wider toward $\pm 90°$. This can be seen in Fig. 2.9, for waves arriving from $0°, 45°$, and $90°$. Due to the front-back ambiguity, a replica of the main lobe always appears at $(180° - \vartheta_s)$ if $\vartheta_s \geq 0$, or at $(-180° - \vartheta_s)$ if $\vartheta_s < 0$. A pattern that depends on the focusing direction is usually referred to as shift-variant.

2.1.2 Uniform circular array

Two of the main weaknesses that uniform linear arrays exhibit, namely the front-back ambiguity and the pattern dependency on the steering direction, can be solved if uniform

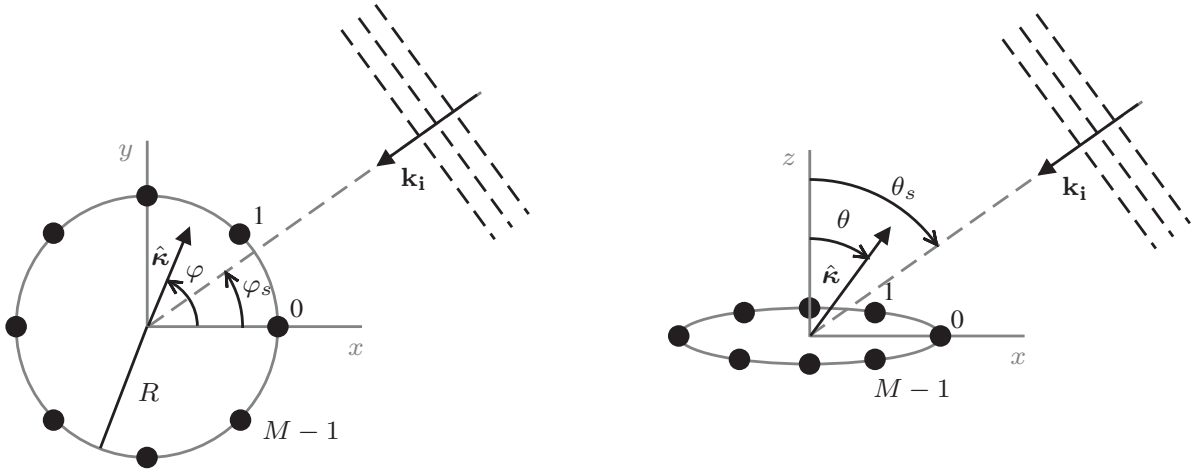

(a) Top view (b) Side view

Figure 2.10: Plane wave impinging on a uniform circular array with M sensors.

circular arrays are used instead. This array geometry is characterized by having M sensors uniformly distributed in a circle, as illustrated in Fig. 2.10. The position of the mth sensor is in this case given by

$$\mathbf{r}_m = R \begin{bmatrix} \cos(2\pi m/M) \\ \sin(2\pi m/M) \\ 0 \end{bmatrix}, \qquad m = 0, \ldots, M-1, \tag{2.21}$$

where R is the radius of the circle. According to geometrical model given in Fig. 2.10, the array steering vector, and the wavenumber vector of a wave arriving from (θ_s, φ_s), are

$$\hat{\boldsymbol{\kappa}} = \begin{bmatrix} \sin\theta\cos\varphi \\ \sin\theta\sin\varphi \\ \cos\theta \end{bmatrix}, \tag{2.22}$$

and

$$\mathbf{k_i} = -k \begin{bmatrix} \sin\theta_s\cos\varphi_s \\ \sin\theta_s\sin\varphi_s \\ \cos\theta_s \end{bmatrix}. \tag{2.23}$$

Using the three previous expressions, the delay-and-sum output can be easily obtained

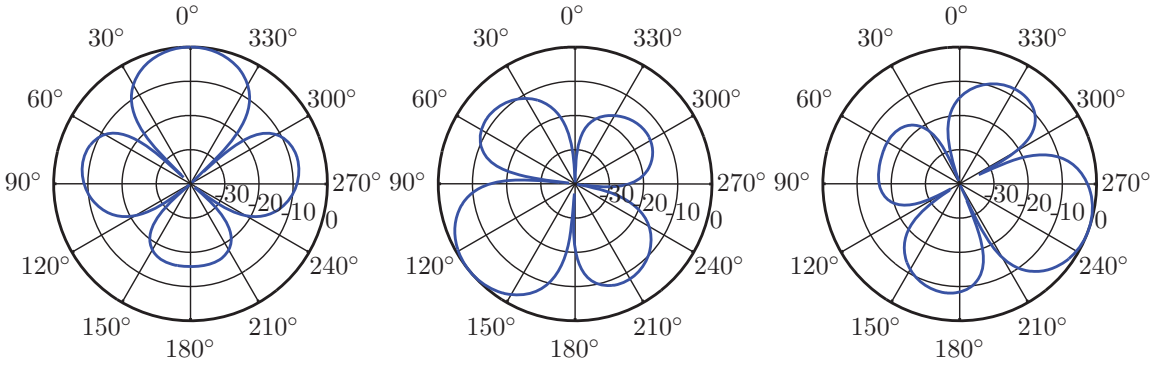

(a) $\varphi_s = 0°$ (b) $\varphi_s = 130°$ (c) $\varphi_s = 250°$

Figure 2.11: Influence of the direction of an incident plane wave on the beamforming pattern of a uniform circular array with 10 sensors. The magnitude is expressed in dB and normalized to $A \times M$. In all cases $d/\lambda = 0.3$ and $\theta_s = \theta = 90°$.

using Eq. (2.4). In a compact form, this can be expressed as [48]

$$b(\theta, \varphi) = \sum_{m=0}^{M-1} w_m e^{jk\rho\cos(\xi - \frac{2\pi m}{M})}, \tag{2.24}$$

where

$$\rho = R\sqrt{(\sin\theta\cos\varphi - \sin\theta_s\cos\varphi_s)^2 + (\sin\theta\sin\varphi - \sin\theta_s\sin\varphi_s)^2}, \tag{2.25}$$

and

$$\cos\xi = R\frac{\sin\theta\cos\varphi - \sin\theta_s\cos\varphi_s}{\rho}. \tag{2.26}$$

In order to obtain a shift-invariant pattern, the weightings w_m must be uniform. In what follows, they are set to unity.

Let us consider a uniform circular array with 10 sensors that captures a plane wave with frequency such that $d/\lambda = 0.3$. It is assumed that the wave propagates in the plane of the array and that the beamformer also looks into this plane. Looking at the right panel of Fig. 2.10, this implies that $\theta_s = \theta = 90°$. The delay-and-sum response for three different azimuth angles φ_s of the incident wave, $0°, 130°$, and $250°$, is shown in Fig. 2.11. At first sight, it can be clearly seen that the circular geometry does not exhibit the front-back ambiguity and that the directivity pattern has practically the same shape regardless the direction of incidence of the wave. However, for a given d/λ and

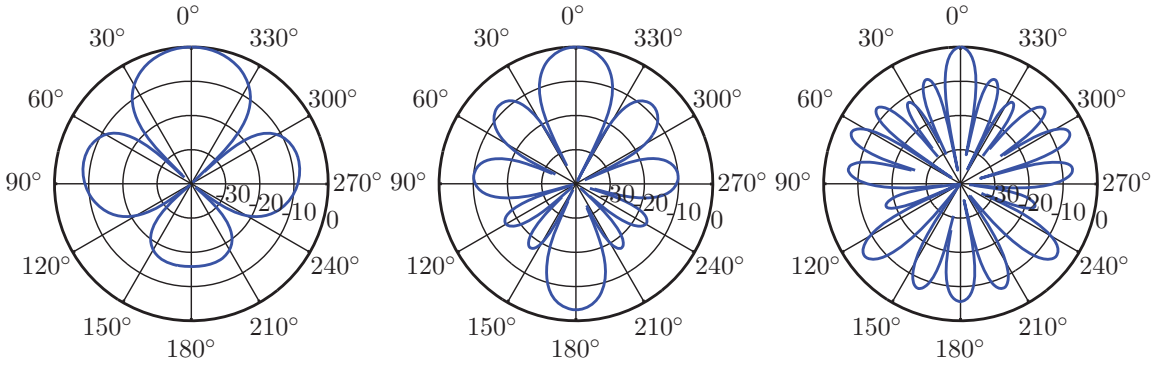

(a) $d/\lambda = 0.3$ (b) $d/\lambda = 0.5$ (c) $d/\lambda = 1.2$

Figure 2.12: Influence of the ratio d/λ on the beamforming pattern of a uniform circular array with 10 sensors. The magnitude is expressed in dB and normalized to $A \times M$. In all cases a plane wave arrives from $(\theta_s, \varphi_s) = (0°, 90°)$ and $\theta = 90°$.

a fixed number of sensors the main lobe is in general wider to that of a uniform linear array; compare, for instance, panels (a) and (b) in Fig. 2.9 with Fig. 2.11.

As can be seen in Fig. 2.12, with increasing d/λ the circular array behaves similarly to a uniform linear array: the main beam becomes more directive and the sidelobes increase in number. Due to the regular geometry of a uniform circular array, aliasing occurs at about $d/\lambda = 0.5$. However, aliasing does not take the form of replicas of the main lobe (grating lobes) as in the case of a uniform linear array, yet in a dramatic increase in level of the sidelobes. It is worth mentioning at this point that the distance between consecutive sensors d does not follow the curvature of the circular geometry, but the straight line between consecutive sensors. Geometrical considerations show that

$$d = 2R\sin(\pi/M). \tag{2.27}$$

Although a uniform circular array is shift-invariant in the azimuthal direction (φ), it should be emphasized that this property is not valid with respect to the polar angle (θ). For this reason, uniform circular arrays are normally steered toward directions contained in the plane of the array, by fixing $\theta = 90°$, and considering 2D sound fields, i.e., only waves propagating in that plane. This is a good assumption as long as waves from other directions are sufficiently attenuated. If that is not the case, but the beamformer still expects a 2D sound field, the resulting map becomes gradually ambiguous to such an extent that the pattern is totally omnidirectional for waves propagating from

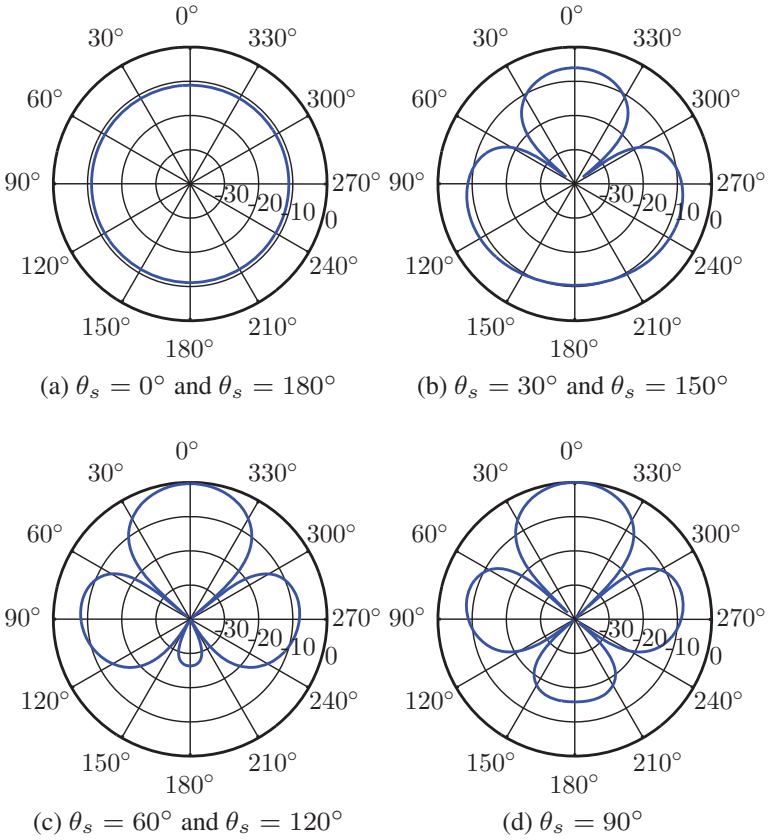

(a) $\theta_s = 0°$ and $\theta_s = 180°$ (b) $\theta_s = 30°$ and $\theta_s = 150°$

(c) $\theta_s = 60°$ and $\theta_s = 120°$ (d) $\theta_s = 90°$

Figure 2.13: Influence of the polar angle of an incident plane wave on the beamforming pattern of a uniform circular array with 10 sensors. The magnitude is expressed in dB and normalized to $A \times M$. In all cases $d/\lambda = 0.3$, $\varphi_s = 0°$ and $\theta = 90°$.

$\theta_s = 0°$ and $\theta_s = 180°$. This can be seen in Fig. 2.13. In practice, waves with polar angles θ_s up to $\pm 30°$ off-plane are generally detected successfully.

2.1.3 Spherical array

Spherical arrays consist of a number of sensors distributed over the surface of a sphere, which can be open (or transparent) or not. Unlike circular arrays, which have difficulties with waves propagating out-of-plane, spherical arrays have the ability to map 3D sound fields effectively. Furthermore, some layouts can provide a shift-invariant pattern for the entire 3D space. This will be later addressed in Sec. 3.1.2. The geometrical model assumed for a spherical array is shown in Fig. 2.14. In this case, the position of the mth microphone is given by

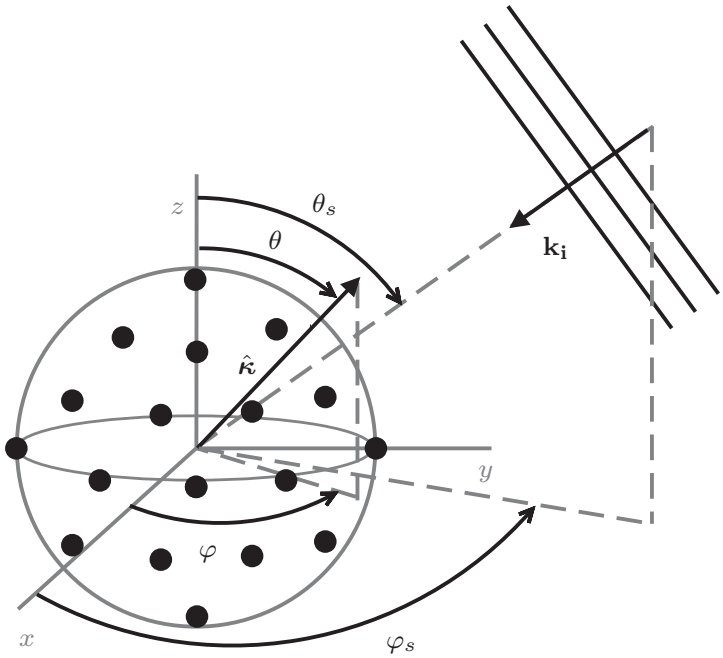

Figure 2.14: Plane wave impinging on a spherical array with M sensors.

$$\mathbf{r}_m = R \begin{bmatrix} \sin\theta_m \cos\varphi_m \\ \sin\theta_m \sin\varphi_m \\ \cos\theta_m \end{bmatrix}, \qquad m = 0, \ldots, M-1, \tag{2.28}$$

where R is the radius of the sphere, and θ_m and φ_m are the polar and the azimuth angles of the mth transducer. The focus direction $\hat{\boldsymbol{\kappa}}$ and the wavenumer vector of an incident plane wave are given by Eqs. (2.22) and (2.23), respectively.

2.2 Performance indicators

It is apparent from the previous section that several aspects, for instance, geometry, number of transducers, and spacing, influence the beamformer response. It is therefore necessary to make use of performance indicators to assess and compare beamforming systems. Most measures of performance found in the literature are often adapted from other fields, such as electromagnetism (antenna theory) and optics. A brief description of the most relevant ones is given in the following.

Measures of beam pattern

Resolution: Defined as the -3 dB width of the main lobe of the directivity pattern and measured in degrees or radians. It is also known as the 3 dB beamwidth, the half-power beamwidth, and the angular resolution. This measure, which is adapted from antenna theory (see, e.g., Ref. [49]) gives the minimum angle at which two incoherent sources can be resolved. Moreover, it is an indicator of directivity. The lower the value, the more directive the beamformer is.

Maximum sidelobe level (MSL): Given by the difference in level in dB between the peak of the highest sidelobe in the beam pattern to the peak of the main lobe [12]. This measure is also adapted from antenna theory and in the antenna community it is commonly referred to as SLL (sidelobe level) [50]. The MSL is complementary to the resolution, as it is not about directivity, yet a descriptor of how sensitive the beamformer is toward unwanted directions. Obviously, the larger the level difference between main- and maximum sidelobe, the better. It can be shown that this measure is more sensitive to noise than the resolution.

Peak-to-zero distance or **Rayleigh resolution limit**: Given by the angular difference between the position of the peak of the main lobe of the beam pattern and the position of its closest null. It determines the ability of the array to resolve two incoherent plane waves based on the Rayleigh criterion [51], adapted from optics theory. This criterion states that two plane waves are resolved when the main peak of the beam pattern of one falls on the null closest to the main peak of the beam pattern of the other one. This measure is an alternative to the resolution based on the -3 dB width, as half the beamwidth between the nulls of the main lobe is approximately equal to the -3 dB beamwidth [52].

Figure 2.15 illustrates how the resolution, the MSL, and the peak-to-zero distance can be extracted from a given beam pattern.

Other measures

Directivity index (DI): Defined as the ratio of the beamformer response in the looking direction to the average response over all directions. Expressed on logarithmic

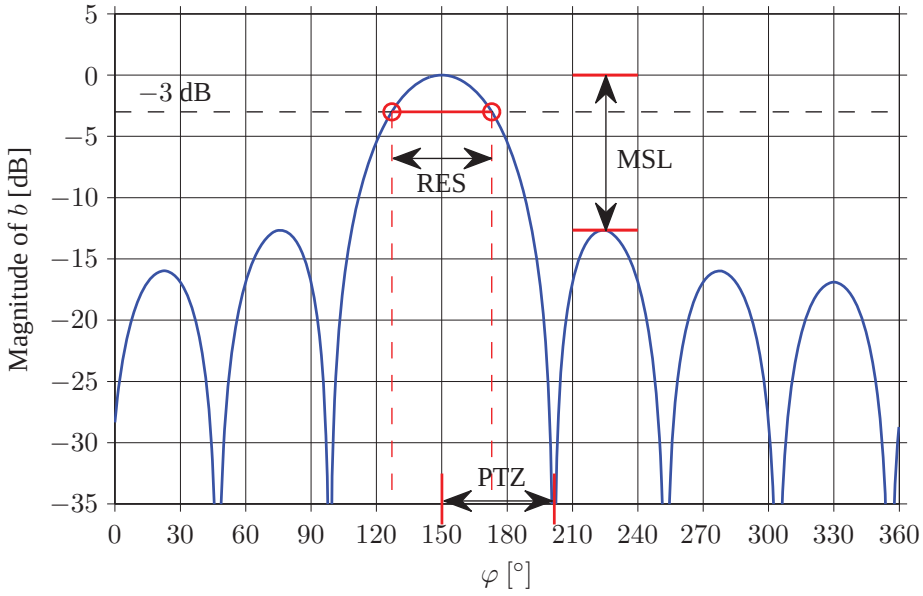

Figure 2.15: Calculation of the resolution (RES), the MSL, and the peak-to-zero (PTZ) distance from a given beam pattern.

scale [52, 53], the DI can be written as

$$\mathrm{DI} = 10 \log \left(\frac{|b(\theta_s, \varphi_s)|^2}{\frac{1}{4\pi} \int_0^{2\pi} \int_0^{\pi} |b(\theta, \varphi)|^2 \sin\theta \, d\theta \, d\varphi} \right). \tag{2.29}$$

This measure can be regarded as the array gain against isotropic noise (noise distributed uniformly over a sphere) [42]. The higher the DI, the better.

Array gain: Reflects the improvement in SNR achieved by using an array. It is defined as the ratio of the SNR at the array output to the SNR at a single sensor subject to different types of noise [4]. Usually isotropic acoustical noise is considered [8].

White noise gain (WNG): Measured as the array gain, but considering that the SNR at every sensor is due to spatially uncorrelated white noise [8]. It can also be regarded as the ratio of the signal power at the output of the beamformer to the sensor self-noise power assuming a unity variance noise [54]. The WNG is an indicator of the robustness of the array against deviations in the practical implementation, such as sensor self-noise, positioning errors, and amplitude and phase variations. The higher the WNG, the more robust the array is. It can be shown that the optimal WNG equals the number of microphones, for frequencies below

the Nyquist frequency, and is achieved with delay-and-sum beamforming with a uniform weighting [42].

Usually, the resolution and the MSL are examined together as they provide direct values related to the beam pattern that complement each other to give an idea of its shape. These two indicators can be seen in Fig. 2.16 as a function of frequency for a delay-and-sum beamformer based on a uniform circular array with 12 sensors and 11.9 cm of radius.[†]. A uniform weighting, a focusing direction of $180°$, and ideal (noise free) conditions are assumed. As can be seen, the resolution improves with increasing frequency, which means that the main beam becomes narrower. On the other hand, the MSL indicates that at low frequencies the sidelobes are non-existent, but they arise with increasing frequency. Inspection of these two performance indicators together suggest that the beamformer response is omnidirectional at the lowest frequencies, but with increasing frequency the directivity increases, although this is accompanied by an increase in level of sidelobes, which stagnates at a certain frequency.

The DI of the array previously examined is showed in Fig. 2.17, together with the WNG. In this case, the DI at the lowest frequencies is 0 dB, which means that the beam pattern is omnidirectional. With increasing frequency, the DI increases progressively, indicating, thus, that the array becomes more and more directive. In contrast to the resolution, the DI provides a value related to the array directivity that considers not only the width of the main lobe, but also the sidelobes. This makes it impossible to predict a beam pattern via the DI, as becomes apparent from the inspection of Fig. 2.17. On the other hand, the WNG is constant across frequency, being equal to 10.8 dB, i.e., 12 in a linear scale, corresponding to the number of array microphones, as expected from the fact that delay-and-sum with uniform weighting provides the optimal WNG. It should be noted that while the resolution, the MSL, and the DI can be extracted from experimental results, this is not possible with the WNG, as this is a theoretical measure.

In the microphone array community, the DI and the WNG are typically preferred for the numerical analysis of array designs, see, e.g., Refs. [8, 19, 54, 55]. The resolution and the MSL are less used, but nevertheless they have proven to be a useful evaluation tool, e.g., in Refs. [12, 56–58]. While the resolution can be related to the DI, as both are measures of directivity, the MSL can be used to examine the robustness

[†] An array with these characteristics is used in Paper A. Its Nyquist frequency is about 2.7 kHz.

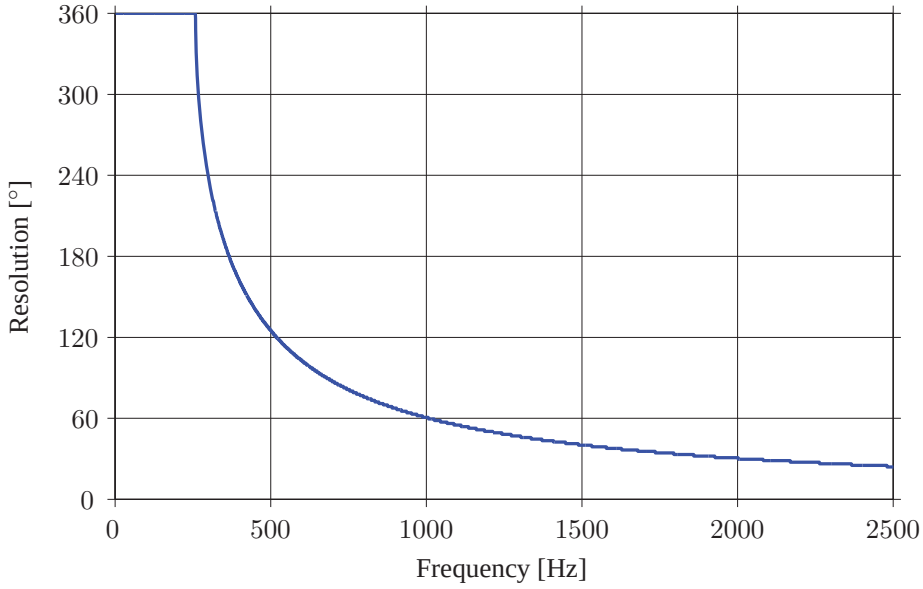

(a) Resolution

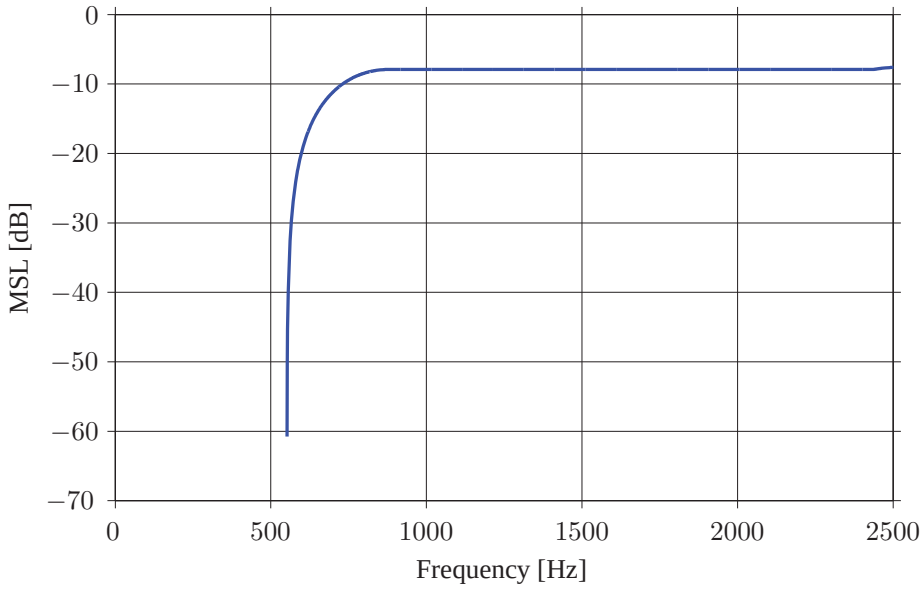

(b) MSL

Figure 2.16: Resolution and MSL obtained with a delay-and-sum beamformer based on a uniform circular array with 12 sensors and 11.9 cm of radius. The array is focused toward 180°.

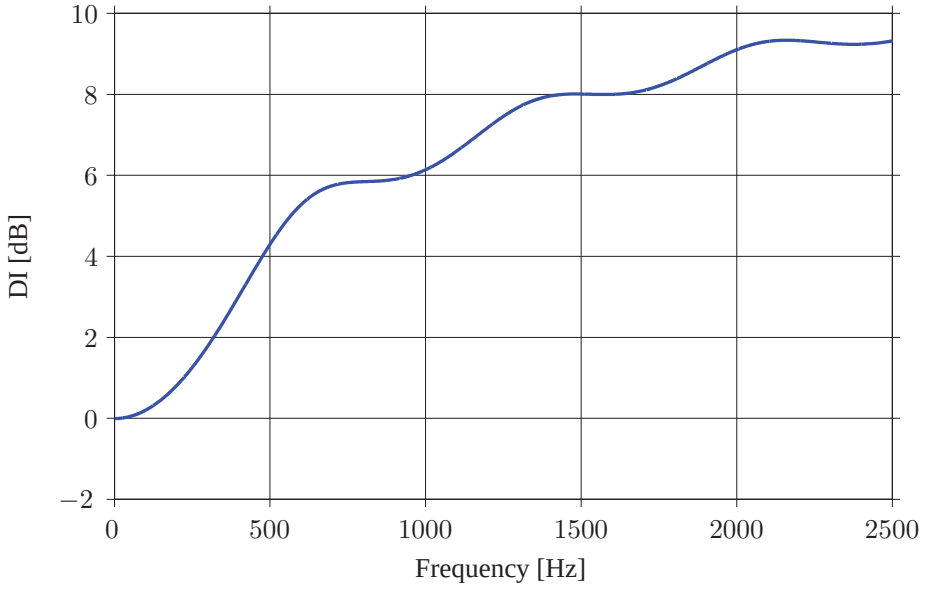

(a) DI

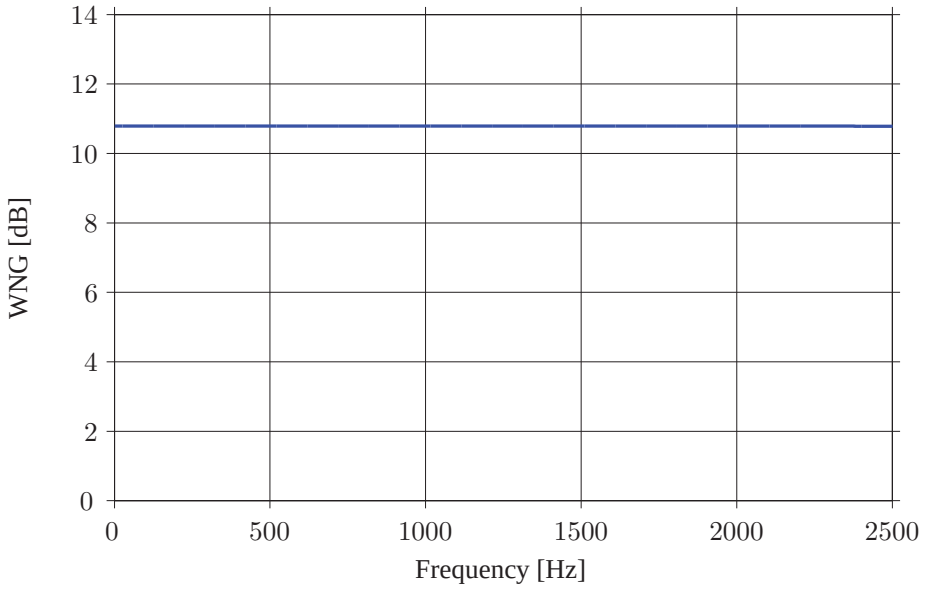

(b) WNG

Figure 2.17: DI and WNG obtained with a delay-and-sum beamformer based on a uniform circular array with 12 sensors and 11.9 cm of radius. The array is focused toward 180°.

of the system, although this is not a direct measure as the WNG is. Since the noise captured by the system affects basically the level of the sidelobes of the beamforming response, this makes the resulting MSL deviate from the MSL that would be obtained in the absence of noise. The higher the deviation, the less robust the system is.

In the contributing papers of this thesis, the performance of the suggested methods is examined basically by means of the resolution and the MSL for the following main reasons:

1. For sound source localization purposes the spatial sensitivity of the array is a very important factor. In this sense, the resolution is a very appropriate parameter. In combination with the MSL, these measures provide a better picture of the behavior of the beam pattern than DI and WNG.

2. Both resolution and MSL can be extracted from experimental data and not only from numerical data as in the case of the WNG[‡], which is crucial for the validation of the methods suggested in the papers.

3. For the reader not familiar with microphone arrays, the resolution and the MSL are simpler to interpret than the DI and the WNG.

[‡]Note that although the DI can also be extracted from experimental measurements, this is rarely seen in the literature.

Chapter 3

Eigenbeamforming

3.1 Introduction

Eigenbeamforming, also known as eigenbeam beamforming, is a rather new category of methods that rely on 'closed' geometries, such as a sphere or a circle. The sound field captured by arrays that fulfill this condition can be decomposed into a sum of orthogonal terms that satisfy the wave equation in the coordinate system that best suits the array geometry. Combination of these orthogonal terms, known as harmonics or phase modes, makes it possible to form a detection beam. An eigenbeamforming system consists of two stages, see Fig. 3.1; in the first stage, the pressure measured with the array is decomposed in a set of harmonics, and in the second stage, usually referred to as *modal beamformer*, the coefficients of the harmonics are weighted and added together to provide the final beamforming output [32]. The fundamental difference from traditional beamforming lays on the fact that the latter is based on applying the signal processing algorithms directly to the signals captured by the microphones. It should be noted that the concept of using phase modes had been already explored in the past in the field of electromagnetism, for antenna design; see, e.g., Refs. [59–68].

Although in principle many array shapes are possible for eigenbeamforming, only those that have a well-defined geometry in the conventional coordinate systems are used in practice. The most popular geometry is the spherical one [69–75], followed by the circular [19, 55, 76–79] and the spheroidal [80].

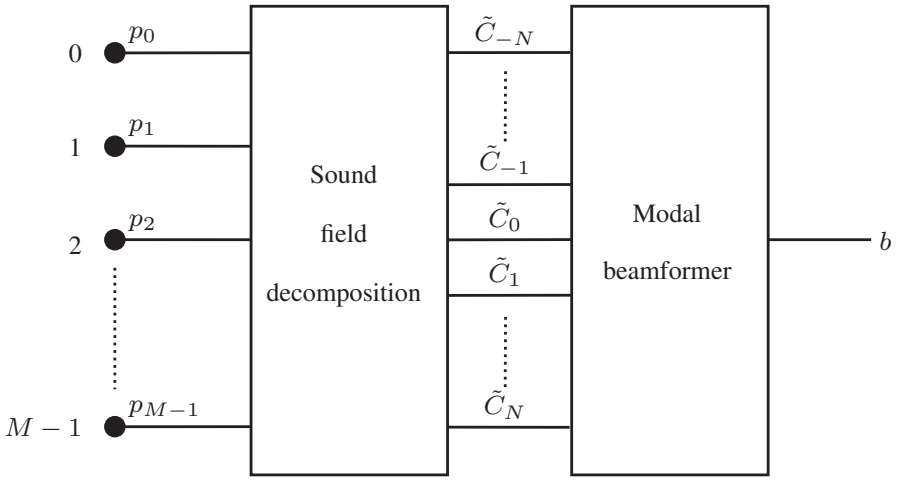

Figure 3.1: Eigenbeamforming procedure. The sound field captured by the array sensors is decomposed in a series of orthogonal functions, whose coefficients are weighted in the modal beamformer stage to yield the final output b.

3.1.1 Eigenbeamforming for circular arrays

The concepts behind eigenbeamforming are here briefly described assuming an open uniform circular array, as the one shown in Fig. 2.10 on page 22. Given the circular symmetry, the sound field can be decomposed in a Fourier series in the azimuth coordinate, φ, so that, at the array radius, the sound pressure can be written in the spatial frequency domain as [10]

$$p(kR, \varphi) = \sum_{n=-\infty}^{\infty} C_n(kR) e^{jn\varphi}, \tag{3.1}$$

where the terms $e^{jn\varphi}$, often referred to as circular harmonics, form a set of orthogonal functions,

$$\frac{1}{2\pi} \int_0^{2\pi} e^{jn\varphi} (e^{j\nu\varphi})^* d\varphi = \delta_{n\nu}, \tag{3.2}$$

where $\delta_{n\nu}$ is the Kronecker delta function, which equals unity when $n = \nu$ and zero otherwise, and $C_n(kR)$ is the nth order Fourier coefficient,

$$C_n(kR) = \frac{1}{2\pi} \int_0^{2\pi} p(kR, \varphi) e^{-jn\varphi} d\varphi. \tag{3.3}$$

If a plane wave with amplitude A, created at φ_s, is present in the sound field, it can be shown that the coefficients become [81]

$$C_n(kR) = AQ_n(kR)e^{-jn\varphi_s}, \tag{3.4}$$

where $Q_n(kR)$ is a function that depends on the boundary conditions of the uniform circular array, that is, for example, whether the array is mounted on a baffle or not, as will be seen later. In the case of a uniform circular array suspended in free-space,

$$Q_n(kR) = (-j)^n J_n(kR), \tag{3.5}$$

where $J_n(kR)$ is a Bessel function of the first kind and order n.

In theory, the sound pressure is represented by infinitely many Fourier coefficients. In practice, it can be shown that the contribution of those orders higher in magnitude than kR is very small [42]. Therefore, the representation of the sound field is often limited, or truncated, to a maximum order N that satisfies

$$N \approx kR. \tag{3.6}$$

It is worth noting that less orders are required for representing the low frequencies compared to the high frequencies.

With an array of transducers, the sound pressure is sampled at discrete positions, rather than in a continuous circle. This implies that the coefficients defined in Eq. (3.3) need to be approximated by

$$\tilde{C}_n(kR) \approx \sum_{m=0}^{M-1} \alpha_m p(kR, \varphi_m) e^{-jn\varphi_m}, \tag{3.7}$$

where the term α_m is an integration factor that ensures the discrete orthogonality property of the circular harmonics

$$\sum_{m=0}^{M-1} \alpha_m e^{jn\varphi_m} \left(e^{j\nu\varphi_m}\right)^* \approx \delta_{n\nu}. \tag{3.8}$$

Given the constant sensor spacing of a uniform circular array, $\alpha_m = 1/M$. An additional consequence of the sampling theorem in space is that the number of array

sensors required to capture the sound field up to order N must be larger than $2N$ ($M > 2N$) [42]. The error due to sampling a continuous circle with a limited number of sensors and the error for considering a finite number of harmonics for representing the sound field are analyzed thoroughly in Refs. [18, 81].

The output of an eigenbeamforming system based on a circular array results from weighting and combining the Fourier coefficients obtained with the decomposition of the sound field, that is,

$$b(kR) = \sum_{n=-N}^{N} w_n(kR)\tilde{C}_n(kR), \tag{3.9}$$

where $w_n(kR)$ is the weighting associated to the nth order Fourier coefficient $C_n(kR)$. Analogous to the influence on the weighting observed in Chapter 2 for delay-and-sum beamforming, the output of the eigenbeamformer strongly depends on the these parameters. When the weightings take the form

$$w_n(kR) = \frac{1}{Q_n(kR)} e^{jn\varphi_l}, \tag{3.10}$$

where φ_l is the looking direction of the array, the beamforming technique is referred to as *circular harmonics beamforming*. This method, described and examined in Papers A and B, provides a response rotationally symmetric around the azimuthal looking direction, i.e., the resulting pattern is shift-invariant. When using these weightings it is particularly important to limit the orders in the beamforming algorithm to a value N close to that given in Eq. (3.6) to avoid amplification of noise. Usually, the maximum number of orders is chosen as $N = \lceil kR \rceil$, where $\lceil \cdot \rceil$ is the ceiling function [81]. If higher orders are considered, the value $Q_n(kR)$ in the denominator tends to zero, boosting, in this way, noise captured in the measurements. Therefore, the truncation of orders can be regarded as a regularization method. The main characteristic of this technique is that the output depends on the number of harmonics taken into account in the algorithm; see Appendix A for further details.

Interestingly, delay-and-sum beamforming can also be characterized in terms of eigenbeamforming, making use of the weightings

$$w_n(kR) = Q_n^*(kR) e^{jn\varphi_l}. \tag{3.11}$$

These weightings also ensure a shift-invariant pattern [16].

Besides circular harmonics beamforming and delay-and-sum beamforming, other methods based on eigenbeam processing with a uniform circular array of microphones can be found in the literature. For instance, Ref. [18] adapts various adaptive methods, such as MUSIC and ESPRIT*, to the circular geometry.

Eigenbeamforming makes it easier to deal with baffled arrays, arrays whose elements are flushed-mounted on the surface of an object or a scatterer. By simply modifying the function $Q_n(kR)$ of Eq. (3.4) according to the baffle type, the scattering effect can be taken into account in the beamforming algorithm. Common baffles suitable for uniform circular arrays are rigid spheres [19, 55] and cylinders [76]. Less popular are rigid baffles with a spheroidal shape [79], which can be oblate or prolate, and baffles with a certain surface impedance [55]. While the scattering effects of spheres, spheroids, and infinitely-long cylinders, have an exact analytical solution, and so does the corresponding Fourier coefficients, that is not the case with the scattering from a finite cylinder.

Arrays with rigid baffles are usually preferred over open arrays for the following two reasons; firstly, the boundary conditions of a baffle are well defined compared to open arrays, which in practice are far from being transparent (their structure, preamplifiers, cables, etc., obviously alter the sound field [82]). Secondly, baffled arrays provide a better response than open arrays; in particular, this is noticeable with delay-and-sum beamforming toward low frequencies, as due to the presence of the baffle, waves need to travel longer distances before reaching the microphones, which results in an effective larger array aperture [78]. Of all common types of rigid baffles for circular arrays, delay-and-sum beamforming performs best with cylinders. The behavior with oblate and prolate spheroidal baffles lies between those of an open array and a sphere, and a sphere and an infinite cylinder, respectively [79]. With circular harmonics beamforming, the performance with scatterers is very similar to that with open arrays. The only difference is that with open arrays the output presents singularities at those frequencies that coincide with the zero-crossings of the Bessel functions in the denominator of the algorithm; see Eqs. (3.5) and (3.10). With this technique, there is no significant difference between different types of baffles.

*ESPRIT stands for ‘estimation of signal parameters via rotational invariance techniques’.

3.1.2 Eigenbeamforming for spherical arrays

Spherical arrays are suitable for decomposing a 3D sound field into a series of orthogonal terms of the form [10]

$$Y_n^m(\theta,\varphi) = \sqrt{\frac{2n+1}{4\pi}\frac{(n-m)!}{(n+m)!}} P_n^m(\cos\theta) e^{jm\varphi}, \tag{3.12}$$

where $P_m^n(\cos\theta)$ is the associated Legendre function of order m and degree n. These terms are commonly referred to as spherical harmonics. In the case of a spherical array of radius R, the pressure at the sphere is given by the Helmholtz equation in spherical coordinates [16],

$$p(kR,\theta,\varphi) = \sum_{n=0}^{\infty}\sum_{m=-n}^{n} C_{mn}(kR) Y_n^m(\theta,\varphi), \tag{3.13}$$

where the terms $C_{mn}(kR)$ follow

$$C_{mn}(kR) = \int_0^{2\pi}\int_0^{\pi} p(kR,\theta,\varphi) Y_n^m(\theta,\varphi)^* \sin\theta d\theta d\varphi. \tag{3.14}$$

Since with an array the pressure is captured at the sensor positions, the coefficients that result from the decomposition of the sound field are in practice approximated by

$$\tilde{C}_{mn}(kR) = \sum_{i=0}^{M-1} \alpha_i p(kR,\theta_i,\varphi_i) Y_n^m(\theta_i,\varphi_i)^*, \tag{3.15}$$

where θ_i and φ_i are angular coordinates of the ith microphone and α_i is an integration factor associated to the ith microphone. This parameter enforces the orthogonality of the spherical harmonics up to order N, such that the resulting coefficients are free of error up to that order [20]. By analogy to the case of eigenbeamforming with a circular sphere, it can be shown that the coefficients $\tilde{C}_{mn}(kR)$ can be weighted before adding them together to form a beam in a particular direction. Eigenbeamforming with spherical arrays is well documented in the literature. The reader interested in this topic is addressed to, e.g., Ref. [16, 54].

A note on the design of spherical arrays for eigenbeamforming

The position of the microphones in a spherical array is not as trivial as in the case of a uniform circular array. There are several strategies to sample a sphere so that the discrete orthogonality property of the spherical harmonics, that is

$$\sum_{i=0}^{M-1} \alpha_i Y_n^m(\theta_i, \varphi_i) Y_\nu^{\mu *}(\theta_i, \varphi_i) = \delta_{n\nu}\delta_{m\mu}, \tag{3.16}$$

is fulfilled. The integration factor of the ith microphone α_i, as well as the relationship between the number of transducers M and the maximum order N that can be captured without error, depends on the sampling scheme. An overview of several sampling schemes is given in details in Ref. [20]. By analogy to the uniform circular array, the most intuitive way to satisfy the orthogonality relationship is by sampling the sphere uniformly so that the transducers are equidistant. In such a case, α_i reduces to a constant. However, a uniform distribution of sensors is only possible with a limited set of arrangements based on regular polyhedra (also called platonic solids) that allow a sphere to fit in; specifically, the tetrahedron (4 faces), the cube (6 faces), the octahedron (8 faces), the dodecahedron (12 faces) and the icosahedron (20 faces). By placing the sensors at the center or at the vertices of each face, the resulting distribution of sensors is uniform. An alternative that presents a distribution close to being uniform is the truncated icosahedron[†], which has 32 faces [69]. Yet another solution is the combination of a non-equidistant sampling with a non-uniform weighting α_i. That is, for instance, the case of the nearly uniform [83], the equiangle [20, 71], and the Gaussian [20, 71, 73, 74, 76] sampling schemes. The equiangle distribution relies on equally spaced samples on θ and φ, whereas the Gaussian sampling scheme is similar, but only half of the samples are considered on θ.

The orthogonality property of the spherical harmonics ensures that the decomposition is independent of the microphone positions, allowing, thus, a shift-invariant beam pattern due to the spherical symmetry.

[†] An example of a truncated icosahedron is a football. It consists of 12 pentagonal faces and 20 hexagonal faces.

3.2 Papers A and B

3.2.1 Synopsis

Paper A suggests an eigenbeamforming technique for a uniform circular array, called circular harmonics beamforming. The technique, conceived for mapping sources distributed from 0 to 360°, is particularly suitable for environmental noise problems. Circular harmonics beamforming is compared numerically to delay-and-sum beamforming for both an open array and an array mounted on an infinitely-long rigid cylinder, by means of the resolution and the MSL. The method is also validated experimentally with an open array.

Paper B extends the investigation carried out in Paper A to the case of a uniform circular array mounted on the equator of a rigid sphere, and validates it numerically and experimentally.

3.2.2 Related work

In 2001, Meyer presented in Ref. [19] a method for beam pattern synthesis based on the decomposition of the sound field into a series of (circular) harmonics that relied on a uniform circular array mounted on a rigid sphere. Although the concept was initially developed for uniform circular arrays, it triggered a series of research projects involving spherical arrays of microphones, pioneered by Meyer and Elko, Ref. [69], and Abhayapala and Ward, Ref. [70], in 2002. Their investigations set the foundations of eigenbeamforming for spherical arrays. In the following years, Rafaely published several articles on the matter, e.g., Refs. [16, 20, 71, 75]. In particular, the principles of eigenbeamforming (in that case referred to as phase-mode processing) were described in Ref. [72], following the approach used in Sec. 3 for the circular geometry, also under the plane wave assumption. In particular, Rafaely analyzed the response of an eigenbeamformer whose weightings provided the so-called *regular beam pattern*, the most directive pattern (for fixed beamforming) [16], and compared it to delay-and-sum expressed in eigenbeamforming terms. The results of that study showed that the directivity achieved with the regular beam pattern exceeds that of delay-and-sum beamforming, specially at low frequencies, at the expense of robustness to noise. That work was later supplemented in Ref. [75] with an overview of various eigenbeamforming methods. Oddly enough, contemporary to Rafaely's research, Pedersen in Ref. [84] and Song

in Ref. [85], following an approach different from Rafaely's, arrived to the expression for eigenbeamforming with a regular beam pattern, considering, though, spherical waves. They called the method *spherical harmonics beamforming*. A year after Song's work was published, Haddad and Hald, in Ref. [86], added a scale factor into spherical harmonics beamforming so that in case of having a rigid sphere, the pressure contribution would be determined correctly, i.e., without the influence of the scattering effect. This version of spherical harmonics beamforming was referred to as *spherical harmonics angularly resolved pressure* (SHARP). This method has been recently extended in Ref. [57] to provide a smoother response, by means of adding regularization filters.

Similarly to Rafaely's article on decomposition of sound fields with spherical arrays, Ref. [71], Teutsch and Kellerman in Ref. [76][‡] presented a theoretical analysis of plane wave decomposition with circular arrays, unbaffled, mounted on a rigid infinitely-long cylindrical baffle, and mounted on a rigid cylinder of finite-length. In addition, they derived eigenbeamforming based on the circular geometry, assuming a continuous aperture instead of the sampled version, i.e., a microphone array. Also, they expressed two adaptive beamforming algorithms ESPRIT and DETECT, in terms of eigenbeamforming and evaluated them with an array mounted on a rigid cylinder, numerically and experimentally.

3.2.3 Discussion

Inspired by the literature on eigenbeamforming with spherical arrays, Paper A adapts the theory behind spherical harmonics beamforming to the 2D case with a circular array, assuming, in this case, plane waves impinging on the array. The proposed beamforming technique, referred to as circular harmonics beamforming, was originally conceived in Paper A for localization of environmental noise sources, but it can obviously be applied to other scenarios where sound sources are distributed over the array azimuth. It should be noted that 1) the approach followed in Paper A to derive circular harmonics beamforming is different from the synthesized derivation given in Sec. 3.1.1; and 2) the article does not include the insight into the technique concerning the influence on the number of orders given in Appendix A.

While delay-and-sum is omnidirectional at low frequencies, circular harmonics beamforming presents a certain directivity, namely a resolution of about 112° in the

[‡]This work is also presented in the PhD Thesis by Teutsch, Ref. [18].

worst case. Indeed, the response of circular harmonics beamforming in terms of directivity is better at the lower frequency range than that of delay-and-sum. At high frequencies, both methods perform similarly. The main drawback of circular harmonics beamforming in comparison with delay-and-sum is its vulnerability to noise, which essentially affects the sidelobe levels. Circular harmonics beamforming implemented with an open uniform circular array presents singularities at a few (single) frequencies, which can be resolved when the array is mounted on a rigid infinitely-long cylinder. In general terms, though, the overall output pattern with the two array configurations is the same. By contrast, the pattern of delay-and-sum with the cylindrical scatterer improves toward low frequencies, as the scatterer makes the array appear larger. Interestingly, with this configuration both the resolution and the MSL at high frequencies is similar for both beamforming techniques. However, at low frequencies, the performance with circular harmonics beamforming still exceeds that of delay-and-sum.

The results of the investigation carried out in Paper A showed that the performance with a rigid infinitely-long cylindrical scatterer was better over that of an open array, especially for delay-and-sum beamforming. Since infinitely-long cylinders are not feasible, they are in practice approximated by finite length cylinders. With regard to that, Teutsch and Kellerman showed in Ref. [76] that a finite cylinder whose length is 1.4 times its radius is enough to approximate an infinitely long cylinder, as its modal response becomes fairly similar. This result was later ratified by Granados in Ref. [87].

As an alternative to cylindrical scatterers of finite-length, Paper B suggests to flush-mount the array on the equator of a rigid sphere, and repeat the comparison carried out in Paper A. The main advantage of this configuration is that the scattering produced by this geometry has an exact analytical solution, in contrast to the finite-length cylinder. With a spherical baffle, circular harmonics beamforming performs in the same manner as in the infinitely-long cylinder case. However, for delay-and-sum the improvement is not as good as with the cylinder, because the effective aperture achieved with the spherical scatterer is smaller.

The novelty of circular harmonics beamforming cannot be entirely attributed to the author of this thesis as Zhang *et al.* in Ref. [88] also derived the same technique under another name and compared it to delay-and-sum for a circular array mounted on a rigid sphere. Their work, thus, resembles the study presented in Paper B, although they assessed the beamforming techniques using DI and WNG, and the analysis was restricted to numerical simulations. In any case, their findings agree in general terms

with those of Paper B. It should be emphasized that Ref. [88] is not cited in Papers A and B as the author of this thesis was not aware of the existence of this work at the time of writing the papers.

The results in Paper B concerning delay-and-sum also agree with those shown by Daigle *et al.*, in Ref. [55], where the performance of delay-and-sum was analyzed for circular arrays mounted on spherical baffles using the DI.

Chapter 4

Deconvolution methods

4.1 Introduction

Beamforming systems cause unavoidable effects, namely the frequency dependence of the array resolution and the appearance of sidelobes, which result in beamformed maps that appear blurred and often difficult to interpret, particularly when several acoustic sources need to be detected simultaneously. Deconvolution methods intend to *deblur* them by removing the artifacts introduced by the array system itself and thereby restoring the original data. These methods rely on the fact that the beamformer output is a linear combination of the spatial distribution of acoustic sources and the so-called *point-spread function*, defined as the beamformer's response to a point source*. Mathematically, the deconvolution problem can be formulated in the frequency domain as follows

$$|b(\mathbf{r})|^2 = \sum_{\mathbf{r}' \in G} s(\mathbf{r}') \cdot H(\mathbf{r}|\mathbf{r}'), \tag{4.1}$$

where $s(\mathbf{r}')$ is the source power distribution at a position $\mathbf{r}'$ that belongs to the grid of points G, and $H(\mathbf{r}|\mathbf{r}')$ is the point-spread function at $\mathbf{r}$ due to a source at $\mathbf{r}'$. It should be emphasized that the source power distribution is non-negative. In matrix notation, the previous expression can be written as

$$\mathbf{b} = \mathbf{H}\mathbf{s}, \tag{4.2}$$

*The point-spread function and the beamformed map are sometimes referred to as the 'dirty beam' and the 'dirty map', respectively.

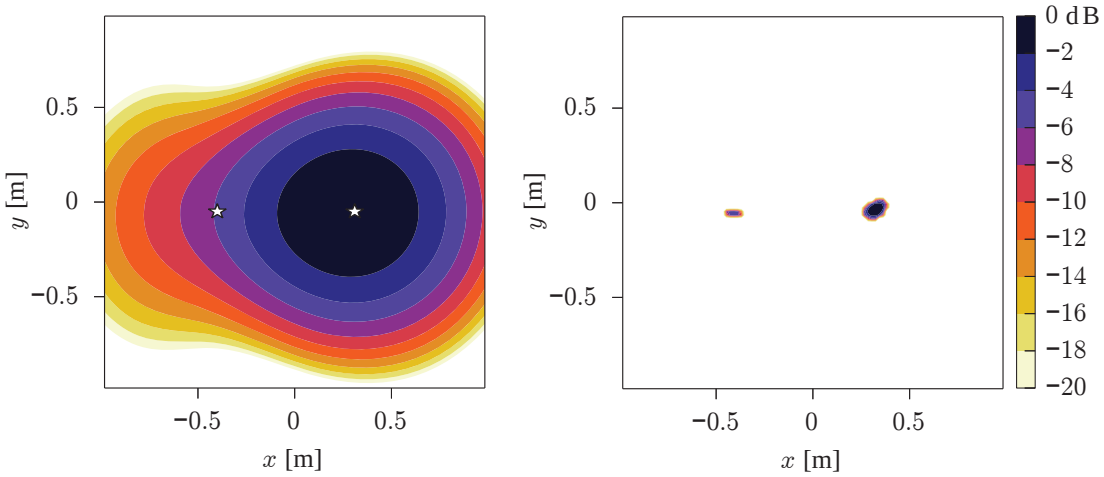

Figure 4.1: Beamformed map (left) and clean map after deconvolution (right). Measurement of two uncorrelated sources located at 2.7 m from the array. The stars in the beamformed map indicate the position of the sources. The level of the right source is 10 dB higher. With beamforming the left source is masked, whereas it becomes visible after deconvolution. Adapted from Ref. [90].

where $\mathbf{b}$ is a vector with the power response of the beamformer, $\mathbf{H}$ is a matrix that in each column contains the point-spread functions of each grid point, and $\mathbf{s}$ is the unknown source power distribution vector. The deconvolution methods try, thus, to compensate for the 'blurring' effect of the point-spread function to recover the original source distribution. Notice that this a discrete inverse problem, and must be treated carefully to avoid an abrupt amplification of noise, which can often lead to a meaningless solution [89]. Deconvolution methods approach this problem by means of iterative algorithms. The resulting plot of the estimated source distribution is a 'clean' version of the beamformed map: the resolution is improved, and the sidelobes are reduced, or even suppressed. This is illustrated in Fig. 4.1.

Deconvolution methods are relevant in many fields that involve image restoration. This problem was first approached for seismology purposes by Robinson [91, 92] back in 1954, inspired by the previous work done by Wiener in that field [93]. Since then, deconvolution has been applied to many other research areas, such as radio astronomy [94], optical microscopy [95] and image processing [96]. It was not until the late nineties, that the aeroacoustic community adapted some of the existing deconvolution methods to deal with sound field visualization problems. That is the case of CLEAN [97] and Richardson-Lucy [98, 99], both originally developed for astronomy and modified for acoustical purposes in Refs. [13] and [100], respectively. While CLEAN acts directly on the beamformed map, i.e., on the image itself, Richardson-

Lucy solves the inverse problem posed in Eq. (4.2) using Bayes' theorem on conditional probabilities. Other algorithms, adapted from classical non-negative least squares (NNLS) procedures [101], seek to solve the following optimization problem

$$\text{minimize} \quad \tfrac{1}{2} \left\| \mathbf{Hs} - \mathbf{b} \right\|_2^2 , \tag{4.3}$$

$$\text{subject to} \quad \mathbf{q} \geq 0. \tag{4.4}$$

That is the case of gradient projection methods, such as the fast Fourier transform-non-negative least squares method (FFT-NNLS) [100], the gradient projection method with Barzilai & Borwein steps [102], and the fast iterative shrinkage-thresholding algorithm (FISTA) [103], examined in Ref. [104] for sound source localization purposes.

Alternatively, there are methods specifically conceived for acoustic purposes. A number of methods are devoted to static incoherent sound fields. The first method developed, called the deconvolution approach for the mapping of acoustic sources (DAMAS) [105, 106], had the main disadvantage that was computationally very heavy. Seeking for efficiency, other algorithms, such as DAMAS2 [107], SC-DAMAS [108], CLEAN-SC [109], the covariance matrix fitting (CMF) [108], and the iterative sidelobe cleaner (ISCA) [110], were implemented based on some assumptions. For example, DAMAS2 relies on a shift-invariant point-spread function, whereas SC-DAMAS, CLEAN-SC and CMF assume source sparsity. Moreover, DAMAS, DAMAS2, CLEAN, and CLEAN-SC have been extended in Ref. [111] to deal with moving sources. There are far less methods capable to deal with coherent sound fields. Examples are DAMAS-C [112], CMF-C [108], the mapping of acoustic sources (MACS) [113], and the wavespace-based coherent deconvolution [114]. In this case, CMF-C and MACS rely on sparsity, whereas the wavespace coherent deconvolution algorithm assumes a shift-invariant point-spread function.

The main drawback of deconvolution procedures is that they are in general computationally challenging. It is therefore necessary to find a compromise between the degree of accuracy, given by the size of the grid and the number of iterations, and the computational run time. Certain techniques, such as DAMAS2, FFT-NNLS, and Richardson-Lucy, rely on a shift-invariant beamformer's point-spread function in order to use spectral procedures (Fourier-based) to reduce the complexity of the calculations, and thus, improve efficiency. Since a shift-invariant point-spread function only depends

on the distance between the source position and the observer position,

$$H(\mathbf{r}|\mathbf{r}') = H(\mathbf{r} - \mathbf{r}'), \tag{4.5}$$

the beamformer output, Eq. (4.1), results in a convolution

$$|b(\mathbf{r})|^2 = s(\mathbf{r}') * H(\mathbf{r} - \mathbf{r}'). \tag{4.6}$$

This relationship makes it possible to tackle the problem in the frequency domain, by means of expressing the convolution as a multiplication, and, thereby, speed up the process,

$$|b(\mathbf{r})|^2 = \mathcal{F}^{-1}\left[\mathcal{F}[s(\mathbf{r}')]\mathcal{F}[H(\mathbf{r})]\right], \tag{4.7}$$

where $\mathcal{F}$ and $\mathcal{F}^{-1}$ are the direct and the inverse FFT.

In general, the assumption of a shift-invariant point-spread function is not valid with 2D imaging using planar-sparse arrays, such as spiral and pseudo-random arrays, unless the source region is small compared to the distance between the array and the source. Therefore, Fourier-based deconvolution approaches are restricted to small regions in space. Otherwise, errors occur. This is examined thoroughly in Ref. [104]. To extend these approaches to a larger, and 3D region, Refs. [107, 115, 116] suggest to make use of a coordinate transformation.

The comparison of deconvolution methods is a cumbersome task because it can be done as function of many different parameters, such as convergence, resolution, computational load, number of iterations, etc. In addition their performance strongly depends on the case under analysis. Readers interested in the comparison of various methods are addressed to Refs. [100, 104, 108, 117, 118].

4.2 Paper C

4.2.1 Synopsis

Paper C adapts three deconvolution methods conceived for planar-sparse arrays, DAMAS2, FFT-NNLS, and Richardson-Lucy, to the circular geometry. The main characteristic of these methods is that they rely on a shift-invariant point-spread function, which has the advantage that the deconvolution can be approached with spectral pro-

cedures to improve computational efficiency. The algorithms are examined via simulations and experimental data with a uniform circular array mounted on a rigid sphere. Their performance is analyzed through the beam patterns obtained with both delay-and-sum beamforming and circular harmonics beamforming as a starting point for the deconvolution process.

4.2.2 Related work

Deconvolution methods have become popular in the recent years as they are capable to provide more accurate maps than beamforming. Initially, they were implemented for planar-sparse arrays, and therefore, most of the existing literature assumes this layout. Although the methods can obviously be applied to eigenbeamforming arrays, they have been rather overlooked. To the author's best knowledge, there is a lack of literature for the circular geometry, and only three references are available for the spherical one, Refs. [119–121]. Pascal and Li in Ref. [119] explore the benefits of using DAMAS and Richardson-Lucy with a uniform spherical array, whereas Schmitt *et al.* in Ref. [120] suggest an NNLS algorithm for a spherical array with a pseudo-random distribution of microphones. On the other hand, Legg and Bradley in Ref. [121] analyze the performance of CLEAN-SC, although they do not specify the array configuration. Surprisingly, none of these works consider eigenbeamforming algorithms, such as spherical harmonics beamforming, as a starting point for the deconvolution process; they simply make use of delay-and-sum. Moreover, only one of the mentioned techniques, Richardson-Lucy, makes use of a shift-invariant array pattern to base the computations on spectral procedures, thereby, lowering the computational running time. Precisely, Richardson-Lucy, together with two other methods that rely on shift-invariant point-spread functions, DAMAS2, and FFT-NNLS, are adapted in Paper C to uniform circular arrays.

4.2.3 Discussion

Paper C introduces for the first time the use of deconvolution methods to circular arrays, and, in addition to it, the use eigenbeamforming as starting point of the deconvolution process.

The results of Paper C indicate that the beamformed maps improve significantly after the deconvolution process in the entire frequency range of interest. In particular,

the resulting maps present a very fine resolution, and the sidelobes are reduced and in some cases even removed.

For a given number of iterations, the maps obtained with the different deconvolution techniques do not present significant differences. In all cases, the main beam becomes narrower with increasing frequency. This actually implies that more iterations are needed at low frequencies in order to achieve the same resolution at all frequencies. In this respect, since circular harmonics beamforming presents a better resolution at low frequencies than delay-and-sum, the deconvolved maps also present a better resolution at these frequencies with this technique. At high frequencies the maps are rather independent on the beamforming technique used prior to deconvolution. However, the sidelobes are more noticeable, though much reduced compared to plain beamforming, with circular harmonics beamforming, as this technique is less robust to noise than delay-and-sum. All in all deconvolution methods are particularly useful when there is more than one source present in the sound field.

Interestingly, if only one source is present in the sound field, the aliasing effect above Nyquist frequencies is removed from the map. This can be explained by the fact that the point-spread function used for the deconvolution is contaminated with aliasing, in such a way that during the deconvolution process the point-spread function matches the beamforming response, which is affected in the same way by aliasing.

Paper C also shows that, apart from providing a better localization of the sound sources present in the sound field, deconvolution methods also give a good estimate of the level of the sources via an integration process. The levels retrieved with the three deconvolution methods under analysis are very similar. However, the levels obtained from the delay-and-sum beamformed map present a better agreement with the average level captured directly with the microphones than the levels estimated with the circular harmonics beamformed map.

During the research on deconvolution methods for the circular geometry, it was observed that the performance of the different methods (DAMAS2, FFT-NNLS, and Richardson-Lucy) depends on the case under analysis. In the examples given in Paper C, Richardson-Lucy converged faster than the other two methods, but this was not systematic; it varied depending on several parameters such as the amplitude of the impinging wave, the frequency, and the angle. It was not the goal of Paper C to judge which method was best, but this could certainly be done in a future study where all the parameters that play a role on the methods where analyzed thoroughly.

The shortcoming of deconvolution methods is that they are time consuming, especially when the frequency range of analysis is broad, as they can only deal with one frequency at a time. With the current computers, these methods are generally restricted to those situations where measurements can be postprocessed at a later stage.

In any case, the results of Paper C indicate a great potential of these methods with other eigenbeamforming systems, e.g., based on spherical arrays.

Chapter 5
Beamforming with holographic virtual arrays

5.1 Introduction

As seen in Chapter 2, for a given number of sensors, an array with larger dimensions benefits the response at low frequencies compared to a smaller array, at the expense of limiting the upper frequency range of operation of the array system. However, the dimensions of the array are usually given by manufacturers, and users cannot do much about that. Motivated by that, beamforming with virtual arrays emerges as an alternative for eigenbeamforming arrays with the aim to improve their performance at low frequencies. The principle behind it is the following: the pressure captured with an array of microphones is used to predict the pressure at a larger and virtual concentric array of the same type, by means of acoustic holography. The predicted pressure is then used to conduct beamforming. It should be noticed that this method assumes sources in the far field of the array, which contrasts with most acoustic holography problems where sources are placed in the near field.

The details of beamforming combined with acoustic holography are given in Papers D and E, for an open circular array and a spherical array mounted on a rigid baffle, respectively. Additionally, Appendix B gives the expressions for acoustic holography for circular arrays both open and mounted on a rigid cylinder of infite length.

In addition to the derivation given in the contributing papers, this method is expressed in eigenbeamforming terms in the following for the case of uniform circular arrays. It is assumed that plane waves traveling perpendicularly to the z-axis impinge

on a (physical) uniform circular array that rests on the xy-plane. The eigenbeamformer output using a holographic virtual circular array with radius R_v is

$$b(kR_v) = \sum_{n=-N_v}^{N_v} w_n(kR_v)\tilde{C}_n(kR_v), \tag{5.1}$$

where this expression follows from Eq. (3.9), but with the limits of the summation set to $-N_v$ and N_v, where $N_v \approx kR_v$. Making use of the acoustic holography expressions given in Appendix B, it can be shown that the weightings for a virtual array when performing delay-and-sum result in

$$w_n(kR_v) = \frac{|Q_n(kR_v)|^2}{Q_n(kR)} e^{jn\varphi_l}. \tag{5.2}$$

As can be seen, these weightings differ from those corresponding to the normal expression of delay-and-sum beamforming (for a physical array); see Eq. (3.11). It should be noted that this derivation is valid for open arrays and for arrays mounted on a rigid cylinder, but not for the case of spherical baffles, as the reconstruction with acoustic holography cannot be expressed in these terms; see the discussion given in Sec. B.3 on page 70.

When circular harmonics beamforming is performed with the virtual array, the weightings become

$$w_n(kR_v) = \frac{1}{Q_n(kR)} e^{jn\varphi_l}. \tag{5.3}$$

Inspection of this expression, independent of R_v, reveals that it totally coincides with the weightings of circular harmonics beamforming performed directly with a physical array; see Eq. (3.10). The only difference in the beamforming algorithm lies in the limits of the summations in Eqs. (5.1) and (3.9), $\pm N_v$ and $\pm N$, respectively. As mentioned in Sec. 3, circular harmonics beamforming requires the truncation of orders higher than about kR to avoid regularization error. Accounting for orders up to about $N_v \approx kR_v$, which is unavoidably higher than kR, will obviously cause a larger error. This shows that computing circular harmonics beamforming with holographic virtual arrays does not present any advantage compared to doing it directly from physical arrays. This also occurs in the case of a spherical array, i.e., the principle works for delay-and-sum, but not for spherical harmonic beamforming.

5.2 Papers D and E

5.2.1 Synopsis

Paper D introduces for the first time the concept of beamforming with holographic virtual arrays. An open uniform circular array is chosen for this purpose. The performance of this method is analyzed by means of simulations and experimental results, making use of the resolution and the MSL.

Paper E adapts the principles given in Paper D to a rigid spherical array, and goes one step beyond with the investigation of the performance as a function of the radius of the virtual array.

5.2.2 Related work

The combination of acoustic holography and beamforming has been examined recently by Fu *et al.* in Ref. [122] for visualization of sound sources with high temperatures. Their method consists of, at a first stage, conducting near-field beamforming with a planar array placed at a (known) distance from the source that prevents the system from being damaged due to the high temperatures. At a second stage, the beamformed map serves as input to acoustic holography, to reconstruct the sound field closer to the source. Both the procedure and the final goal of this work differ fundamentally from beamforming based on holographic virtual arrays for sound source localization.

During the preparation of the work presented in Paper D, it was found out that there was a lack on literature about acoustic holography for circular arrays. This method, introduced in Refs. [9, 123, 124] in the beginning of the 1980's, was conceived for array measurements in the near-field of a source to predict the sound field closer to it, with the aim to visualize the source radiation characteristics. In the first years, planar NAH, based on measurements with planar arrays, was the main focus. However, already in the paper by Maynard *et al.* from 1985, Ref. [9], the method was expressed in spherical and cylindrical coordinates, in addition to the Cartesian. The possibilities that spherical arrays offered for spherical NAH became soon of interest; see, e.g., Refs. [17, 82, 125, 126]. A peculiarity of spherical NAH that contrasts with planar NAH is that, due to the closed surface of spherical arrays, the sound field can be reconstructed in the entire 3D space without restrictions, as long as the reconstruction field is free of sources [127].

The principles of spherical NAH can easily be adapted to the circular geometry.

Since this geometry has one less dimension than the spherical one, circular arrays can predict an entire 2D sound field from measurements in a closed curve (a ring). Although acoustic holography with circular arrays can be regarded as a particular case of cylindrical acoustic holography, the circular geometry has not been much examined. In particular, Cho *et al.* in Ref. [128] and Lee and Bolton in Ref. [129] made use of an open circular array for statistical optimized near-field acoustic holography (SONAH) and for patch near-field acoustic holography, respectively. The goal of both studies was to measure sources placed in the interior of the array. However, beamforming with virtual arrays, as described in Paper D, assumes sources outside the array. Moreover, with this technique both the measurement and the reconstruction with acoustic holography are carried out in the far field of the sources.

5.2.3 Discussion

The combination of acoustic holography and beamforming, by means of using virtual arrays for the beamforming procedure, has been examined in this PhD project for the first time. It should be noticed that due to a lack of literature in acoustic holography for interior problems with circular arrays, the expressions for this reconstruction technique had to be derived explicitly for Paper D.

The results of Papers D and E have shown that when the method is implemented with delay-and-sum, the performance at low frequencies exceeds that obtained with conventional delay-and-sum beamforming, to the detriment of the high frequencies, as the spacing between the 'sensors' of the virtual array is larger. It is thus recommended to perform beamforming directly from the physical array at high frequencies, while taking advantage of holographic virtual arrays at low frequencies. The success of the method depends on the dimensions of the virtual array, as the reconstruction process outside the physical array is an ill-posed problem that leads to an error in the estimated sound field that increases with increasing the distance from the array to the reconstruction point [126]. This implies that with increasing radius of the virtual array, noise is amplified progressively. As a consequence, the value of the radius of the virtual array is crucial for the success of the proposed beamforming technique. This is analyzed in Paper E for a virtual spherical array.

In contrast to the positive effect of the suggested technique on delay-and-sum, this new method does not exhibit any improvement when circular harmonics and spherical

harmonic beamforming are used for its implementation, as seen in Sec. 5.1 for circular arrays. This indicates that the method is not general, and therefore, it should be tested with other beamforming algorithms. On the other hand, delay-and-sum beamforming with holographic virtual arrays should be compared to circular/spherical harmonics beamforming in a future follow up study. Some preliminary results not shown in this dissemination suggest that this technique can be more robust and present a better resolution and MSL than circular/spherical harmonics beamforming at certain frequencies. In a future investigation it could be helpful to address this question using other well-known performance indicators, such as the DI and the WNG, besides the resolution and the MSL.

As shown in Sec. 5.1, beamforming with holographic virtual arrays can be expressed in eigenbeamforming terms. However, in the case of circular arrays, this is only possible when they are either open or mounted on an infinitely-long cylinder, due to some limitations imposed by the implementation of acoustic holography for this geometry; see Appendix B.

Despite the intrinsic limitations of acoustic holography, and the fact that this technique does not benefit circular harmonics beamforming, the implementation of beamforming using holographic virtual arrays is a new concept that at the moment has showed positive results for delay-and-sum. The findings during the PhD project aim at setting the ground for future research.

Chapter 6

Conclusions

6.1 Summary and conclusions

This dissertation has examined the use of uniform circular arrays for sound source localization purposes using beamforming. Uniform circular arrays are suitable for 2D sound fields in which waves propagate along the array plane, as they provide a 360° azimuthal coverage. That is often the need in many environmental noise problems where sound sources are placed in the far field. A fundamental characteristic of beamforming based on uniform circular arrays is that the output pattern is rotationally symmetric in the azimuthal direction, and thus, the system can be equally fair in all looking directions from 0 to 360°.

Traditionally, sound source localization problems have been approached mainly with planar-sparse arrays, and to some extent, with spherical arrays. Surprisingly, the use of circular arrays for this purpose has not been explored much in the literature. The work carried out during the present PhD project contributes to fill this gap. Taking delay-and-sum beamforming as a reference, the present study has suggested several options to improve the performance of uniform circular arrays and extend their operative frequency range in order to cope with broadband sources. In all cases, it has been assumed that the acoustic sources where incoherent, static, and located in the far field. The goal of Papers A to D is to improve the performance of uniform circular arrays in two different ways: by means of designing new processing techniques (Papers A, C, and D), and by means of changing the physical characteristics of the array (Paper B).

The progress and findings of the PhD project can be seen as a journey toward the improvement of uniform circular arrays. Curiously, the existing literature on spherical

arrays inspired the initial work on uniform circular arrays reflected in Papers A and B, while the outcome of Papers C and D showed to have potential with spherical arrays. In fact, Paper E closes this circle, by adapting the results of Paper D to the spherical geometry.

The first contribution of this thesis, presented in Paper A and complemented by Sec. 3 and Appendix A, is the derivation and examination of an eigenbeamforming method, circular harmonics beamforming, that results from adapting spherical harmonics beamforming, a method for spherical arrays, to the circular geometry. The outcome of this study shows that a slightly better performance can be achieved when the array is mounted on a rigid cylinder of infinite length compared to the case where the microphones are simply suspended in the free space. Inspired by the properties of a theoretical rigid cylindrical scatterer of infinite length, and motivated by the difficulty of its practical implementation, Paper B suggests the use of a rigid spherical baffle, as its scattering behavior is, unlike the case of a rigid finite cylinder, well described analytically.

On the other hand, Paper C suggests the use of deconvolution methods to improve the visualization of the beamformed maps and recover the levels of the impinging waves with accuracy. From a given map, these methods make use of iterative procedures to estimate the sound sources present in the sound field. Since uniform circular arrays are shift-invariant, they can benefit from those deconvolution methods that rely on a shift-invariant point-spread function, thereby handling the inverse problem in the (spatial) Fourier domain to achieve a lower computational load. Paper C adapts, for the first time, three methods originally conceived for planar-sparse arrays, namely, DAMAS2, FFT-NNLS, and Richardson-Lucy, to the circular geometry, and shows the potential of using eigenbeamforming, such as circular harmonics beamforming, as input to the deconvolution process.

Finally, Papers D and E contribute to the current literature by suggesting a new method adequate for circular (Paper D) and spherical arrays (Paper E), based on the combination of beamforming with acoustic holography. Its principle relies on applying beamforming to a holographic virtual array with larger dimensions than the physical array to improve the performance at low frequencies.

The main contributions of this thesis to the existing literature are highlighted in the following:

- Development, examination, and validation of circular harmonics beamforming, an eigenbeamforming technique for uniform circular arrays.
- Extension of circular harmonics beamforming to uniform circular arrays mounted on a rigid spherical scatterer.
- Adaptation of three deconvolution methods, namely DAMAS2, FFT-NNLS, and Richardson-Lucy, to uniform circular arrays, and examination and validation using both delay-and-sum and circular harmonics beamforming prior to the deconvolution process.
- Development, examination, and validation of delay-and-sum beamforming with holographic virtual arrays for the improvement of the performance at low frequencies, for both circular and spherical arrays.
- Derivation of the equations governing acoustic holography for circular arrays for interior domain problems.

6.2 Future work

The findings of the PhD project have given rise to some questions and challenges that should be addressed in the near future.

Deconvolution methods

A natural continuation of the work done in the project on deconvolution methods is the extension of Fourier-based algorithms to the 3D case, using spherical arrays (with shift-invariant point-spread functions). The main challenge is to implement the deconvolution problem as a function of both the azimuth and the polar angle.

Beamforming with holographic virtual arrays

The study on beamforming using holographic virtual arrays has revealed that delay-and-sum beamforming benefits from using this method, but that is not the case of

circular harmonics and spherical harmonics beamforming. Therefore, the method should be implemented with other beamforming techniques and examined to prove its generalization.

Some preliminary studies not shown in this dissertation suggest that delay-and-sum implemented with holographic virtual arrays is more robust to noise than circular harmonics and spherical harmonics beamforming. Furthermore, it seems that at some frequencies, both the resolution and the MSL are better. It is therefore necessary to compare the methods thoroughly, making use of the usual performance indicators.

New technology

The findings of the thesis have been focused toward the enhancement of beamforming at low frequencies. However, if the aim was to improve the performance at high frequencies, this could be achieved by adding more transducers, as this would lower the spacing between transducers, and hence, increase the Nyquist frequency. However, with conventional microphones, this solution is usually not viable, as systems become way too expensive. One alternative would be to use microelectromechanical (MEMS) microphones, as they are small, and, more importantly, cheap. Despite the fact that, at the moment, MEMS microphones are far from being as stable as conventional microphones, this technology is still developing and has very good prospects. Advances in MEMS technology will, for sure, lead to very attractive array systems.

A completely different approach could make use of acoustic fibers*, as these allow to measure the sound field in all the points of the fiber. This technology is based on sending an optical pulse into the fiber, and awaiting the reflections scattered back from the fiber glass walls. By measuring the time lag between the signal sent and the reflections received, the acoustic signal is extracted. Although at the moment acoustic fibers are only used for measuring sound pressures, they also seem adequate for beamforming purposes. Since fibers allow to scan a sound field in a continuous manner, beamformers that made use of this technology would be able to provide maps free of aliasing. In this sense, a single fiber shaped in the form of a ring would be enough to build a continuous circular beamformer.

*Such as the iDAS^{TM} ('intelligent distributed acoustic sensor'), manufactured by the British company Silixa.

Appendix A
Insight into circular harmonics beamforming

According to Paper A, the starting point to develop circular harmonics beamforming is that, in the presence of a single source in the far field, the ideal beamforming output should be a delta function located at the angular position of the source φ_s

$$b_{\text{ideal}}(\varphi, \varphi_s) = B\delta(\varphi - \varphi_s), \tag{A.1}$$

where B is a scale factor. Due to the circular geometry, the beamforemer output is expansible in a set of circular harmonics,

$$b_{\text{ideal}}(\varphi, \varphi_s) = \sum_{n=-\infty}^{\infty} I_n e^{jn\varphi}, \tag{A.2}$$

where I_n is the nth Fourier coefficient obtained with an ideal beamformer due to a source located at φ_s. The Fourier coefficients are given by the inverse Fourier series

$$I_n = \frac{1}{2\pi} \int_0^{2\pi} b_{\text{ideal}}(\varphi, \varphi_s) e^{-jn\varphi} \mathrm{d}\varphi = B e^{-jn\varphi_s}. \tag{A.3}$$

Insertion of Eq. (A.3) into Eq. (A.2) yields

$$b_{\text{ideal}}(\varphi, \varphi_s) = B \sum_{n=-\infty}^{\infty} e^{jn(\varphi - \varphi_s)}. \tag{A.4}$$

In order to implement this expression, the number of modes of the Fourier series needs to be truncated at N,

$$b(\varphi, \varphi_s) = B \sum_{n=-N}^{N} e^{jn(\varphi-\varphi_s)}. \tag{A.5}$$

By making use of trigonometric identities, this equation can be rewritten as

$$b(\varphi, \varphi_s) = B \frac{\sin\left((N+1/2)(\varphi-\varphi_s)\right)}{\sin\left((\varphi-\varphi_s)/2\right)}. \tag{A.6}$$

Inspection of this expression reveals that when $N \to \infty$ the output becomes a delta function, as [130]

$$\lim_{N\to\infty} \frac{1}{2\pi} \frac{\sin((N+1/2)x)}{\sin(x/2)} = \delta(x), \tag{A.7}$$

which, in effect, agrees with the starting point of this derivation.

Alternatively, the expression given in Eq. (A.6) can be expressed using the Chebyshev polynomial of second kind,

$$U_n(\cos\theta) = \frac{\sin\left((n+1)\theta\right)}{\sin\theta}. \tag{A.8}$$

Therefore, with $n = 2N$ and $\theta = (\varphi - \varphi_s)/2$,

$$b(\varphi, \varphi_s) = B U_{2N}(\cos((\varphi-\varphi_s)/2)). \tag{A.9}$$

One of the main characteristics of circular harmonics beamforming is that the output depends on the number of harmonics taken into account in the calculation. In addition, for a given number of harmonics, the output is rather independent of whether the circular array is mounted or not into a rigid baffle. Note that the number of harmonics used in the algorithm depends on the frequency and the radius of the array, R, as well as the number of microphones, M, as $N = \lceil kR \rceil$ up to a maximum order equal to $M/2 - 1$ [77, 78]. Figure A.1 shows the normalized beamforming output for different values of N. In this case, a source is simulated at $180°$. As can be seen, the main lobe becomes narrower with increasing N, which agrees with the fact that, when N tends to infinity, the output approaches a delta function centered at the angular position of the source. On the other hand, the resolution and the MSL decrease with increasing the number of orders, as shown in Figs. A.2 and A.3 as a function of the number of orders.

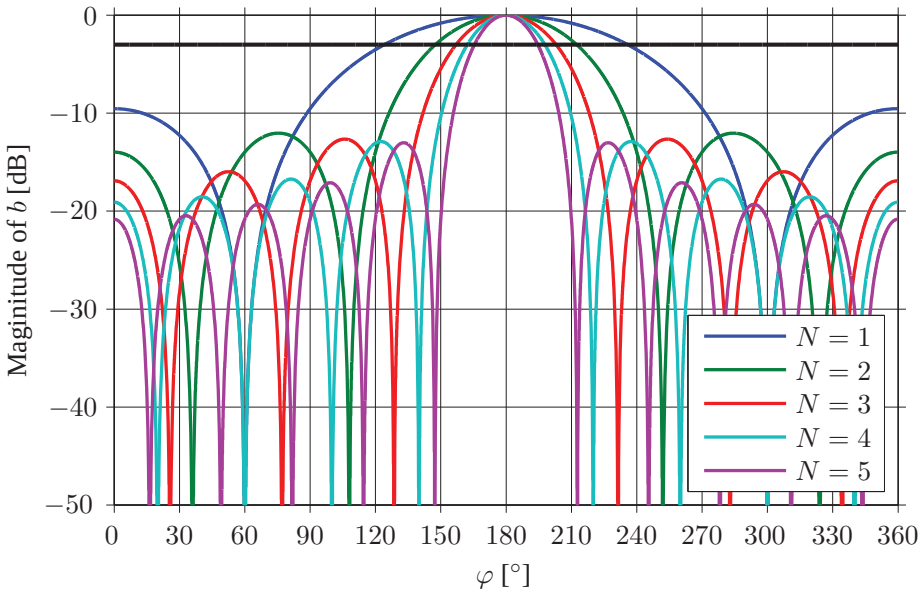

Figure A.1: Normalized output of a circular harmonics beamformer, for different values of N. A straight black line indicates -3 dB.

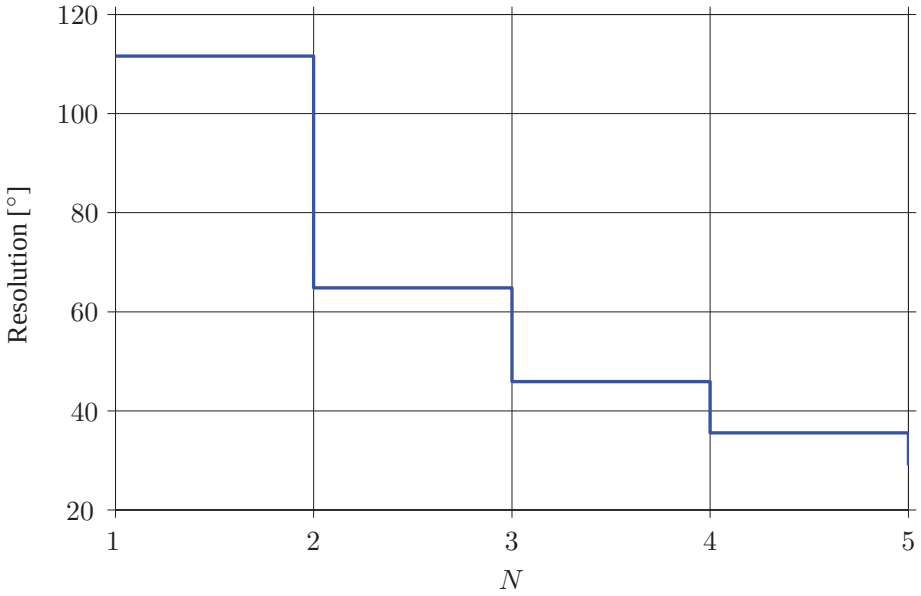

Figure A.2: Resolution as a function of the number of orders taken into account in the calculation of circular harmonics beamforming.

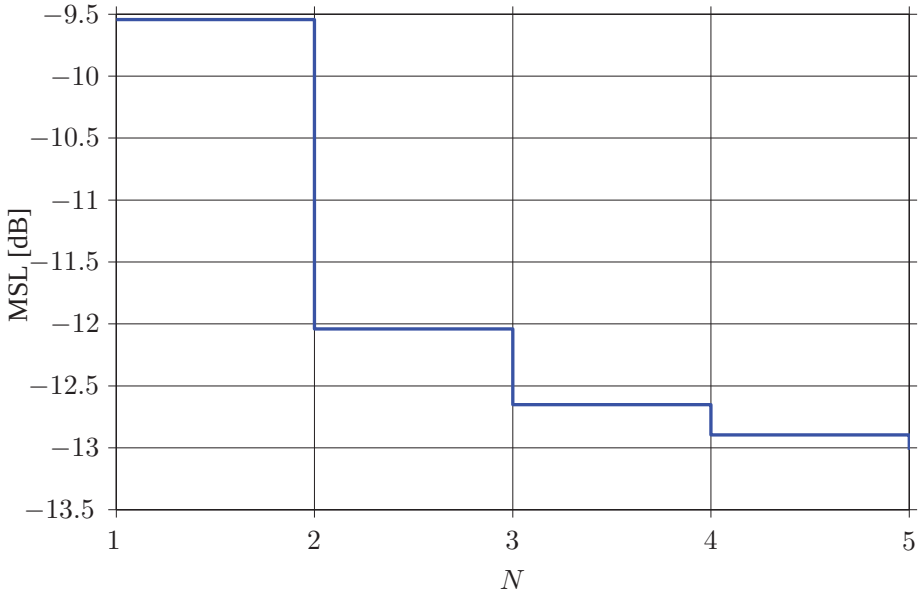

Figure A.3: MSL as a function of the number of orders taken into account in the calculation of circular harmonics beamforming.

Appendix B
Acoustic holography with uniform circular arrays

B.1 Open array

Let us consider a uniform circular array of microphones placed at the $xy-$plane ($z = 0$) that captures a plane wave that travels perpendicularly to the $z-$axis, i.e., the wavefronts are parallel to to the $z-$axis. In what follows the time dependency $e^{-j\omega t}$ is omitted.

After solving the Helmholtz equation in cylindrical coordinates and applying the boundary conditions (basically that the sound field at the origin must be finite), the sound pressure results in

$$p(kr, \varphi) = \sum_{n=-\infty}^{\infty} A_n J_n(kr) e^{jn\varphi}, \tag{B.1}$$

where A_n is an expansion coefficient of order n. This expression can be used to determine the sound pressure at an arbitrary point of the sound field by means of acoustic holography. For this purpose the values of the coefficients A_n are needed. Since the pressure at the uniform circular array (at $r = R$) is known,

$$p(kR, \varphi) = \sum_{n=-\infty}^{\infty} A_n J_n(kR) e^{jn\varphi}. \tag{B.2}$$

The coefficients can be computed making use of the continuous orthogonality property of the circular harmonics given in Eq. (3.2) on page 34. After some rearranging, they

result in

$$A_n = \frac{\int_0^{2\pi} p(kR,\varphi)e^{-jn\varphi}d\varphi}{2\pi J_n(kR)}. \tag{B.3}$$

This expression implies a continuous integral of the sound pressure. However, the pressure is known at a number of discrete positions, as the sound field is sampled with M microphones. Using the discrete orthogonality relationship of the circular harmonics given in Eq. (3.8) on page 35 the coefficients A_n result in

$$A_n = \frac{\frac{1}{M}\sum_{i=0}^{M-1} p(kR,\varphi_i)e^{-jn\varphi_i}}{J_n(kR)}. \tag{B.4}$$

B.2 Rigid cylindrical scatterer of infinite length

Let us now consider that the circular array is mounted on a rigid cylinder of infinite length. The total pressure will present the contributions of the incident pressure and the scattered pressure: $p_t = p_i + p_s$ [131]. The incident sound pressure corresponds to that that would occur if the cylinder was not present, i.e., the pressure given in Eq. (B.1). Its associated radial velocity follows

$$v_{kr,i}(r,\varphi) \propto \frac{dp_i(kr,\varphi)}{dr} = \sum_{n=-\infty}^{\infty} A_n \frac{dJ_n(kr)}{dr} e^{jn\varphi}. \tag{B.5}$$

On the other hand, the scattered pressure follows from solving the Helmholtz equation in cylindrical coordinates considering an exterior boundary problem (applying the Sommerfeld radiation condition),

$$p_s(kr,\varphi) = \sum_{n=-\infty}^{\infty} B_n H_n^{(1)}(kr) e^{jn\varphi}, \tag{B.6}$$

where B_n is an expansion coefficient and $H_n^{(1)}(kr)$ is a Hankel function of the first kind and order n. The associated radial velocity follows

$$v_{kr,s}(r,\varphi) \propto \frac{dp_s(kr,\varphi)}{dr} = \sum_{n=-\infty}^{\infty} B_n \frac{dH_n^{(1)}(kr)}{dr} e^{jn\varphi}. \tag{B.7}$$

Imposing the boundary condition at the surface of the cylinder, that is, the total radial velocity is zero at $r = R$ provides the relationship between A_n and B_n,

$$\sum_{n=-\infty}^{\infty} \left[A_n \frac{dJ_n(kr)}{dr}\bigg|_{r=R} + B_n \frac{dH_n^{(1)}(kr)}{dr}\bigg|_{r=R} \right] e^{jn\varphi} = 0. \tag{B.8}$$

From this expression it follows that

$$B_n = -A_n \frac{J_n'(kR)}{H_n'^{(1)}(kR)}, \tag{B.9}$$

where $J_n'(kR)$ and $H_n'^{(1)}(kR)$ are the derivatives of the Bessel function and the Bessel function evaluated at $r = R$, respectively. Insertion of this relationship into the expression of the scattered pressure, Eq. (B.6), yields

$$p_s(kr, \varphi) = -\sum_{n=-\infty}^{\infty} A_n \frac{J_n'(kR)}{H_n'^{(1)}(kR)} H_n^{(1)}(kr) e^{jn\varphi}. \tag{B.10}$$

Finally the total pressure is

$$p(kr, \varphi) = \sum_{n=-\infty}^{\infty} A_n \left[J_n(kr) - \frac{J_n'(kR)}{H_n'^{(1)}(kR)} H_n^{(1)}(kr) \right] e^{jn\varphi}. \tag{B.11}$$

Following the same procedure carried out in the previous section to determine the coefficients A_n we obtain the following relationship:

$$A_n = \frac{\frac{1}{M}\sum_{i=0}^{M-1} p(kR, \varphi_i) e^{-jn\varphi_i}}{J_n(kR) - \frac{J_n'(kR)}{H_n'^{(1)}(kR)} H_n^{(1)}(kR)}. \tag{B.12}$$

Inserting this expression into the total pressure provides the sound pressure at any other position. It should be emphasized that this solution is only valid if the plane waves propagate perpendicularly to the cylinder so that the pressure along the z-axis is constant and the wavefronts match perfectly the symmetry of the scatterer.

B.3 Rigid spherical scatterer

In this section we consider a uniform circular array mounted on a rigid sphere. It can be shown that the pressure due to the incident waves and the scattered ones can be written in spherical coordinates as follows [82]

$$p(kr,\theta,\varphi)=\sum_{n=0}^{\infty}\sum_{m=-n}^{n}A_{mn}\left(j_n(kr)-\frac{j_n'(kR)}{h_n'^{(1)}(kR)}h_n^{(1)}(kr)\right)Y_n^m(\theta,\varphi), \quad \text{(B.13)}$$

where A_{mn} is an expansion coefficient of order mnth, $j_n(kr)$ and $h_n^{(1)}(kr)$ are the spherical Bessel and the spherical Hankel function of the first kind and order n, and $j_n'(kR)$ and $h_n'^{(1)}(kR)$ their derivatives with respect to r, evaluated at $r=R$.

The total sound pressure on the surface of the sphere, i.e., at $r=R$, is

$$p(kR,\theta,\varphi)=\sum_{n=0}^{\infty}\sum_{m=-n}^{n}A_{mn}\left(j_n(kR)-\frac{j_n'(kR)}{h_n'^{(1)}(kR)}h_n^{(1)}(kR)\right)Y_n^m(\theta,\varphi). \quad \text{(B.14)}$$

The coefficients A_{mn} can be found making use of the continuous orthogonality property of the spherical harmonics,

$$\int_0^{2\pi}\int_0^{\pi}Y_n^m(\theta,\varphi)Y_\nu^{\mu*}(\theta,\varphi)\sin\theta d\theta d\varphi=\delta_{n\nu}\delta_{m\mu}. \quad \text{(B.15)}$$

Following a similar procedure as in the case of the array mounted on an infinitely-long baffle, they result in

$$A_{mn}=\frac{\int_0^{2\pi}\int_0^{\pi}p(kR,\theta,\varphi)Y_n^{m*}(\theta,\varphi)\sin\theta d\theta d\varphi}{j_n(kR)-\frac{j_n'(kR)}{h_n'^{(1)}(kR)}h_n^{(1)}(kR)}. \quad \text{(B.16)}$$

Inspection of this equation reveals that the pressure in the entire sphere is needed for the computation of the coefficients. This implies that the microphones are required to be distributed over the entire sphere, and not only on the equator, as in the case of the circular array. By analogy to the case of the cylindrical scatterer derived in the previous section, where the pressure along the z-axis was constant as plane waves propagating perpendicularly to the cylinder were assumed, the approach for the circular array on the sphere given in Eq. (B.16) has a solution only when the pressure is constant on θ.

However, this corresponds to a very particular sound field, far from being planar. To overcome this limitation, the reconstruction with a circular array mounted on a sphere can be achieved by solving a system of equations based on an elementary wave expansion [132], similarly to the approach given in Ref. [133] for spherical arrays. This topic, though, is out of the scope of this dissertation.

Bibliography

[1] J. Billingsley and R. Kinns, "The acoustic telescope," *J. Sound Vib.*, vol. 48, no. 4, pp. 485–510, 1976.

[2] U. Michel, "History of acoustic beamforming," in *Proc. of BeBeC 2006, Berlin, Germany*, 2006.

[3] C. Zhang, D. Florncio, D. E. Ba, and Z. Zhang, "Maximum likelihood sound source localization and beamforming for directional microphone arrays in distributed meetings," *IEEE Trans. Multimedia*, vol. 10, no. 3, pp. 538–548, 2008.

[4] D. H. Johnson and D. E. Dudgeon, *Array signal processing: Concepts and techniques*. Prentice Hall, 1993.

[5] R. P. Dougherty, "Functional beamforming," in *Proc. of BeBeC 2014, Berlin, Germany*, 2014.

[6] L. J. Griffiths and C. W. Jim, "An alternative approach to linear constrained adaptive beamforming," *IEEE Trans. Antennas Propag.*, vol. 30, no. 1, pp. 27–34, 1982.

[7] R. O. Schmidt, "Multiple emitter location and signal parameter estimation," *IEEE Trans. Antennas Propag.*, vol. 34, no. 3, pp. 276–280, 1986.

[8] M. Brandstein and D. Ward, eds., *Microphone arrays – Signal processing techniques and applications*. Springer, 2001.

[9] J. D. Maynard, E. G. Williams, and Y. Lee, "Nearfield acoustic holography: I. Theory of generalized holography and the development of NAH," *J. Acoust. Soc. Am.*, vol. 78, no. 4, pp. 1395–1413, 1985.

[10] E. G. Williams, *Fourier Acoustics: Sound radiation and nearfield acoustic holography*. Academic, London, 1999.

[11] J. Bourgeois and W. Minker, *Time-domain beamforming and blind source separation – Speech input in the car environment*. Springer, 2009.

[12] J. J. Christensen and J. Hald, "Brüel & Kjær technical review – Beamforming," 2004.

[13] R. P. Dougherty and R. W. Stoker, "Sidelobe suppression for phased array aeroacoustic measurement," in *Proc. of AIAA Toulouse, France*, 1998.

[14] J. R. Underbrink and R. P. Dougherty, "Array design for non-intrusive measurement of noise sources," in *Proc. of Noise-Con 96, Bellevue, WA*, 1996.

[15] J. R. Underbrink, *Aeroacoustic measurements*, ch. 3. Aeroacoustic phased array testing in low speed wind tunnels, pp. 98–129. Springer, 2002.

[16] B. Rafaely, Y. Peled, M. Agmon, D. Khaykin, and E. Fisher, *Speech processing in modern communication – Challenges and perspectives*, vol. 3, ch. 11. Spherical microphone array beamforming, pp. 281–305. Springer, 2010.

[17] E. G. Williams and K. Takashima, "Vector intensity reconstructions in a volume surrounding a rigid spherical microphone array," *J. Acoust. Soc. Am.*, vol. 127, no. 2, pp. 773–783, 2010.

[18] H. Teutsch, *Modal array signal processing: Principles and applications of acoustic wavefield decomposition*. Springer, 2007.

[19] J. Meyer, "Beamforming for a circular microphone array mounted on spherically shaped objects," *J. Acoust. Soc. Am.*, vol. 109, no. 1, pp. 185–193, 2001.

[20] B. Rafaely, "Analysis and design of spherical microphone arrays," *IEEE Trans. Signal Process.*, vol. 13, no. 1, 2005.

[21] M. Marschall, S. Favrot, and J. Buchholz, "Robustness of a mixed-order Ambisonics microphone array for sound field reproduction," in *Proc. of AES 132nd Convention, Budapest, Hungary*, 2012.

[22] S. Favrot and M. Marschall, "Metrics for performance assessment of mixed-order Ambisonics spherical microphone arrays," in *Proc. of AES 25th UK Conference, York, UK*, 2012.

[23] M. Marschall and J. Chang, "Sound-field reconstruction performance of a mixed-order Ambisonics microphone array," in *Proc. Meetings on Acoustics*, vol. 19, 2013.

[24] S. Favrot, M. Marschall, J. Käshbach, J. Buchholz, and T. Weller, "Mixed-order Ambisonics recording and playback for improving horizontal directionality," in *Proc. of AES 131st Convention, New York City, USA*, 2011.

[25] M. Kleider, B. Rafaely, B. Weiss, and E. Bachmat, "Golden-ratio sampling for scanning circular microphone arrays," *IEEE Trans. Audio, Speech, Language Process.*, vol. 18, no. 8, pp. 2091–2098, 2010.

[26] A. Parthy, C. T. Jin, and A. van Schaik, "Acoustic holography with a concentric rigid and open spherical microphone array," in *Proc. of ICASSP, Taipei, Republic of China*, pp. 2173–2176, 2009.

[27] C. T. Jin, N. Epain, and A. Parthy, "Design, optimization and evaluation of a dual-radius spherical microphone array," *IEEE/ACM Trans. Audio, Speech, Language Process.*, vol. 22, no. 1, pp. 193–204, 2014.

[28] I. Balmages and B. Rafaely, "Open-sphere designs for spherical microphone arrays," *IEEE Trans. Audio, Speech, Language Process.*, vol. 15, no. 2, pp. 727–732, 2007.

[29] S. C. Chan and H. H. Chen, "Uniform concentric circular arrays with frequency-invariant characteristics - theory, design, adaptive beamforming and DOA estimation," *IEEE Trans. Signal Process.*, vol. 55, no. 1, pp. 165–177, 2007.

[30] H. H. Chen, S. C. Chan, and K. L. Ho, "Adaptive beamforming using frequency invariant uniform concentric circular arrays," *IEEE Trans. Circuits Syst – I: Reg. Papers*, vol. 54, no. 9, pp. 1938–1949, 2007.

[31] Z. Li and R. Duraiswami, "Hemispherical microphone arrays for sound capture and beamforming," in *Proc. of IEEE Workshop on ASPAA, New Paltz, NY, USA*, pp. 106 – 109, 2005.

[32] G. W. Elko and J. Meyer, *Handbook of speech processing*, ch. 50. Microphone arrays, pp. 1021–1041. Springer, 2002.

[33] D. Fernandez-Comesana, J. Wind, H. de Bree, and K. R. Holland, "'Virtual arrays', a novel broadband source localization technique," in *Proc. of Novem 2012, Sorrento, Italy*, 2012.

[34] A. Farina and R. Ayalon, "Recording concert hall acoustics for posterity," in *Proc. of AES 24th Int. Conf. Multichannel Audio, Banff, Canada*, no. 38, 2003.

[35] F. Jacobsen, *Handbook of signal processing in acoustics*, ch. 68. The Microflown particle velocity sensor, pp. 1283–1291. Springer, 2008.

[36] F. Jacobsen and Y. Liu, "Near field acoustic holography with particle velocity transducers," *J. Acoust. Soc. Am.*, vol. 118, no. 5, pp. 3139–3144, 2005.

[37] F. Jacobsen and V. Jaud, "Statistically optimized near field acoustic holography using an array of pressure-velocity probes," *J. Acoust. Soc. Am.*, vol. 121, no. 3, pp. 1550–1558, 2007.

[38] Y.-B. Zhang, F. Jacobsen, C.-X. Bi, and X.-Z. Chen, "Near field acoustic holography based on the equivalent source method and pressure-velocity transducers," *J. Acoust. Soc. Am.*, vol. 126, no. 3, pp. 1257–1263, 2009.

[39] E. Fernandez-Grande, F. Jacobsen, and Q. Leclère, "Sound field separation with sound pressure and particle velocity measurements," *J. Acoust. Soc. Am.*, vol. 132, no. 6, pp. 3818–3825, 2012.

[40] A. Torras-Rosell, S. Barrera-Figueroa, and F. Jacobsen, "An acousto-optic beamformer," *J. Acoust. Soc. Am.*, vol. 132, no. 1, pp. 144–149, 2012.

[41] A. Torras-Rosell, *New measurement techniques: Optical methods for characterizing sound fields*. PhD thesis, Technical University of Denmark, 2014.

[42] H. L. Van Trees, *Optimum array processing. Part IV of Detection, estimation and modulation theory*. Wiley, 2002.

[43] R. P. Dougherty, *Aeroacoustic measurements*, ch. 2. Beamforming in acoustic testing. Springer, 2002.

[44] H. Wang and M. Kaveh, "Coherent signal-subspace processing for the detection and estimation of angles of arrival of multiple wide-band sources," *IEEE Trans. Acoust., Speech, Signal Process.*, vol. 33 (4), pp. 823–831, 1985.

[45] D. Khaykin and B. Rafaely, "Coherent signals direction-of-arrival estimation using as spherical microphone array: frequency smoothing approach," in *IEEE Workshop on Applications of Signal Processing to Audio and Acoustics, New Paltz, NY*, 2009.

[46] J. J. Christensen and J. Hald, "Improvements of cross spectral beamforming," in *Proc. of Inter-Noise 2003, Seogwipo, Korea*, 2003.

[47] J. Hald, *Handbook of signal processing in acoustics*, ch. 9. Beamforming and wavenumber processing, pp. 131–144. Springer, 2008.

[48] R. E. Collin and F. J. Zucker, *Antenna theory. Part 1*, pp. 163–165. McGraw-Hill, 2nd ed., 1969.

[49] J. D. Kraus, *Antennas*. McGraw-Hill, 2nd ed., 1988.

[50] A. W. Rudge, K. Milne, A. D. Olver, and P. Knight, eds., *IEE Electromagnetic wave series 16: The Handbook of Antenna Design*, vol. 2. Peter Peregrinus Ltd, 1983.

[51] Lord Rayleigh, "XXXI. Investigations in optics, with special reference to the spectroscope," *Lond. Edinb. Dublin Philos. Mag.*, vol. 8, no. 49, 1879.

[52] J. D. Kraus and R. J. Marhefka, *Antennas for all applications*. McGraw-Hill, 3rd ed., 2001.

[53] M. R. Bai, J.-G. Ih, and J. Benesty, *Acoustic array systems: theory, implementation, and application*. John Wiley & Sons, 2013.

[54] J. Meyer and G. W. Elko, *Audio signal processing for next-generation multimedia communication systems*, ch. 2. Spherical microphone Arrays for 3D sound recording. Springer, 2004.

[55] G. A. Daigle, M. R. Stinson, and J. G. Ryan, "Beamforming with air-coupled surface waves around a sphere and circular cylinder (L)," *J. Acoust. Soc. Am.*, vol. 117, no. 6, pp. 3373–3376, 2005.

[56] J. Hald and J. J. Christensen, "A novel beamformer array design for noise source location from intermediate measurement distances," *J. Acoust. Soc. Am.*, vol. 112, no. 5, p. 2448, 2002.

[57] J. Hald, "Spherical beamforming with enhanced dynamic range," *SAE Int. Passeng. Cars - Mech. Syst.*, vol. 6, no. 2, pp. 1334–1341, 2013.

[58] M. Marschall, *Capturing and reproducing realistic acoustic scenes for hearing research*. PhD thesis, Technical University of Denmark, 2014.

[59] W. R. LePage, C. S. Roys, and S. Seely, "Radiation from circular current sheets," in *Proc. of IRE*, vol. 38, pp. 1069–1072, 1950.

[60] T. T. Taylor, "A synthesis method for circular and cylindrical antennas composed of discrete elements," *IRE Trans. Antennas Propag.*, pp. 251– 261, 1952.

[61] C. E. Hickman, H. P. Neff, and J. D. Tillman, "The theory of a single-ring circular antenna array," *Trans. Am. Inst. Electr. Eng.*, vol. 80, no. 2, pp. 110–115, 1961.

[62] G. Ziehm, "Optimum directional pattern synthesis of circular arrays," *Radio Electron. Eng.*, vol. 28, no. 5, pp. 341–355, 1964.

[63] I. D. Longstaff, P. E. K. Chow, and D. E. N. Davies, "Directional properties of circular arrays," in *Proc. IEE*, vol. 114, pp. 713–718, 1967.

[64] T. Rahim and D. E. N. Davies, "Effect of directional elements on the directional response of circular antenna arrays," in *Proc. IEE Pt. H*, vol. 129, pp. 18–22, 1982.

[65] D. E. N. Davies, *The handbook of antenna design*, vol. 2, ch. 12. Circular arrays. Peregrinus, London, 1983.

[66] M. R. Jones and H. D. Griffiths, "Prediction of circular array phase mode characteristics," *Electronics Letters*, vol. 24, no. 13, pp. 811 – 812, 1988.

[67] H. D. Griffiths, "The use of circular arrays for direction finding applications," in *IEE Colloquium on Passive Direction Finding*, 1989.

[68] C. P. Mathews and M. D. Zoltowski, "Eigenstructure techniques for 2-D angle estimation with uniform circular arrays," *IEEE Trans. Signal Process.*, vol. 42, no. 9, pp. 2395–2407, 1994.

[69] J. Meyer and G. W. Elko, "A highly scalable spherical microphone array based on an orthonormal decomposition of the soundfield," in *Proc. IEEE ICASSP 2002, Orlando, Florida, USA*, vol. 2, pp. 1781–1784, 2002.

[70] T. D. Abhayapala and D. B. Ward, "Theory and design of high order sound field microphones using spherical microphone arrays," in *Proc. IEEE ICASSP 2002, Orlando, Florida, USA*, vol. 2, pp. 1949–1952, 2002.

[71] B. Rafaely, "Plane-wave decomposition of the sound field on a sphere by spherical convolution," *J. Acoust. Soc. Am.*, vol. 116, no. 4, pp. 2149–2157, 2004.

[72] B. Rafaely, "Phase-mode versus delay-and-sum spherical microphone array processing," *IEEE Signal Process. Lett.*, vol. 12, no. 10, pp. 713 – 716, 2005.

[73] M. Park and B. Rafaely, "Sound-field analysis by plane-wave decomposition using spherical microphone array," *J. Acoust. Soc. Am.*, vol. 118, no. 5, pp. 3094–3103, 2005.

[74] B. Rafaely and B. Weiss, "Spatial aliasing in spherical microphone arrays," *IEEE Trans. Signal Process.*, vol. 55, no. 3, pp. 1003–1010, 2007.

[75] B. Rafaely, "Spatial sampling and beamforming for spherical mircrophone arrays," in *Proc. of IEEE HSCMA 2008, Trento, Italy*, pp. 5–8, 2008.

[76] H. Teutsch and W. Kellermann, "Acoustic source detection and localization based on wavefield decomposition using circular microphone arrays," *J. Acoust. Soc. Am.*, vol. 120, no. 5, pp. 2724–2736, 2006.

[77] E. Tiana-Roig, F. Jacobsen, and E. Fernandez-Grande, "Beamforming with a circular microphone array for localization of environmental noise sources," *J. Acoust. Soc. Am.*, vol. 128, no. 6, pp. 3535–3542, 2010.

[78] E. Tiana-Roig, F. Jacobsen, and E. Fernandez-Grande, "Beamforming with a circular array of microphones mounted on a rigid sphere (L)," *J. Acoust. Soc. Am.*, vol. 130, no. 3, pp. 1095–1098, 2011.

[79] S. Holmes, "Circular harmonics beamforming with spheroidal baffles," in *Proc. of ICA 2013 Montreal, Montreal, Canada*, 2013.

[80] S. Holmes, "Spheroidal beamforming. Circular harmonics beamforming with spheroidal baffles & spheroidal harmonics beamforming," Master's thesis, Technical University of Denmark, 2012.

[81] E. Tiana-Roig, "Beamforming techniques for environmental noise," Master's thesis, Technical University of Denmark, 2009.

[82] F. Jacobsen, G. Moreno-Pescador, E. Fernandez-Grande, and J. Hald, "Near field acoustic holography with microphones on a rigid sphere (L)," *J. Acoust. Soc. Am.*, vol. 129, no. 6, pp. 3461–3464, 2011.

[83] I. H. Sloan and R. S. Womersley, "External systems of points and numerical integration on the sphere," *Adv. Comput. Math.*, vol. 21, pp. 107–125, 2004.

[84] S. Petersen, "Localization of sources using 3D microphone array," Master's thesis, University of Southern Denmark, 2004.

[85] W. Song, *Beamforming applied to psychoacoustics*. PhD thesis, Aalborg University, 2007.

[86] K. Haddad and J. Hald, "3D localization of acoustic sources with a spherical array," in *Proc. of Acoustics'08 Paris, Paris, France*, 2008.

[87] A. Granados, "Scattering of sound by a finite cylinder." Technical University of Denmark, 2012.

[88] C. Zhang, K.-A. Chen, and G.-Y. Chen, "Beam pattern design and performance analyses for circular array with spherical baffles," *J. Electronic Science and Technology of China*, vol. 7, no. 3, 2009.

[89] P. C. Hansen, *Discrete inverse problems. Insight and algorithms*. SIAM, 2010.

[90] O. Lylloff, E. Fernandez-Grande, E. Tiana-Roig, F. T. Agerkvist, J. Hald, and M. S. Andersen, "Improving the efficiency of deconvolution algorithms for sound source localization," *J. Acoust. Soc. Am. (to be published)*, 2014.

[91] E. A. Robinson, *Predictive decomposition of time series with applications to seismic exploration*. PhD thesis, MIT, Cambridge, Massachusetts, USA, 1954.

[92] E. A. Robinson, "Predictive decomposition of time series with applications to seismic exploration," *Geophysics*, vol. 32, no. 3, pp. 418–484, 1967.

[93] N. Wiener, *The extrapolation, interpolation, and smoothing of stationary time series with engineering applications*. MIT Press, 1949.

[94] J. L. Starck, E. Pantin, and F. Murtagh, "Deconvolution in astronomy: A review," *Publications of the Astronomical Society of the Pacific*, no. 114, pp. 1051–1069, 2002.

[95] J.-B. Sibarita, "Deconvolution microscopy," *Adv. Biochem. Eng. Biotechnol.*, no. 95, pp. 201– 243, 2005.

[96] M. Bertero and P. Boccacci, *Introduction to inverse problems in imaging*. Institute of Physics Publishing, 1998.

[97] J. A. Högbom, "Aperture synthesis with a non-regular distribution of interferometer baselines," *Astron. Astrophys. Suppl.*, vol. 15, pp. 417–426, 1974.

[98] W. H. Richardson, "Bayesian-based iterative method of image restoration," *J. Optical Soc. Am.*, vol. 62, no. 1, pp. 55–59, 1972.

[99] L. B. Lucy, "An iterative technique for the rectification of observed distributions," *Astron. J.*, vol. 79, no. 6, pp. 745–754, 1974.

[100] K. Ehrenfried and L. Koop, "Comparison of iterative deconvolution algoritms for the mapping of acoustic sources," *AAIA J.*, vol. 45, pp. 1584–1595, 2007.

[101] C. L. Lawson and R. J. Hanson, *Solving least squares problems*. SIAM, 1995.

[102] J. Barzilai and J. M. Borwein, "Two-point step size gradient methods," *IMA J. Numer. Ana.*, vol. 8, no. 1, pp. 141–148, 1988.

[103] A. Beck and M. Teboulle, "A fast iterative shrinkage-thresholding algorithm for linear inverse problems," *SIAM J. Imaging Sci.*, vol. 2, no. 1, pp. 183–202, 2009.

[104] O. Lylloff, "Efficient nonnegative least squares solvers for beamforming deconvolution," Master's thesis, Technical University of Denmark, 2014.

[105] T. F. Brooks and W. M. Humphreys, "A deconvolution approach for the mapping of acoustic sources (DAMAS) determined from phased microphone arrays," in *Proc. of the 10th AIAA/CEAS Aeroacoustics Conference, Manchester, UK*, 2004.

[106] T. F. Brooks and W. M. Humphreys, "A deconvolution approach for the mapping of acoustic sources (DAMAS) determined from phased microphone arrays," *J. Sound Vib.*, vol. 294, pp. 856–879, 2006.

[107] R. P. Dougherty, "Extension of DAMAS and benefits and limitations of deconvolution in beamforming," in *Proc. of the 11th AIAA/CEAS Aeroacoustics Conference (26th AIAA Aeroacoustics Conference), Monterey, California*, 2005.

[108] T. Yardibi, J. Li, P. Stoica, and L. N. Cattafesta III, "Sparsity constrained deconvolution approaches for acoustic source mapping," *J. Acoust. Soc. Am.*, vol. 123, no. 5, pp. 2631–2642, 2008.

[109] P. Sijtsma, "CLEAN based on spatial source coherence," *Int. J. Aeroacoust.*, vol. 6, no. 4, pp. 357–374, 2007.

[110] D. Fernandez-Comesana, E. Fernandez-Grande, E. Tiana-Roig, and K. R. Holland, "A novel deconvolution beamforming algorithm for virtual phased arrays," in *Proc. of Inter-Noise 2013, Innsbruck, Austria*, 2013.

[111] V. Fleury and J. Bult, "Extension of deconvolution algoritms for the mapping of moving acoustic sources," *J. Acoust. Soc. Am.*, vol. 129, no. 3, pp. 1417–1428, 2011.

[112] T. F. Brooks and W. M. Humphreys, "Extension of DAMAS phased array processing for spatial coherence determination (DAMAS-C)," in *Proc. of the 12th AIAA/CEAS Aeroacoustics Conference, Cambridge, MA, USA*, no. AAIA–2006-2654, 2006.

[113] T. Yardibi, J. Li, P. Stoica, N. S. Zawodny, and L. N. Cattafesta III, "A covariance fitting approach for correlated acoustic source mapping," *J. Acoust. Soc. Am.*, vol. 127, no. 5, pp. 2920–2931, 2010.

[114] C. Bahr and L. Cattafesta, "Wavespace-based coherent deconvolution," in *18th AIAA/CEAS Aeroacoustics Conference (33rd AIAA Aeroacoustics Conference), Colorado Springs, USA*, no. AAIA 2012-2227, 2012.

[115] A. Xenaki, F. Jacobsen, E. Tiana-Roig, and E. Fernandez-Grande, "Improving the resolution of beamforming measurements on wind turbines," in *Proc. of ICA 2010, Sidney, Australia*, 2010.

[116] A. Xenaki, F. Jacobsen, and E. Fernandez-Grande, "Improving the resolution of three-dimensional acoustic imaging with planar phased arrays," *J. Sound Vib.*, vol. 331, no. 8, pp. 1939–1950, 2012.

[117] T. Yardibi, N. S. Zawodny, C. Bahr, F. Liu, L. N.Cattafesta III, and J. Li, "Comparison of microphone array processing techniques for aeroacoustic measurements," *Int. J. Aeroacoust.*, vol. 9, no. 6, pp. 733–762, 2010.

[118] Z. Chu and Y. Yang, "Comparison of deconvolution methods for the visualization of acoustic sources based on cross-spectral imaging function beamforming," *Mech. Syst. Signal Process.*, 2014.

[119] J.-C. Pascal and J.-F. Li, "Resolution improvement of beamformers using spherical microphone array," in *Proc. of Acoustics'08 Paris, Paris, France*, 2008.

[120] A. Schmitt, L. Lamotte, and F. Deblauwe, "Source identification inside cabin using inverse methods," in *Proc. of BeBec 2010, Berlin, Germany*, 2010.

[121] M. Legg and S. Bradley, "Comparison of CLEAN-SC for 2D and 3D scanning surfaces," in *Proc. of BeBec 2012, Berlin, Germany*, 2012.

[122] Q. Fu, M. Li, L. Wei, and D. Yang, "An improved method combining beamforming and acoustical holography for the reconstruction of the sound pressure on structure surface," *Acta Acust. united Ac.*, vol. 100, no. 1, pp. 166–183, 2014.

[123] E. G. Williams and J. D. Maynard, "Holographic imaging without the wavelength resolution limit," *Phys. Rev. Lett.*, vol. 45, no. 7, pp. 554–557, 1980.

[124] E. G. Williams, J. D. Maynard, and E. Skudrzyk, "Sound source reconstructions using a microphone array," *J. Acoust. Soc. Am.*, vol. 68, no. 1, pp. 340–344, 1980.

[125] E. G. Williams, N. Valdivia, and P. C. Herdic, "Volumetric acoustic vector intensity imager," *J. Acoust. Soc. Am.*, vol. 120, no. 4, pp. 1887–1897, 2006.

[126] A. Granados, F. Jacobsen, and E. Fernandez-Grande, "Regularised reconstruction of sound fields with a spherical microphone array," in *Proc. Meetings on Acoustics*, vol. 19, 2013.

[127] E. Fernandez-Grande, *Near-field acoustic holography with sound pressure and particle velocity measurements*. PhD thesis, Technical University of Denmark, 2012.

[128] Y. T. Cho, J. S. Bolton, and J. Hald, "Source visualization by using statistically optimized near-field acoustical holography in cylindrical coordinates," *J. Acoust. Soc. Am.*, vol. 118, no. 4, pp. 2355–2364, 2005.

[129] M. Lee and J. S. Bolton, "Patch near-field acoustical holography in cylindrical geometry," *J. Acoust. Soc. Am.*, vol. 118, no. 6, pp. 3721–3732, 2005.

[130] G. B. Arfken and H. J. Weber, *Mathematical methods for physicists*. Elsevier Academic Press, 2005.

[131] F. Jacobsen and P. M. Juhl, *Fundamentals of general linear acoustics*. Wiley, 2013.

[132] D. N. Zotkin, R. Duraiswami, and N. A. Gumerov, "Plane-wave decomposition of acoustical scenes via spherical and cylindrical microphone arrays," *IEEE Trans. Audio, Speech, Language Process.*, vol. 18, no. 1, pp. 2–16, 2010.

[133] E. Fernandez-Grande and T. Walton, "Reconstruction of sound fields with a spherical microphone array," in *Proc. of Inter-Noise 2014, Melbourne, Australia*, 2014.

Papers A-E

Errata list

The following typos have been detected in the contributing articles after publication:

Paper A The index q in the second sum of Eq. (14) should read h.

Paper B The function $b_n(kR)$ in Eq. (7) should read $b_q(kR)$.

Paper D The parameter w_i in Eq. (8) should read w_m.

Paper E The function $p(kR, \theta_i, \varphi_i)$ in Eq. (17) should read $\tilde{p}(kR, \theta_i, \varphi_i)$.

Paper A

Beamforming with a circular microphone array for localization of environmental noise sources[a)]

Elisabet Tiana-Roig,[b)] Finn Jacobsen, and Efrén Fernández Grande
Acoustic Technology, Department of Electrical Engineering, Technical University of Denmark, Ørsteds Plads 352, 2800 Kongens Lyngby, Denmark

(Received 11 May 2010; revised 7 September 2010; accepted 13 September 2010)

It is often enough to localize environmental sources of noise from different directions in a plane. This can be accomplished with a circular microphone array, which can be designed to have practically the same resolution over 360°. The microphones can be suspended in free space or they can be mounted on a solid cylinder. This investigation examines and compares two techniques based on such arrays, the classical delay-and-sum beamforming and an alternative method called circular harmonics beamforming. The latter is based on decomposing the sound field into a series of circular harmonics. The performance of the two signal processing techniques is examined using computer simulations, and the results are validated experimentally. © *2010 Acoustical Society of America*.
[DOI: 10.1121/1.3500669]

PACS number(s): 43.60.Fg, 43.50.Rq [EJS] Pages: 3535–3542

I. INTRODUCTION

Acoustical beamforming is a signal processing technique used to localize sound sources using microphone arrays. Unlike other array techniques such as statistically optimized near-field acoustical holography (SONAH), which are based on near-field measurements,[1,2] beamforming is based on far-field measurements, i.e., the array must be placed relatively far from the sources in order to determine their "position" by processing the signals captured by the microphones.[3]

The goal of the present work is the design of beamformers for localization of environmental noise sources. In outdoors measurements, the sound field is basically generated by sources placed far from the measurement point, in the far field. At the measurement point, the direction of propagation of the waves can be considered essentially parallel to the ground, which implies that the sound field can be assumed to be two-dimensional. For such purposes, it is suitable to use circular arrays as these are able to map the sound field over 360°.

The techniques developed for the circular geometry are delay-and-sum beamforming (DSB) and circular harmonics beamforming (CHB). The first technique is the classical beamforming technique, which is widely used since it is very robust in the presence of background noise.[4] By contrast, CHB is a novel technique that belongs to a more recent category called eigenbeamforming. All techniques in this group are based on decomposing the sound field into a summation of harmonics.[5–8] CHB has been developed by adapting the theory of spherical harmonics beamforming to the two-dimensional case using circular harmonics (CH).

II. DECOMPOSITION OF THE SOUND FIELD USING CH

A. Circular apertures

Consider a circular aperture of radius R in the xy-plane and a plane wave with amplitude P_0 that impinges on the aperture in a direction perpendicular to the z-axis in free space. The incident pressure at any point of the aperture can be written in polar coordinates,

$$p(kR,\varphi) = P_0 e^{j\mathbf{k_i}\cdot\mathbf{r}}\big|_{r=R} = P_0 e^{jkR\cos(\varphi-\varphi_i)}, \tag{1}$$

where $\mathbf{k_i}$ and φ_i are the wave number vector and the angle of the incident wave. The temporal term $e^{-j\omega t}$ has been suppressed. This expression can be expanded in series of circular waves,[9]

$$e^{jkR\cos(\varphi-\varphi_i)} = J_0(kR) + \sum_{n=1}^{\infty} 2j^n \cos(n(\varphi-\varphi_i))\, J_n(kR), \tag{2}$$

where J_n is a Bessel function of order n. Developing this expression further, the pressure of the incident plane wave becomes

$$p(kR,\varphi) = P_0 \sum_{n=-\infty}^{\infty} j^n J_n(kR) e^{jn(\varphi-\varphi_i)}. \tag{3}$$

The pressure can now be represented by an infinite number of CH $e^{jn\varphi}$ (or modes) using the principle of a Fourier series. The pressure on the (unbaffled) aperture can be expressed as a function of the angle of the source φ_s using the relationship $\varphi_i = \varphi_s + \pi$,

$$p(kR,\varphi) = P_0 \sum_{n=-\infty}^{\infty} (-j)^n J_n(kR) e^{jn(\varphi-\varphi_s)}. \tag{4}$$

[a)]Portions of this work were presented in "Beamforming with a circular microphone array for localization of environmental sources of noise," Proceedings of Inter-Noise 2010, Lisbon, Portugal, June 2010.

[b)]Author to whom correspondence should be addressed. Electronic mail: etr@elektro.dtu.dk

Author's complimentary copy

When the same aperture is mounted on a rigid, infinite cylinder, the incident wave is scattered by the cylinder. The pressure on the baffled aperture is the superposition of the incident pressure and the scattered pressure, $p = p_i + p_s$. The scattered pressure at positions on the aperture becomes[10]

$$p_s(kR, \varphi) = \sum_{n=0}^{\infty} A_n \cos(n\varphi)(J_n(kR) + jY_n(kR)), \tag{5}$$

where the terms A_n are a set of coefficients and Y_n is a Neumann function of order n. Making use of the Hankel functions of first kind, $H_n(\cdot) = J_n(\cdot) + jY_n(\cdot)$, the previous expression can be rewritten as

$$p_s(kR, \varphi) = \sum_{n=-\infty}^{\infty} B_n H_n(kR) e^{jn\varphi}. \tag{6}$$

The terms B_n are obtained by imposing that the total velocity in the radial direction vanishes on the surface of the rigid cylinder, $u_{i,r} + u_{s,r} = 0$,

$$B_n = -P_0 (-j)^n \frac{J_n'(kR)}{H_n'(kR)} e^{-jn\varphi_s}, \tag{7}$$

where J_n' and H_n' are the derivatives of the Bessel and Hankel functions with respect to the radial dimension. Using the expressions given in Eqs. (4) and (6) for the incident and the scattered wave, together with the coefficients obtained in Eq. (7), the total pressure at the surface of the rigid cylinder becomes

$$p(kR, \varphi) = P_0 \sum_{n=-\infty}^{\infty} (-j)^n \times \left(J_n(kR) - \frac{J_n'(kR) H_n(kR)}{H_n'(kR)} \right) e^{jn(\varphi - \varphi_s)}. \tag{8}$$

Comparing Eqs. (3) and (8) with a Fourier series in the exponential form[11] shows that the pressure on the baffled or the unbaffled apertures can be represented as

$$p(kR, \varphi) = \sum_{n=-\infty}^{\infty} C_n e^{jn\varphi}, \tag{9}$$

where the Fourier coefficients C_n for the two cases are

$$C_n(kR, \varphi_s) = P_0 Q_n(kR) e^{-jn\varphi_s}, \tag{10}$$

with

$$Q_n(kR) = \begin{cases} (-j)^n J_n(kR) & \text{unbaffled}, \\ (-j)^n \left(J_n(kR) - \frac{J_n'(kR) H_n(kR)}{H_n'(kR)} \right) & \text{baffled}. \end{cases} \tag{11}$$

The modulus of the first four coefficients C_n is shown in Fig. 1, for baffled and unbaffled apertures. At low values of kR, the zero order mode is constant and equals 0 dB in both cases, whereas all the other modes have a slope of $10 \times n$ dB per decade. When the aperture is baffled, the response is offset by 6 dB compared with the unbaffled case. With increasing values of kR, more and more harmonics gain strength. However, for the unbaffled aperture the response exhibits some dips that imply that signals that have components around these dips cannot be totally resolved. This problem disappears when the cylindrical baffle is used.

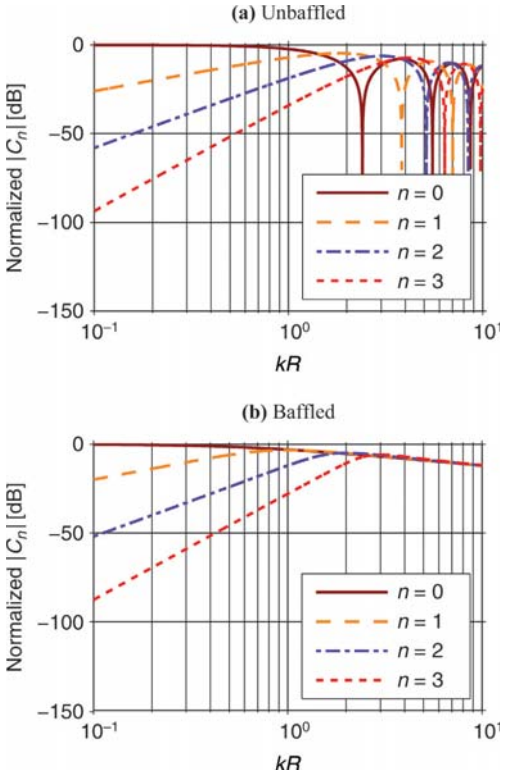

FIG. 1. (Color online) Normalized modulus of the four lowest Fourier coefficients of the pressure on an unbaffled circular aperture (top) and on a circular aperture mounted on a rigid cylindrical baffle of infinite length (bottom).

Since the curves of the Fourier coefficients are functions of kR, variation of R implies that the curves are scaled in frequency (or wave number), and vice-versa. For instance, when R is increased, the response is shifted toward low frequencies, whereas a decrease of R results in a shift toward high frequencies.

B. Implementation using microphone arrays

In principle, infinitely many Fourier terms are needed to represent the sound pressure. However, in practice the number of harmonics must be truncated to a maximum order, N. As a rule of thumb,

$$N \approx kR \tag{12}$$

is usually chosen as a first approximation.[8,12,13] The reason for this is that the amplitude of the Bessel functions in the Fourier coefficients [see Eqs. (10) and (11)] is small when the order of the Bessel functions n exceeds its argument (kR). Thus, the overall contribution of modes $|n| > kR$ is very small.

Besides, microphone arrays rather than "ideal" continuous apertures are used in real-life applications, which implies

Author's complimentary copy

that apertures are sampled at discrete points. Assuming that an aperture is sampled with M omnidirectional microphones placed equidistantly, the Fourier coefficients become

$$\tilde{C}_n = \frac{1}{M}\sum_{m=1}^{M} \tilde{p}(kR, \varphi_m) e^{-jn\varphi_m}, \tag{13}$$

where $\tilde{p}$ is the *measured* pressure at the mth microphone placed at an angle φ_m.

The sampling procedure introduces an error in the Fourier coefficients. For example, it can be shown that in the case of an unbaffled circular array, the Fourier coefficients resulting after the sampling are, theoretically,[12–14]

$$\begin{aligned}\tilde{C}_n(kR) = {} & P_0(-j)^n J_n(kR) e^{-jn\varphi_s} \\ & + P_0 \sum_{q=1}^{\infty} (-j)^g J_g(kR) e^{jg\varphi_s} \\ & + P_0 \sum_{q=1}^{\infty} (-j)^h J_h(kR) e^{jh\varphi_s},\end{aligned} \tag{14}$$

where $g = Mq - n$ and $h = Mq + n$. Note that the first term is identical to the Fourier coefficient of the continuous aperture; see Eq. (10), whereas the remaining terms are residuals caused by the sampling. Further examination of Eq. (14) reveals that the first term is the dominant one when $M > 2|n|$. Since the highest mode excited is N,

$$M > 2N. \tag{15}$$

In fact, inserting the approximation for N given in Eq. (12) into Eq. (15) yields the Nyquist sampling criterion:

$$M > 2kR \quad \Rightarrow \quad M > 2\frac{2\pi}{\lambda}R \quad \Rightarrow \quad \frac{\lambda}{2} > d, \tag{16}$$

where λ is the wavelength and d is the distance between two consecutive microphones. Hence, by fulfilling the relationship between M and N given in Eq. (15), the Nyquist criterion is satisfied.[14]

III. BEAMFORMING TECHNIQUES

A. CHB

The beamformer response is the output of the beamformer as a function of the steering angle, i.e., the angle at which the main beam of the beamformer is pointing. Ideally, the beamformer response should assume a maximum when the beamformer is steered toward the source at φ_s, and should be zero in all other directions; that is,

$$b_{\text{ideal}}(\varphi) = A\delta(\varphi - \varphi_s), \tag{17}$$

where A is a scale factor. This can be described in terms of a Fourier series,

$$b_{\text{ideal}}(\varphi) = \sum_{n=-\infty}^{\infty} I_n e^{jn\varphi}, \tag{18}$$

$$I_n = \frac{1}{2\pi}\int_0^{2\pi} b_{\text{ideal}}(\varphi) e^{-jn\varphi}\, \mathrm{d}\varphi = A e^{-jn\varphi_s}. \tag{19}$$

It follows that

$$b_{\text{ideal}}(\varphi) = A\sum_{n=-\infty}^{\infty} e^{-jn\varphi_s} e^{jn\varphi}. \tag{20}$$

Using Eq. (10), the output of the ideal beamformer becomes

$$b_{\text{ideal}}(kR, \varphi) = A\sum_{n=-\infty}^{\infty} \frac{C_n(kR, \varphi_s)}{P_0 Q_n(kR)} e^{jn\varphi}. \tag{21}$$

In real implementations, the number of modes must be truncated at a reasonable value, N, and the aperture must be sampled by a number of microphones, M. Thus

$$b_{N,\text{CH}}(kR, \varphi) = A\sum_{n=-N}^{N} \frac{\tilde{C}_n(kR, \varphi_s)}{P_0 Q_n(kR)} e^{jn\varphi}. \tag{22}$$

Comparing with Eq. (10), Eq. (22) be rewritten as

$$b_{N,\text{CH}}(kR, \varphi) = A\sum_{n=-N}^{N} \frac{\tilde{C}_n(kR, \varphi_s)}{C_n(kR, \varphi)}. \tag{23}$$

When the beamformer is steered toward the position of the source, φ equals φ_s, so the quotients approximate unity and the output assumes a maximum. Note that, when using unbaffled arrays, Eq. (23) has singularities at the frequencies where the Fourier coefficients have dips; see Fig. 1. At such frequencies, the CH beamformer is not capable of resolving the location of the source properly.

Inserting the approximated coefficients given by Eq. (13) into Eq. (22), the CH beamformer output becomes

$$\begin{aligned}& b_{N,\text{CH}}(kR, \varphi) \\ & = \frac{A}{MP_0}\sum_{m=1}^{M}\left(\tilde{p}(kR, \varphi_m)\sum_{n=-N}^{N}\frac{1}{Q_n(kR)} e^{-jn(\varphi_m - \varphi)}\right).\end{aligned} \tag{24}$$

Ideally, this should be zero at all angles different from φ_s. However, since a limited number of microphones are used, the response exhibits a main lobe around φ_s and side lobes at other angles.

B. DSB

The delay-and-sum (DS) technique aligns the signals from the microphones of the array by introducing appropriate delays and finally adds them together.[3,15,16] The delays are determined by the steering direction of the array. The output assumes its maximum when the focusing direction coincides with the position of the source.

In this investigation, the output of a DS beamformer is implemented in the frequency domain using matched field

Author's complimentary copy

processing. This method uses phase shifts to align the signals in phase. Assuming that the beamformer is steered toward the direction φ, the beamformer output is

$$b_{\mathrm{DS}}(kR,\varphi) = A\sum_{m=1}^{M} w_m \tilde{p}(kR,\varphi_m)\cdot p^*(kR,\varphi_m,\varphi), \quad (25)$$

where

(1) w_m is the weighting coefficient of the mth microphone;
(2) $\tilde{p}(kR,\varphi_m)$ is the pressure measured at the mth microphone position due to a plane wave generated by a source at φ_s; and
(3) $p^*(kR,\varphi_m,\varphi)$ is the *theoretical* complex conjugated pressure that would be captured at the mth microphone due to plane wave generated at φ. Note that the argument φ is used to emphasize that this is the variable that defines the focusing direction of the beamformer.

In general, the source position is unknown, and therefore the beamformer must map over all possible source positions, i.e., $0 \le \varphi < 2\pi$. The key point is that when the beamformer is focused toward the position of the source φ_s, the second and the third terms of Eq. (25) become equal in magnitude but opposite in phase. In these circumstances, the microphone signals are aligned in time, and therefore the maximum output of the beamformer is reached.

In the case of an unbaffled array, the theoretical pressure is simply the closed form for a plane wave, so the beamformer output is

$$\begin{aligned} b_{\mathrm{DS}}(kR,\varphi) &= A\sum_{m=1}^{M} w_m \tilde{p}(kR,\varphi_m) P_0 e^{-j\mathbf{k}_i\cdot\mathbf{r}}\Big|_{r=R} \\ &= \frac{AP_0}{M}\sum_{m=1}^{M}\tilde{p}(kR,\varphi_m)e^{jkR\cos(\varphi_m-\varphi)}. \end{aligned} \quad (26)$$

Since all microphones have equal "importance," the weights w_m have been set to $1/M$. For the baffled array, the output of the beamformer is obtained by introducing Eq. (9) into Eq. (25), and taking into account that the number of modes used for the processing is truncated at a number N,

$$\begin{aligned} &b_{N,\mathrm{DS}}(kR,\varphi) \\ &= \frac{AP_0}{M}\sum_{m=1}^{M}\left(\tilde{p}(kR,\varphi_m)\sum_{n=-N}^{N} Q_n^*(kR)e^{-jn(\varphi_m-\varphi)}\right). \end{aligned} \quad (27)$$

This expression is also valid for the unbaffled case, although it is not as precise as Eq. (26) because of the truncation.

Further analysis of Eq. (27) reveals that the beamformer output can be written, according to Eqs. (10) and (13), as

$$b_{N,\mathrm{DS}}(kR,\varphi) = A\sum_{n=-N}^{N}\tilde{C}_n(kR,\varphi_s)\cdot C_n^*(kR,\varphi). \quad (28)$$

As opposed to CHB, where the beamformer output could be expressed as the ratio of the approximated coefficients to the theoretical ones [see Eq. (23)], the output of the DS beamformer is a multiplication of these terms. Therefore, in the case of unbaffled arrays, the singularities that can be present in CHB because of the dips of the Fourier coefficients are totally resolved with a DS beamformer.

C. Beamformer performance—Resolution and maximum side lobe level (MSL)

The resolution of a beamformer is defined as the −3 dB width of the main lobe of the beampattern. This parameter is of interest because it gives an approximation to the minimum angular difference between two incoherent sources that is necessary in order to distinguish them from each other.

The beamformer output will usually exhibit side lobes. This is an unwanted effect as the beamformer seems to be sensitive not only in the focusing direction but also in the direction of the side lobes. Therefore, it is convenient to evaluate the beamformer response by means of the MSL. This parameter is the difference in level between the peak of the highest side lobe and the peak of the main lobe.

IV. SIMULATIONS

The performance of circular arrays with CHB and DSB has been evaluated by means of simulations. The circular arrays have radii of 10 and 20 cm and 10 and 20 microphones, respectively. The number of microphones and the radius of each array were chosen by setting the same maximum frequency that could be represented without any sampling error (around 2.7 kHz); see Sec. II B. The simulations were carried out under ideal conditions, i.e., without background noise. The source was placed at 180°, but the source position has a very limited influence on the results. The amplitude of the waves impinging on the array was the same at all frequencies.

A. Simulations with CHB

The resolution and the MSL obtained with CHB and an unbaffled circular array are shown in Fig. 2, for the range from 50 Hz to 3.5 kHz. The number of orders used in the CHB algorithm given in Eq. (24) followed $N = \lceil kR \rceil$, where $\lceil\cdot\rceil$ is the ceiling function. The maximum value of N was $M/2 - 1$ in order to fulfill Eq. (15).

As can be seen, the resolution and the MSL are constant for a certain interval. This depends on the number of orders N used for the processing. The fact that the main lobe becomes narrower from interval to interval indicates an improvement in the resolution. More intervals, i.e., more orders, result in a better resolution, which is the case of the array of largest radius. The MSL follows the same behavior as the resolution, improving when the number of orders is increased. The staircase pattern in these two measures is also obtained with spherical harmonics beamforming.

At some frequencies an "unexpected" response occurs, e.g., around 2.1 kHz for the array of 10 cm and 2.8 kHz for the array of 20 cm. This phenomenon is due to the dips in the Fourier coefficients obtained with unbaffled arrays. The frequencies where this phenomenon occurs cannot be resolved as precisely as the neighboring frequencies. This

Author's complimentary copy

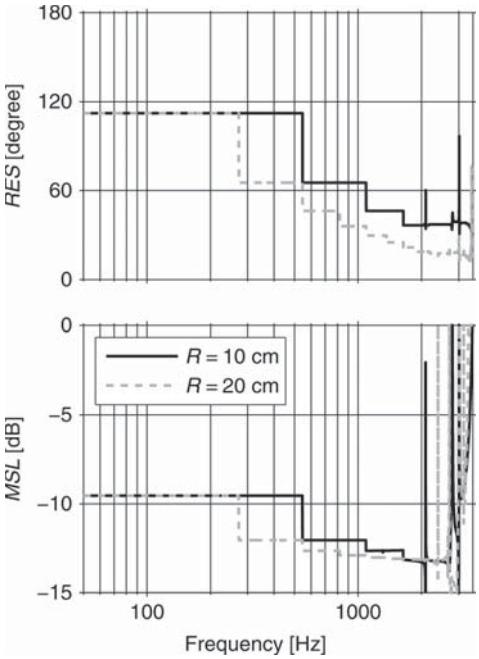

FIG. 2. Resolution and MSL using CHB and unbaffled arrays of radii 10 and 20 cm and 10 and 20 microphones, respectively. The source is placed at 180°.

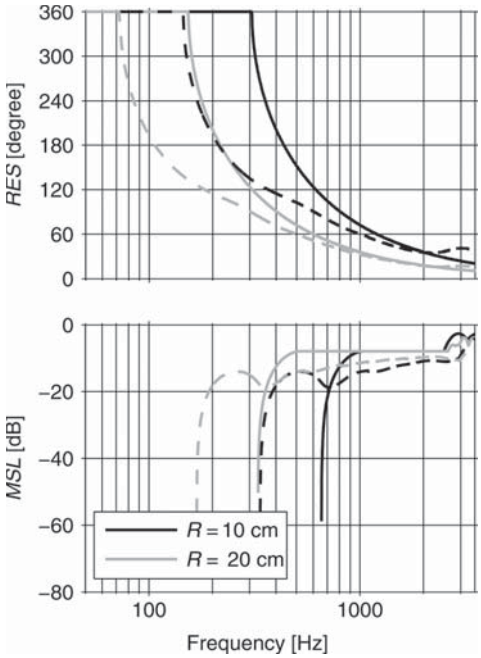

FIG. 3. Resolution and MSL using DSB and circular arrays of radius 10 and 20 cm and 10 and 20 microphones, respectively. Solid lines: Unbaffled arrays; dashed lines: Baffled arrays. The source is placed at 180°.

effect is avoided when the array is mounted on a rigid cylindrical baffle. The overall behavior of the CH beamformers when baffled arrays are used is very similar to the unbaffled case but without the problem of unresolved frequencies.

The arrays can be used up to a maximum frequency without any sampling error. For the arrays under analysis, this occurs at about 2.7 kHz. Above this frequency, the effect of the sampling error can be seen especially in the MSL (the magnitude of the side lobes is higher than in the previous interval of frequencies).

B. Simulations with DSB

The resolution and the MSL obtained under ideal conditions using DSB are shown in Fig. 3 for both baffled and unbaffled arrays. In the case of baffled arrays, the number of orders used in the DSB algorithm, stated in Eq. (27), was $N = \lceil kR \rceil + 1$, up to a maximum $N = M/2 - 1$ according to Eq. (15).

It is apparent that the resolution is 360° at low frequencies in all cases, and the MSL is non-existent, meaning that the beamformer is omnidirectional. From a certain frequency depending on the radius of the array, the resolution improves continuously until high frequencies. The curves decay in a similar way for both kinds of arrays, but in the baffled case they exhibit small smooth fluctuations. The MSL curves begin at a certain frequency and grow progressively until a maximum level is reached. In the case of unbaffled arrays, this level remains constant, whereas for baffled arrays the MSL exhibits ripples while it increases toward high frequencies. Nevertheless, the MSL is better for baffled arrays than for unbaffled.

In both cases, the performance improves with increasing radius of the array and is better in the case of baffled arrays. Furthermore, it can be seen that the baffled array of 10 cm of radius has resolution and MSL similar to the unbaffled array of radius 20 cm. Thus it can be concluded that mounting an array on an infinite baffle makes it seem to be "larger" than in the unbaffled case. Similar characteristics are found when DSB is applied to spherical arrays.

In general the resolution obtained with DSB is much worse than the resolution obtained with CHB. At high frequencies, the MSL with DSB is worse than with CHB for unbaffled arrays; but the opposite is the case for baffled arrays.

V. EXPERIMENTAL RESULTS

A prototype array with a radius of 11.9 cm has been tested in an anechoic room with a volume of about 1000 m^3. The array was constructed by mounting twelve 1/4 in. microphones, Brüel & Kjær (B&K) Type 4935, on a circular frame, corresponding to a microphone for every 30°. The implemented prototype is shown in Fig. 4.

The array and the source, a loudspeaker, were controlled by a B&K PULSE Analyzer. In all the measurements the loudspeaker was driven by a signal from the generator, pseudorandom noise of 1 s of period, 3.2 kHz of bandwidth, and 1 Hz of resolution. The microphones signals were recorded with the analyzer and postprocessed with the beamforming algorithms DSB and CHB.

The normalized outputs obtained with both CHB and DSB are shown on top of Fig. 5, whereas the simulated outputs are provided in the bottom. To account for the background noise introduced in the measurements, the simulations were carried out with a signal-to-noise ratio (SNR) of 30 dB at the input of each microphone due to uniformly distributed noise.

Author's complimentary copy

FIG. 4. (Color online) Circular array with radius of 11.9 cm and 12 microphones. Prototype by Brüel & Kjær.

The results agree very well with the theoretical ones for both techniques. A few differences deserve to be mentioned in the case of CHB. The side lobes are somewhat deformed and blurred compared with the simulations. The output is not only distorted at the frequencies that coincide with the dips in the Fourier coefficients, but also at frequencies in their vicinity. This phenomenon is particularly pronounced around 1.7 kHz. These differences are suspected to be caused by the CH beamformer algorithm itself, because of the fact that the approximated Fourier coefficients are compared with the theoretical ones in a ratio. When the approximate coefficients match the theoretical ones, the beamformer output is similar to the pattern expected under ideal conditions.

The agreement between measurements and simulations can be further examined by studying the resolution and the MSL. These quantities are shown in Fig. 6. The resolution using CHB is very similar to the one obtained with the simulation. The response follows the simulation curve rather accurately even at the frequencies where singularities occur. Some small deviations can be observed at the lowest frequencies, which are attributed to the influence of background noise. In contrast to the resolution, the MSL deviates somewhat from the simulation. In general, this measure is slightly higher than the expected one and worsens near singularities. At frequencies below 100 Hz a significant influence of background noise in the measurement becomes apparent.

For DSB, there are only a few differences compared with the simulations. The first is that the resolution equals 360° up to a frequency 20 Hz higher than expected. The second difference is that the first side lobe appears at 634 Hz instead of 556 Hz as obtained in the simulation. Yet another difference is that MSL is better than expected in the range from 1950 Hz to about 2300 Hz. These differences are again mainly attributed to the differences between the measured pressure and the theoretical one. However, the beampattern as well as the resolution and the MSL are not as much affected by these differences as in the case of CHB. This characteristic

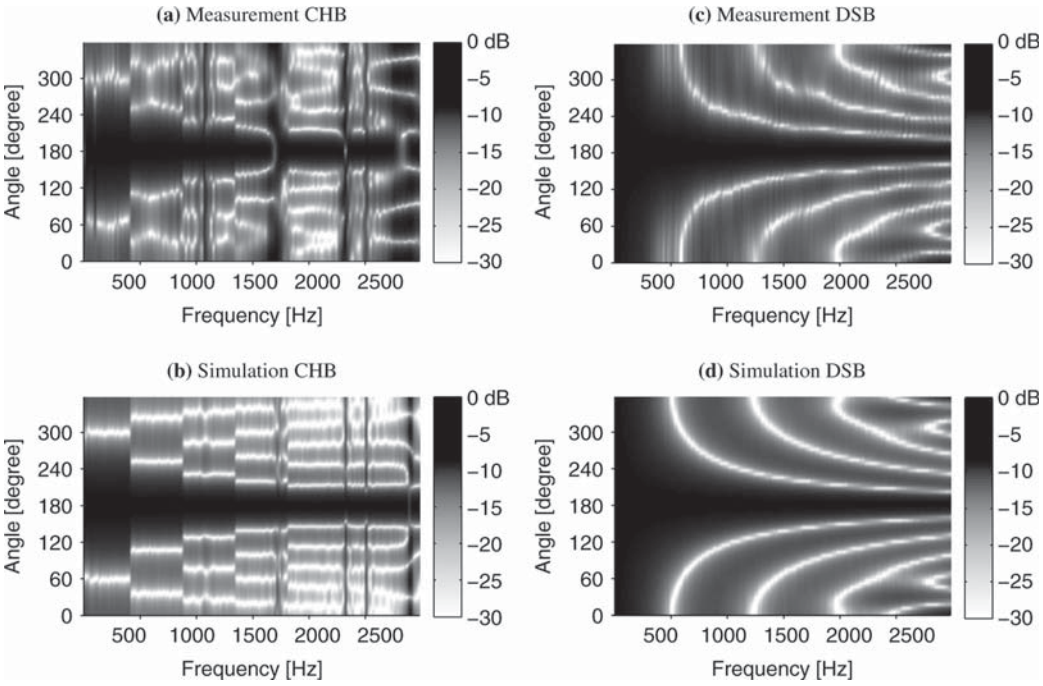

FIG. 5. Normalized output using CHB [(a), (b)] and DSB [(c), (d)] and an unbaffled array with a radius of 11.9 cm with 12 microphones. The source is placed at 180°. The top panels (a) and (c) show the measurements performed with a prototype, whereas the corresponding simulation is presented in the bottom panels (b) and (d). For the simulation, an SNR of 30 dB in each microphone is considered.

Author's complimentary copy

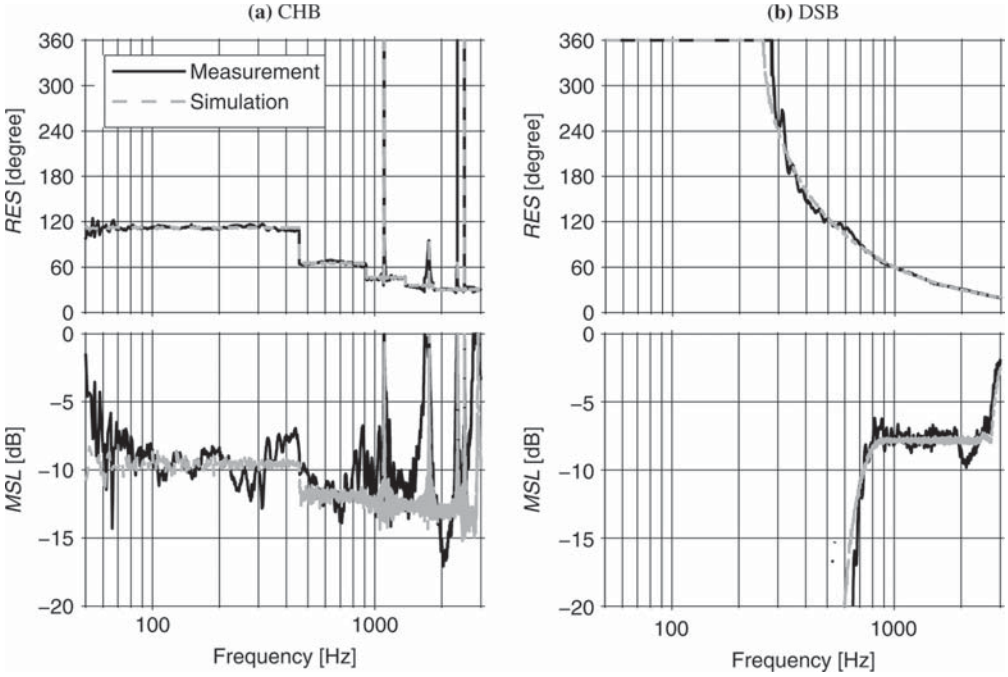

FIG. 6. Resolution and MSL using CHB (left) and DSB (right) and an unbaffled array with a radius of 11.9 cm with 12 microphones. The source is placed at 180°. The theoretical case obtained by simulation is also shown. The SNR in each microphone is set to 30 dB for the simulation.

and the fact that the influence of background noise is lower than CHB demonstrate that DSB is a more robust algorithm.

VI. CONCLUSIONS

Two different beamforming techniques based on circular arrays have been examined theoretically and experimentally, CHB and the well-known DSB. CHB is an adaptation of the spherical harmonics beamforming technique to a circular geometry.

The prototype used for the experimental investigation gave very satisfactory results: The beampatterns, the resolution, and the MSL were found to be in extremely good agreement with simulations for both CHB and DSB.

For a given array, CHB has better resolution and lower MSL in a wider frequency range than DSB has. Regardless of the technique, these quantities improve with increasing frequency. The frequency range is limited at low frequencies by the influence of background noise in the case of CHB and by the fact that the output becomes omnidirectional for DSB. At high frequencies, the limitation is in both cases given by the increase of the sampling error.

Keeping the number of microphones constant, the beamformer response is scaled in frequency when the radius of the array is modified. However, when the radius of the array is kept constant but the number of microphones is increased, the response improves toward higher frequencies since the spacing between the microphones becomes smaller. In fact, by increasing the number of microphones, the array behaves more similarly to a continuous aperture.

A given ratio between the number of microphones and the radius of the array determines the upper frequency above which a sampling error occurs. In such case, the overall performance improves considerably toward lower frequencies when increasing the radius. However, the number of microphones should be increased accordingly, otherwise the upper limit frequency would be reduced.

In the presence of background noise, DSB is more robust than CHB, and CH beamformers exhibit singularities, i.e., frequencies that cannot properly be resolved, when unbaffled circular arrays are used. This problem would be solved if it were feasible to mount the arrays on rigid cylindrical baffles of infinite length. The performance of DS beamformers would also improve substantially by mounting the arrays on rigid cylindrical baffles of infinite length, but this is not realistic.

CHB can be used in the entire frequency range except at the frequencies that cannot be properly resolved due to the nature of this technique. At such frequencies, it is convenient to use DSB instead. In addition to this, DSB should not be underestimated in environments with a poor SNR because of its robustness.

ACKNOWLEDGMENTS

The authors would like to thank Karim Haddad and Jørgen Hald, Brüel & Kjær, for lending us a circular microphone array and other equipment for the beamforming measurements. We would also like to thank Julien Jourdan and Marton Marschall for their notes about spherical harmonics beamforming, which became very helpful for the present work.

[1]J. Maynard, E. Williams, and Y. Lee, "Nearfield acoustic holography: I. Theory of generalized holography and the development of NAH," J. Acoust. Soc. Am. **78**(4), 1397–1413 (1985).
[2]J. Hald, "Basic theory and properties of statistically optimized near-field acoustical holography," J. Acoust. Soc. Am. **125**(4), 2105–2120 (2009).
[3]J. Hald, "Beamforming and wavenumber processing," in *Handbook of Signal Processing in Acoustics*, edited by D. Havelock, S. Kuwano, and M. Vorländer (Springer, New York, 2008), Chap. 9, pp. 131–144.

Author's complimentary copy

[4]J. Bitzer and K. Uwe Simmer, "Superdirective microphone arrays," in *Microphone Arrays. Signal Processing Techniques and Applications*, edited by M. Brandstein and D. Ward (Springer, Berlin, 2001), Chap. 2, p. 26.
[5]B. Rafaely, "Plane-wave decomposition of the sound field on a sphere by spherical convolution," J. Acoust. Soc. Am. **116**(4), 2149–2157 (2004).
[6]W. Song, W. Ellermeier, and J. Hald, "Using beamforming and binaural synthesis for the psychoacoustical evaluation of target sources in noise," J. Acoust. Soc. Am. **123**(2), 910–924 (2008).
[7]H. Teutsch and W. Kellermann, "Acoustic source detection and localization based on wavefield decomposition using circular microphone arrays," J. Acoust. Soc. Am. **120**(5), 2724–2736 (2006).
[8]H. Teutsch, *Modal Array Signal Processing: Principles and Applications of Acoustic Wavefield Decomposition* (Springer, Berlin, 2007), pp. 150–188.
[9]P. Morse and H. Feshbach, *Methods of Theoretical Physics* (McGraw-Hill, New York, 1953), Vol. I, p. 828.
[10]P. Morse, *Vibration and Sound*, 2nd ed. (McGraw-Hill, New York, 1948), pp. 347–348.
[11]E. Williams, *Fourier Acoustics: Sound Radiation and Nearfield Acoustic Holography* (Academic Press, London, 1999), pp. 4–5.
[12]C. Mathews and M. Zoltowski, "Eigenstructure techniques for 2-D angle estimation with uniform circular arrays," IEEE Trans. Signal Process. **42**(9), 2395–2407 (1994).
[13]D. E. N. Davies, "Circular arrays," in *The Handbook of Antenna Design*, edited by A. W. Rudge, K. Milne, A. D. Olver, and P. Knight (Peter Peregrinus Ltd., London, 1983), Vol. II, Chap. 12, pp. 298–310.
[14]H. Van Trees, *Optimum Array Processing. Part IV of Detection, Estimation, and Modulation Theory* (Wiley, New York, 2002), pp. 280–284.
[15]D. Johnson and D. Dudgeon, *Array Signal Processing Concepts and Techniques* (Prentice Hall, Englewood Cliffs, NJ, 1993), pp. 112–119.
[16]G. Elko and J. Meyer, "Microphone arrays," in *Springer Handbook of Speech Processing*, edited by J. Benesty, M. Sondhi, and Y. Huang (Springer-Verlag, Berlin, 2008), Chap. 50, pp. 1021–1042.

Author's complimentary copy

Paper B

Beamforming with a circular array of microphones mounted on a rigid sphere (L)

Elisabet Tiana-Roig,[a] Finn Jacobsen, and Efren Fernandez-Grande
Acoustic Technology, Department of Electrical Engineering, Technical University of Denmark, Ørsteds Plads 352, 2800 Kongens Lyngby, Denmark

(Received 4 November 2010; revised 6 July 2011; accepted 7 July 2011)

Beamforming with uniform circular microphone arrays can be used for localizing sound sources over 360°. Typically, the array microphones are suspended in free space or they are mounted on a solid cylinder. However, the cylinder is often considered to be infinitely long because the scattering problem has no exact solution for a finite cylinder. Alternatively one can use a solid sphere. This investigation compares the performance of a circular array mounded on a rigid sphere with that of such an array in free space and mounted on an infinite cylinder, using computer simulations. The examined techniques are delay-and-sum and circular harmonics beamforming, and the results are validated experimentally. © *2011 Acoustical Society of America*. [DOI: 10.1121/1.3621294]

PACS number(s): 43.60.Fg [EJS] Pages: 1095–1098

I. INTRODUCTION

During the past decade, studies on the performance of circular arrays of microphones for localizing sound sources over 360° have been reported. For example, Meyer[1] utilized modal beamforming to generate a desired beampattern for a circular microphone array mounted around a rigid sphere. Daigle *et al.*[2] considered delay-and-sum beamforming with circular arrays mounted on the surface of sound absorbing spheres and cylinders and showed that the achieved beamwidth improved over that of arrays mounted on hard spheres and cylinders. Instead of delay-and-sum beamforming, Teutsch and Kellermann[3] analyzed various algorithms based on decomposing the sound field into a series of modes for a circular array mounted on a cylinder. Still in the field of modal beamforming Tiana-Roig *et al.*[4] adapted the theory of spherical harmonics beamforming to the two-dimensional case using circular harmonics. The resulting circular harmonics beamformer was compared to the classical delay-and-sum beamformer using both a circular array suspended in free space and one mounted on a rigid, infinite cylinder. This letter to the editor repeats the comparison for the case of a circular array mounted on a rigid sphere.

II. PLANE WAVE DECOMPOSITION

Consider a plane wave, $e^{j\mathbf{k_i}\cdot\mathbf{r}}$, generated by a source placed in the far field, at a polar angle θ_s and azimuth angle φ_s, that impinges on a rigid sphere with radius R. The pressure on the surface of the sphere, at a point with spherical coordinates $[R, \theta, \varphi]$, can be written as[5,6]

$$p(kR,\theta,\varphi) = 4\pi \sum_{q=0}^{\infty} b_q(kR) \sum_{n=-q}^{q} Y_q^n(\theta,\varphi) Y_q^n(\theta_s,\varphi_s)^*, \quad (1)$$

where

$$b_q(kR) = (-j)^q \left(j_q(kR) - \frac{j_q'(kR)}{h_q'(kR)} h_q(kR) \right), \quad (2)$$

$$Y_q^n(\theta,\varphi) \equiv \sqrt{\frac{(2q+1)}{4\pi}\frac{(q-n)!}{(q+n)!}} P_q^n(\cos\theta) e^{jn\varphi}. \quad (3)$$

In the function b_n, which accounts for the effect of the rigid scatterer, j_q is a spherical Bessel function of order q, h_q is a spherical Hankel function of first kind and order q, and j_q' and h_q' are their derivatives. On the other hand, Y_q^n is a spherical harmonic, in which P_q^n is a Legendre function of degree q and order n. Note that in Eq. (1) the temporal term $e^{-j\omega t}$ is omitted; and the angles of the position of the source $[\theta_s, \varphi_s]$ are used instead of the angles of the incident wave $[\theta_i, \varphi_i]$, these being related by $\theta_s = \pi - \theta_i$ and $\varphi_s = \varphi_i + \pi$ because the unit vector of the incident wave $\hat{\mathbf{k}}_\mathbf{i}$ is opposite to the unit vector of the position of the source $\hat{\mathbf{r}}_\mathbf{s}$, $\hat{\mathbf{k}}_\mathbf{i} = -\hat{\mathbf{r}}_\mathbf{s}$.

Now a circular aperture of radius R is mounted at the equator of the rigid sphere, in the xy plane. Because the polar angle at all positions of the aperture is constant, i.e., $\theta = \pi/2$, its pressure can be represented in a Fourier series in the φ coordinate.[5] The resulting Fourier coefficients are

$$C_n = \frac{1}{2\pi}\int_0^{2\pi} p(kR, \pi/2, \varphi) e^{-jn\varphi} \mathrm{d}\varphi. \quad (4)$$

Inserting Eq. (1), it can be shown that the coefficients become

$$C_n(kR) = \sum_{q=|n|}^{\infty} (2q+1) b_n(kR) \times \frac{(q-|n|)!}{(q+|n|)!} P_q^{|n|}(0) P_q^{|n|}(\cos\theta_s) e^{-jn\varphi_s}. \quad (5)$$

Figure 1 shows the magnitude of the first four coefficients assuming a source located in the plane of the aperture, i.e., at $\theta_s = \pi/2$. The advantage of this configuration is that its behavior resembles the one of a circular aperture mounted

[a]Author to whom correspondence should be addressed. Electronic mail: etr@elektro. dtu.dk

Author's complimentary copy

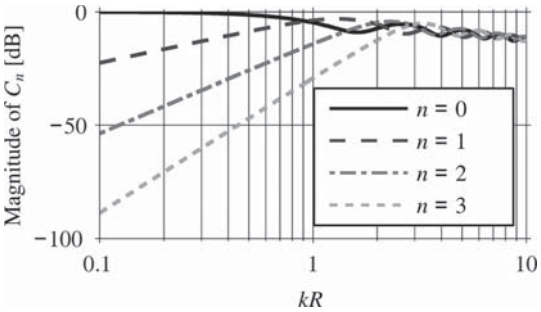

FIG. 1. Magnitude of the Fourier coefficients of the pressure on a circular aperture mounted on the equator of a rigid sphere.

on a rigid cylinder of infinite length,[4] for which all frequencies can be resolved by means of beamforming procedures.

III. BEAMFORMING ALGORITHMS

Circular harmonics beamforming (CHB) is a technique implemented specifically for circular arrays of microphones based on the decomposition of the sound field using the principles of a Fourier series. The beamformer output is[4]

$$b_{N,\mathrm{CHB}}(kR,\varphi)=\frac{A}{M}\sum_{m=1}^{M}\tilde{p}(kR,\varphi_m)\sum_{n=-N}^{N}\frac{1}{Q_n(kR)}e^{-jn(\varphi_m-\varphi)}, \tag{6}$$

where A is a scale factor, M is the number of microphones, $\tilde{p}$ and φ_m are the measured pressure and the azimuth angle of the mth microphone, and N is the maximum order taken into account. $Q_n(kR)$, which is related to the Fourier coefficients as $Q_n(kR)=C_n(kR)/e^{-jn\varphi_s}$, depends on the configuration of the array:

$$Q_n(kR)=\begin{cases}(-j)^n J_n(kR) & \text{Free space}\\ (-j)^n\left(J_n(kR)-\dfrac{J_n'(kR)H_n(kR)}{H_n'(kR)}\right) & \text{Rigid cylinder of infinite length}\\ \displaystyle\sum_{q=|n|}^{\infty}(2q+1)b_n(kR)\frac{(q-|n|)!}{(q+|n|)!} & \text{Equator of a rigid sphere}\\ \quad\times P_q^{|n|}(0)P_q^{|n|}(0)\end{cases} \tag{7}$$

Whereas the expressions for the array suspended in free field and mounted on an infinitely long cylinder are taken from Ref. 4, the value for the array on the sphere follows from Eq. (5). Note that in all cases the sound sources are assumed to be in the plane of the array, i.e., $\theta_s=\pi/2$.

Another technique that can be implemented for the circular geometry is delay-and-sum beamforming (DSB). This technique aligns the signals of the microphones by introducing appropriate delays and finally adds the signals together.[7] Implemented in the frequency domain using matched field processing, the beamformer output is[4]

$$b_{N,\mathrm{DSB}}(kR,\varphi)=\frac{A}{M}\sum_{m=1}^{M}\tilde{p}(kR,\varphi_m)\sum_{n=-N}^{N}Q_n^*(kR)e^{-jn(\varphi_m-\varphi)}. \tag{8}$$

The output of the unbaffled array can be also written as

$$b_{\mathrm{DSB}}(kR,\varphi)=\frac{A}{M}\sum_{m=1}^{M}\tilde{p}(kR,\varphi_m)e^{jkR\cos(\varphi_m-\varphi)}, \tag{9}$$

which is more precise than Eq. (8) because it does not imply a truncation at an order N.

Ideally, the beamformers output should be zero at all angles φ different from the angle of the sound source, φ_s. However, because a limited number of microphones is used, rather than a continuous aperture, the response exhibits a main lobe around φ_s and side lobes at other angles. Therefore, it is convenient to evaluate the performance of the beamformer in terms of resolution, defined as the -3 dB width of the main lobe, and maximum side lobe level (MSL), which is given by the difference in level between the peaks of the highest side lobe and the main lobe.

IV. SIMULATION STUDY

The performance of CHB and DSB using a circular array mounted on the equator of a rigid sphere has been compared to other configurations such as a circular array suspended in free space or a circular array mounted on a rigid cylinder of infinite length by means of computer simulations. The impinging plane waves were perpendicular to the plane of the array and were created by a source placed at $\theta_s=90°$ and $\varphi_s=180°$. (Note, however, that the azimuth angle has a very limited influence on the results.) The maximum order of the algorithms followed $N\approx kR$ for CHB and $N\approx kR+1$ for DSB,[4] up to a maximum $N=M/2-1$ to satisfy the Nyquist criterion: $\lambda/2>d$, where d is the distance between the microphones, or equivalently, $M>2kR$.[8,9] An array with 10 cm of radius and 10 microphones was considered.

The left panels of Fig. 2 show the performances of the unbaffled array and the array mounted on a sphere using CHB and considering ideal conditions, i.e., without background noise. The behavior of the array mounted on a rigid cylinder is not depicted because the curves coincide with the ones of the array on the sphere in the frequency range of interest. As can be seen, by mounting the array on the sphere, the performance is very similar to the one of the unbaffled array but improves particularly at those frequencies where the unbaffled array presents peaks. Note that from 2.7 kHz on the MSL worsens dramatically because in this range the Nyquist criterion is no longer fulfilled and consequently aliasing occurs.

The resolution and the MSL with DSB can be seen in the right column of Fig. 2. In this case, the response of the array mounted on a cylinder of infinite length is also shown. With this technique, the performance of the array mounted on the sphere is better than the one with an unbaffled array, especially toward low frequencies. However, it is not as good as in the case of the array mounted on an infinitely long cylinder. Actually, by mounting the array on a cylinder or on a sphere, the apparent distance between microphones increases, and this improves the performance of DSB at low frequencies. This is in agreement with the observations of Daigle *et al.*, although they claimed that the array has an effectively larger aperture when mounted on a physical

Author's complimentary copy

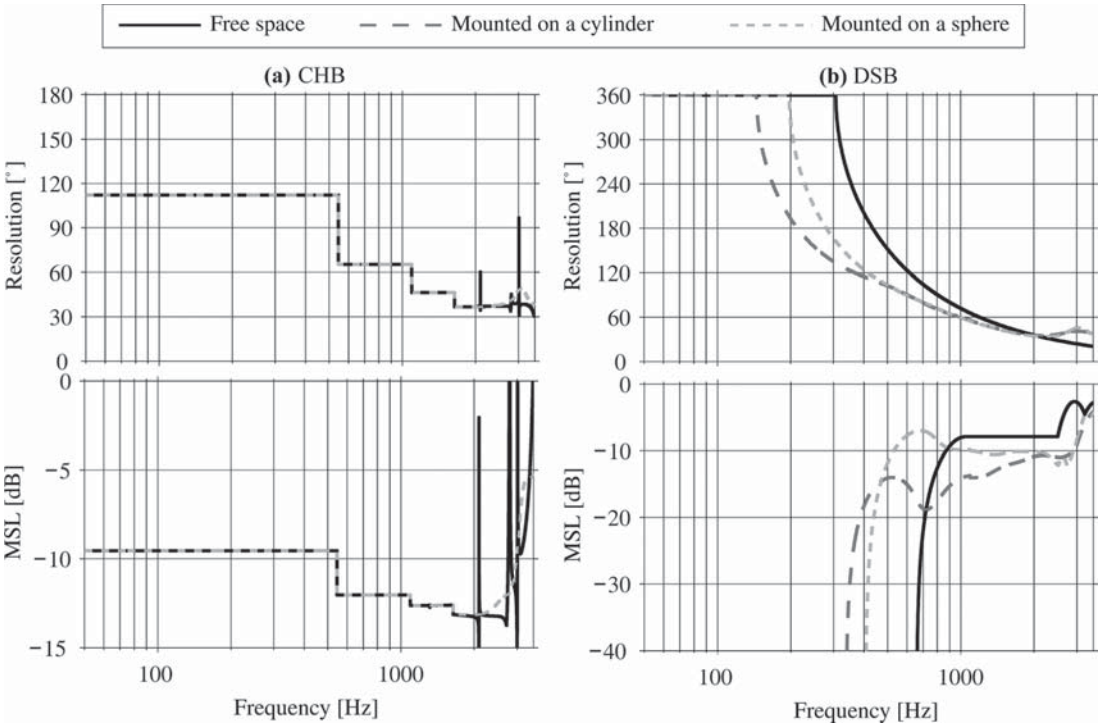

FIG. 2. Resolution and MSL using CHB (left) and DSB (right) and a circular array of radius 10 cm and 10 microphones when the microphones are suspended in free space, mounted on the equator of a rigid sphere, and mounted on a rigid cylinder of infinite length. For ease of comparison, the case of the cylinder with CHB is not plotted because it coincides with the case of the sphere. In all cases, the source is in the far field at $[\theta_s, \varphi_s] = [90°, 180°]$.

structure independently of the beamforming technique,[2] whereas the present study has revealed that this is not the case with CHB.

V. EXPERIMENTAL RESULTS

A circular array mounted on a rigid sphere has been tested in an anechoic room. The prototype array consisted of 16 1/4 in. microphones, Brüel & Kjær (B&K) type 4958, mounted on the equator of a rigid sphere with a radius of 9.75 cm, corresponding to a microphone for every 22.5°. With this configuration, the array can operate free of aliasing up to about 4.5 kHz.

The array and the source, a loudspeaker, were controlled by a B&K PULSE analyzer. The loudspeaker was driven by a signal from the generator, pseudorandom noise of 1 s of period, 6.4 kHz of bandwidth, and 1 Hz of resolution. The microphone signals were recorded with the analyzer and post-processed with the beamforming algorithms CHB and DSB.

Figure 3 shows the output of the array using CHB and DSB when a source is located 4 m away but at the very same height and at an azimuth angle $\varphi_s = 180°$. It can be seen that with the two techniques, the array is capable of localizing the sound source in the frequency range of interest with exception of DSB at the frequencies below about 300 Hz due to the fact that this technique behaves omnidirectionally at such values.

The performance of the array is also illustrated in Fig. 4, where the resolution and the MSL for both CHB and DSB are shown. The predictions made with computer simulations are also depicted. To account for the background noise introduced in the measurements, the simulations were carried out with a signal-to-noise ratio (SNR) of 30 dB at the input of each microphone due to uniformly distributed noise.

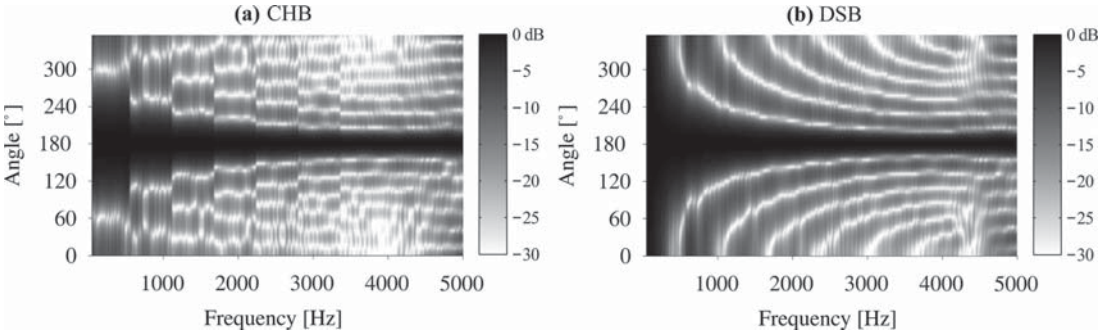

FIG. 3. Normalized output with CHB (left) and DSB (right) using a circular array with 16 microphones mounted on the equator of a rigid sphere with radius of 9.75 cm. The source is in the far field at $[\theta_s, \varphi_s] = [90°, 180°]$.

Author's complimentary copy

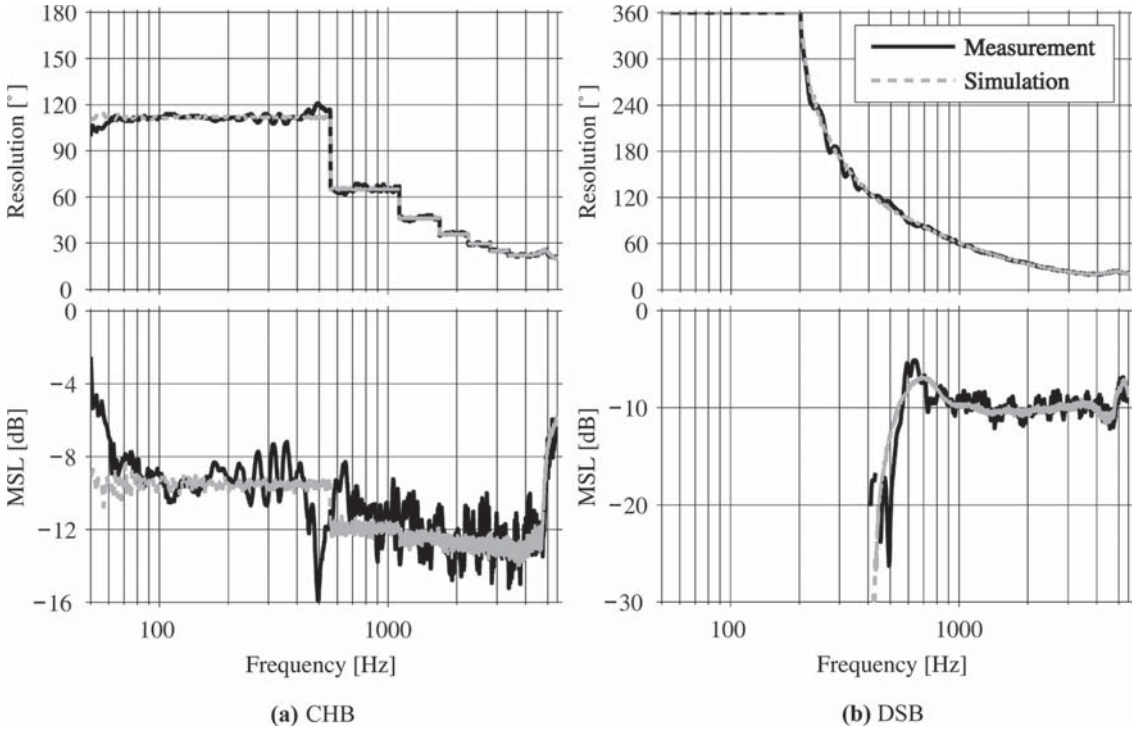

FIG. 4. Resolution and MSL with CHB (left) and DSB (right) using a circular array of radius 9.75 cm and 16 microphones mounted on the equator of a rigid sphere. The source is in the far field at $[\theta_s, \varphi_s] = [90°, 180°]$. For the simulation, the SNR in each microphone is 30 dB.

For CHB, the simulations and the measurements agree in terms of resolution in most of the frequency range. Small deviations from the expected values are observed at the lowest frequencies and around 500 Hz. In terms of MSL, the measurements oscillate around the expected values as occurs with circular arrays suspended in free space.[4] The differences detected in the resolution at low frequencies and about 500 Hz also appear in the MSL. At low frequencies, the difference is attributed to a presence of background noise higher than expected. At about 500 Hz, the performance is better than expected because the MSL is much lower than the predictions. The good agreement with the simulations is also found in the case of DSB. Just in the range from 400 to 600 Hz, the MSL differs from the expected value.

Other measurements with the source placed at different positions revealed that the behavior of the array is practically independent of its azimuth angle. Because the beamforming algorithms given in Sec. III expect a source placed at a polar $\theta_s = 90°$, i.e., at the plane of the array, the performance is optimal when this happens. However, it can be shown that sources placed in the range $\theta_s = 90° \pm 45°$ can still be localized.

VI. CONCLUSIONS

A beamformer consisting of a uniform circular array of microphones mounted on the equator of a rigid sphere has been examined using CHB and DSB. A simulation study has revealed that this configuration is an improved version of a circular array suspended in free space. Particularly, with CHB, the array mounted on the sphere behaves identically to the unrealistic case of an array with the same dimensions mounted on a rigid cylinder of infinite length. Therefore, the array on the sphere is a simple solution of special interest as alternative to beamformers based on cylinders of finite length because these are often approximated by infinitely long cylinders to overcome the problem that an exact analytical expression for such cylinders does not exist.

Various experiments using a prototype array have proved the validity of the model.

[1]J. Meyer, "Beamforming for a circular microphone array mounted on spherically shaped objects," J. Acoust. Soc. Am. **109**(1), 185–193 (2001).
[2]G. A. Daigle, M. R. Stinson, and J. G. Ryan, "Beamforming with air-coupled surface waves around a sphere and circular cylinder (L)," J. Acoust. Soc. Am. **117**(6), 3373–3376 (2005).
[3]H. Teutsch and W. Kellermann, "Acoustic source detection and localization based on wavefield decomposition using circular microphone arrays," J. Acoust. Soc. Am. **120**(5), 2724–2736 (2006).
[4]E. Tiana-Roig, F. Jacobsen, and E. Fernández Grande, "Beamforming with a circular microphone array for localization of environmental noise sources," J. Acoust. Soc. Am. **128**(6), 3535–3542 (2010).
[5]E. Williams, *Fourier Acoustics: Sound Radiation and Nearfield Acoustic Holography* (Academic, London, 1999), pp. 4–5, 224–230.
[6]B. Rafaely, "Plane-wave decomposition of the sound field on a sphere by spherical convolution," J. Acoust. Soc. Am. **116**(4), 2149–2157 (2004).
[7]D. Johnson and D. Dudgeon, *Array Signal Processing Concepts and Techniques* (Prentice Hall, Englewood Cliffs, NJ, 1993), pp. 112–119.
[8]H. Van Trees, *Optimum Array Processing. Part IV of Detection, Estimation, and Modulation Theory* (Wiley, New York, 2002), pp. 280–284.
[9]C. Mathews and M. Zoltowski, "Eigenstructure techniques for 2-D angle estimation with uniform circular arrays," IEEE Trans. Signal Process. **42**(9), 2395–2407 (1994).

Author's complimentary copy

Paper C

Deconvolution for the localization of sound sources using a circular microphone array[a)]

Elisabet Tiana-Roig[b)] and Finn Jacobsen
Acoustic Technology, Department of Electrical Engineering, Technical University of Denmark, Ørsteds Plads 352, DK-2800 Kongens Lyngby, Denmark

(Received 14 September 2012; revised 18 June 2013; accepted 10 July 2013)

During the last decade, the aeroacoustic community has examined various methods based on deconvolution to improve the visualization of acoustic fields scanned with planar sparse arrays of microphones. These methods assume that the beamforming map in an observation plane can be approximated by a convolution of the distribution of the actual sources and the beamformer's point-spread function, defined as the beamformer's response to a point source. By deconvolving the resulting map, the resolution is improved, and the side-lobes effect is reduced or even eliminated compared to conventional beamforming. Even though these methods were originally designed for planar sparse arrays, in the present study, they are adapted to uniform circular arrays for mapping the sound over 360°. This geometry has the advantage that the beamforming output is practically independent of the focusing direction, meaning that the beamformer's point-spread function is shift-invariant. This makes it possible to apply computationally efficient deconvolution algorithms that consist of spectral procedures in the entire region of interest, such as the deconvolution approach for the mapping of the acoustic sources 2, the Fourier-based non-negative least squares, and the Richardson–Lucy. This investigation examines the matter with computer simulations and measurements. © *2013 Acoustical Society of America*. [http://dx.doi.org/10.1121/1.4816545]

PACS number(s): 43.60.Fg [BEA] Pages: 2078–2089

I. INTRODUCTION

Beamforming with phased arrays of microphones is a well established method for visualization of sound fields. However, because the sound field is mapped with a discrete number of microphones, beamforming techniques present intrinsic limitations, specifically the frequency dependence of the array resolution and the appearance of side lobes that contaminate the beamforming map with sometimes unexpected results.[1] These two factors make it difficult to interpret the map and therefore to visualize the actual sound field accurately.

The focus of the present investigation is on the improvement of the performance of uniform circular arrays (UCAs) for mapping the sound field over 360° around the array to localize sound sources in the far field. This array geometry has lately been of interest in various studies about environmental noise localization, conferencing, and measurements in ducts among others; see, for instance, Refs. 2–9. It has been shown that a better performance in terms of resolution and level of the side lobes can be achieved by mounting the array on a scatterer such as a sphere or a cylinder[3,4,6] or by designing other techniques than delay-and-sum (DS) beamforming, for example, circular harmonics (CH) beamforming.[5] Nevertheless these solutions are not sufficient to result in a clear and unambiguous beamforming map.

In the recent years, the aeroacoustic community has suggested various methods to improve the beamforming map in two-dimensional (2D) imaging using planar sparse arrays to map the sound field in a region parallel to the plane of the array. These methods rely on the fact that the map is a convolution of the acoustic sources and the beamformer's point-spread function (PSF), which is defined as the response of the beamformer to a point source. By means of deconvolution, the distribution of the sources can be recovered presenting a better resolution and reduced (or even suppressed) side lobes in comparison with direct beamforming. Examples of deconvolution methods can be found in Refs. 10–12 for static uncorrelated noise sources, in Refs. 13–15 for correlated noise sources, and in Ref. 16 for moving sources. The main problem is that these methods require a high computational effort due to the fact that they are based on iterative algorithms. To improve the efficiency, certain techniques use spectral (Fourier-based) procedures for the deconvolution, but these can only be applied when the beamformer's PSF is shift-invariant, that is, when the response of the beamformer to a point source depends only on the distance between the focusing point of the beamformer and the position of the point source. However, for 2D imaging, the assumption that the PSF is shift-invariant is only a good approximation when the source region is small compared with the distance between the array and the source. Therefore the use of such deconvolution approaches is restricted to a small region in space unless it is expanded to a larger (and 3D) region by making use of a coordinate transformation.[10,17,18]

Interestingly, one could think of adapting the existing deconvolution methods to a UCA to improve its performance. Contrary to the case of planar sparse arrays for which

[a)]Portions of this work were presented in "Acoustical source mapping based on deconvolution approaches for circular microphone arrays," Proceedings of Inter-Noise 2011, Osaka, Japan, September 2011.

[b)]Author to whom correspondence should be addressed. Electronic address: etr@elektro.dtu.dk

Author's complimentary copy

the PSF is shift-variant *per se*, beamformers based on UCAs have a practically shift-invariant PSF along the region of interest,[2,19] i.e., 360°, and consequently this scenario seems particularly adequate for the use of Fourier-based deconvolution methods. In the following, the main deconvolution methods that rely on a shift-invariant PSF, namely, the deconvolution approach for the mapping of the acoustic sources 2 (DAMAS2), the Fourier-based non-negative least squares (FFT-NNLS), and the Richardson–Lucy (RL) will be reformulated for the case of plane waves impinging on a UCA. The first method, DAMAS2, introduced by Dougherty in Ref. 10, is an extension of DAMAS of Brooks and Humphreys (Ref. 13). The second algorithm, FFT-NNLS, was adapted from the classical NNLS procedures[20] by Ehrenfried and Koop in Ref. 11. Finally RL, which was initially developed by Richardson and Lucy (Refs. 21 and 22) for image restoration in astronomy, was also adapted for acoustical purposes in Ref. 11. All these methods will be examined by means of computer simulations and experimental results.

II. CONVOLUTIONAL FORMULATION FOR UNIFORM CIRCULAR ARRAYS

A beamformer based on a UCA of microphones is capable of mapping the sound field over 360° in the plane of the array to find the direction of sound sources located in that plane. By electronically steering the beamformer, the sound field is scanned in a grid of azimuth angles φ, from 0 to 360°, to detect the propagating acoustic waves that impinge on the array and thereby to identify the direction of the sound sources that emit them. When a single source is present, the beamformer output exhibits a main lobe around the azimuth of the source, whereas other directions are contaminated with side lobes; see Fig. 1.

The characteristics of the beampattern, i.e., the shape of the main lobe and the side lobes, are given by the beamformer's PSF. This function was originally defined as the beamformer response to a point source with unit strength at an arbitrary position of a grid located in a plane parallel to the array plane.[10–12] However, this definition needs to be reformulated for a UCA because the goal is to look into all possible azimuth angles around a UCA beamformer instead of looking to a plane parallel to the array.

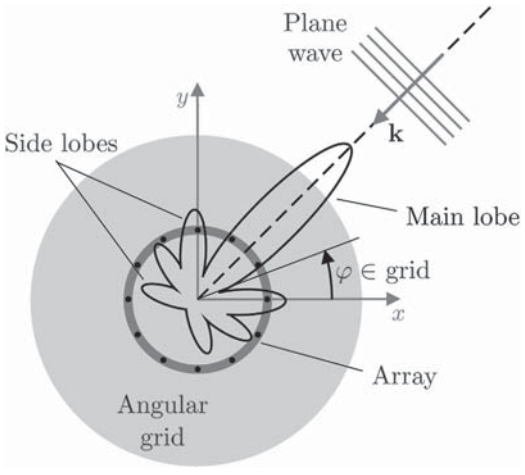

FIG. 1. Illustration of beamforming with a UCA for detecting the location of a distant sound source.

In the current study, the sources are considered to be sufficiently far from the array position, and therefore waves captured by the array can be regarded to be planar. This assumption implies that the direction of the waves can be identified, although the distance to the sources that emit them cannot be estimated—this would require a near-field scenario. Under the plane wave assumption, the PSF can be redefined as the beamformer response to a plane wave of unit amplitude created by a source in the far field of the array. Then in the presence of incoherent sources, the beamformer output is related to the PSF as

$$b(\varphi) = \sum_{\varphi' \in G} s(\varphi') H(\varphi|\varphi'), \tag{1}$$

where $s(\varphi')$ contains information regarding the direction and the strength (at the array position) of a plane wave created by a source located at an azimuth angle φ' contained on the grid G, whereas $H(\varphi \,|\, \varphi')$ is the PSF at φ due to a source at φ'. From now on s will be referred to as the source distribution.

From this expression, it becomes apparent that the information regarding sound sources can be recovered from the measured beamformer map and the beamformer's PSF. This is done by means of a deconvolution procedure, imposing that the distribution of sound sources must be non-negative $[s(\varphi') \geq 0]$. This is an inverse problem, which in matrix notation can be rewritten as

$$\mathbf{b} = \mathbf{H}\mathbf{s}, \tag{2}$$

where the vectors $\mathbf{b}$ and $\mathbf{s}$ contain the information about the beamformer output and the source distribution, respectively, and $\mathbf{H}$ is a matrix that in each column contains the PSF for one source located at an angle φ' of the grid. Often the matrix $\mathbf{H}$ can be singular, which implies that there may be infinitely many solutions for $\mathbf{s}$.[11]

For a beamformer based on a UCA, the focusing direction can be steered to any position in the plane where the array lies without changing the beampattern significantly due to the symmetry of the array.[2,19] This implies that the overall shape of the beamformer's PSF remains practically the same independently of its looking direction as shown in Fig. 2. A PSF that satisfies this condition is called to be shift-invariant because it depends only on the difference of the actual focus point φ and the azimuth of a source φ',

$$H(\varphi|\varphi') = H(\varphi - \varphi'). \tag{3}$$

Inserting this property into Eq. (1) leads to

$$b(\varphi) = \sum_{\varphi' \in G} s(\varphi') H(\varphi - \varphi'), \tag{4}$$

which corresponds to a discrete circular convolution of $s(\varphi)$ and $H(\varphi)$. Making use of the convolution theorem, Eq. (3) can be expressed with the discrete Fourier transform,

Author's complimentary copy

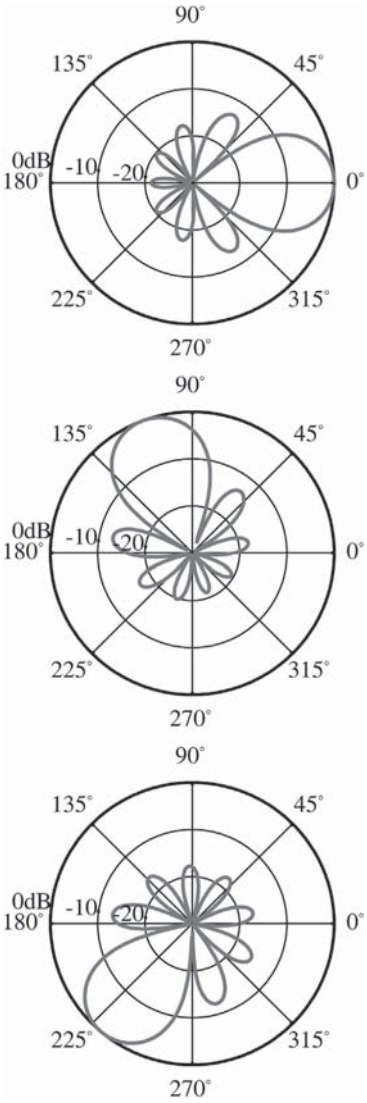

FIG. 2. PSF of a particular UCA focused to different directions (0°, 110°, and 230°).

and thus one can take advantage of the computational efficiency of this operation,

$$b(\varphi) = \mathcal{F}^{-1}[\mathcal{F}[s(\varphi)]\,\mathcal{F}[H(\varphi)]], \tag{5}$$

where the operators $\mathcal{F}$ and $\mathcal{F}^{-1}$ stand for the direct and the inverse Fourier transforms, respectively. This relationship is a key issue for deconvolution methods based on spectral approaches. Note that this equation requires that the PSF used for the calculation of the beamformer output, $H(\varphi)$, considers a source placed at an azimuth $\varphi' = 0$, according to Eq. (3).

III. DECONVOLUTION METHODS

From the mid 2000s the aeroacoustic array community has suggested various deconvolution methods, such as the DAMAS family of algorithms[10–16] or the NNLS algorithms,[11] to visualize sound sources with accuracy from a given beamforming map. These methods use iterative procedures to solve the inverse problem expressed by Eqs. (1) and (2).

Among the the existing methods, DAMAS2[10] and FFT-NNLS,[11] appear to be especially attractive for a UCA to map the sound field over 360°, because they rely on a shift-invariant PSF to solve the deconvolution problem as formulated in Eq. (5).

Yet another method that can be adapted to a UCA for localizing sound sources is RL, even though this was initially conceived for deconvolution problems in statistical astronomy.[21,22] Unlike DAMAS2 and FFT-NNLS, this method solves the inverse problem given by Eq. (5) from a statistical point of view following from Bayes' theorem on conditional probabilities.

In any case, the three methods aim to find an estimate of the source distribution s, $\tilde{s}$, that convolved with the PSF gives an estimate of the beamformer output, $\tilde{b}$, as similar as possible to the real beamformer output.

An overview and a comparison of the performances of RL, DAMAS2, and FFT-NNLS for planar sparse arrays for localizing sound sources in a small region of a plane parallel to the array plane can be found in Ref. 11.

In what follows DAMAS2, FFT-NNLS, and RL are adapted for the case of UCAs when sources in the far field of the array are assumed. In this sense, the estimate of the source distribution, $\tilde{s}$, will provide information about the direction of the impinging waves and their level at the array position.

A. DAMAS2

DAMAS2 addresses the inverse problem formulated in Sec. II directly as stated in Eq. (5), which follows from Eqs. (1) and (2) considering a shift-invariant PSF. The algorithm consists of the following steps:

1. Step 0

Initialize the iteration index, $n = 0$, and use an estimate of s, $\tilde{s}^{(0)}$ to start. Typically this value is set to zero for the entire region of interest, i.e.,

$$\tilde{s}^{(0)}(\varphi) := 0, \quad \forall \varphi \in G. \tag{6}$$

Compute the value α, which is given by the discrete integral of the PSF,

$$\alpha = \sum_{\varphi \in G} H(\varphi - \varphi'), \tag{7}$$

for a source located at an angle φ', e.g., $\varphi' = 0°$.

Calculate the FFT of $H(\varphi)$,

$$F_H = \mathcal{F}[H(\varphi)]. \tag{8}$$

2. Step 1

Compute the estimate of the beamformer map b as

$$\tilde{b}^{(n)}(\varphi) := \mathcal{F}^{-1}[\mathcal{F}[\tilde{s}^{(n)}(\varphi)]\,F_H]. \tag{9}$$

Note that this expression follows from Eq. (5). In the original algorithm implemented for planar sparse arrays given by Dougherty in Ref. 10, the preceding expression is scaled by a Gaussian filter to smooth the retrieved sound distribution

Author's complimentary copy

and to minimize the influence of high wave-number noise, i.e., background noise induced by sources outside the region of interest.[11] However, for the case of UCAs, this filter is not necessary as all sources are placed inside the entire region of interest, between 0° and 360°.

3. Step 2

Apply a non-negativity constraint to update the value of $\tilde{s}$

$$\tilde{s}^{(n+1)}(\varphi) := \max\left(\tilde{s}^{(n)}(\varphi) + \frac{b(\varphi) - \tilde{b}^{(n)}(\varphi)}{\alpha}, 0\right).$$

4. Step 3

Increment the iteration index, $n = n + 1$.

5. Remaining steps

Repeat steps 1–3 until the standard deviation of the residual $r^{(n)}$ converges to zero. The residual is defined as the difference between the estimated beamforming map and the actual map

$$r^{(n)}(\varphi) := \tilde{b}^{(n)}(\varphi) - b(\varphi). \tag{10}$$

B. FFT-NNLS

Unlike DAMAS2, FFT-NNLS tries to minimize the square sum of the residuals, that is

$$\min\|\mathbf{Hs}-\mathbf{b}\|_2. \tag{11}$$

This can be solved by a gradient-type minimization procedure as suggested in Ref. 11. The steps are the following:

1. Step 0

Initialize the iteration index, $n = 0$, and $\tilde{s}^{(0)}$ before starting the iterative procedure. As in DAMAS2, $\tilde{s}^{(0)}$ is usually set to zero; see Eq. (6). Besides, compute F_H as in Eq. (8).

2. Step 1

Compute the residual vector $r^{(n)}$ from a given solution $\tilde{s}^{(n)}$ as follows:

$$r^{(n)}(\varphi) := \mathcal{F}^{-1}[\mathcal{F}[\tilde{s}^{(n)}(\varphi)]\, F_H] - b(\varphi).$$

Note that the first term of this difference is the estimate of the beamformer output at the nth iteration, $\tilde{b}^{(n)}$, as in Eq. (9).

3. Step 2

Calculate the gradient $w^{(n)}$ as

$$w^{(n)}(\varphi) := -\mathcal{F}^{-1}[\mathcal{F}[r^{(n)}(\varphi)]\, F_H].$$

4. Step 3

Use the following projection of the gradient

$$\bar{w}^{(n)}(\varphi) := \begin{cases} 0 & \text{if } w^{(n)}(\varphi) < 0 \text{ and } \tilde{s}^{(n)}(\varphi) = 0, \\ w^{(n)}(\varphi) & \text{otherwise.} \end{cases}$$

5. Step 4

Compute the auxiliary value $g^{(n)}$ as

$$g^{(n)}(\varphi) := \mathcal{F}^{-1}[\mathcal{F}[\bar{w}^{(n)}(\varphi)]\, F_H].$$

6. Step 5

Calculate an optimal step factor λ as

$$\lambda := -\frac{\sum_{\varphi} g^{(n)}(\varphi) r^{(n)}(\varphi)}{\sum_{\varphi} (g^{(n)}(\varphi))^2}.$$

7. Step 6

Update the solution $\tilde{s}^{(n+1)}$ using the non-negativity constrain as follows

$$\tilde{s}^{(n+1)}(\varphi) := \max(\tilde{s}^{(n)}(\varphi) + \lambda \bar{w}^{(n)}(\varphi), 0).$$

8. Step 7

Increment the iteration index, $n = n + 1$.

9. Remaining steps

Repeat steps 1–7 until the standard deviation of the residual $r^{(n)}$ converges to zero.

C. RL

For imaging deblurring purposes, RL assumes a shift-invariant PSF. One iteration cycle of the algorithm can be written as

$$\tilde{s}^{(n+1)}(\varphi) = \frac{1}{\alpha}\tilde{s}^{(n)}(\varphi)\left[\frac{b}{\tilde{s}^{(n)}(\varphi) * H(\varphi)} * H(\varphi)\right], \tag{12}$$

where the initial value is

$$\tilde{s}^{(0)}(\varphi) = \frac{1}{\alpha} b(\varphi). \tag{13}$$

If the initial value $\tilde{s}^{(0)}$ is non-negative (so the non-negativity constraint is fulfilled), RL guarantees that all generated solutions $\tilde{s}^{(n)}$ will be non-negative. Note that the scaling factor α given in the two previous expressions was not present in the original formulation. The reason for this is that normalized data was of concern, so that $\alpha = 1$. However, for the current investigation, the data is not normalized, and this value must represent the discrete integral of the PSF,[11] given in Eq. (7).

Making use of the Fourier transform to compute the convolutions the method consists of the following steps:

1. Step 0

Initialize the iteration index, $n = 0$, set the initial value of $\tilde{s}$, $\tilde{s}^{(0)}$, using Eq. (13) and compute F_H as in Eq. (8).

2. Step 1

Compute an estimate of the beamformer output as

$$\tilde{b}^{(n)}(\varphi) := \mathcal{F}^{-1}[\mathcal{F}[\tilde{s}^{(n)}(\varphi)]\, F_H].$$

Author's complimentary copy

3. Step 2

Calculate the ratio between the actual beamformer output and the estimated one,

$$x^{(n)}(\varphi) := \frac{b(\varphi)}{\tilde{b}^{(n)}(\varphi)}.$$

4. Step 3

Update the value $\tilde{s}$ according to the following expression

$$\tilde{s}^{(n+1)}(\varphi) := \frac{1}{\alpha}\tilde{s}^{(n)}(\varphi)\mathcal{F}^{-1}[\mathcal{F}[x^{(n)}(\varphi)]\,F_H].$$

5. Step 4

Increment the iteration index, $n = n + 1$.

6. Remaining steps

Repeat steps 1–4 until the standard deviation of the residual $r^{(n)}$ [defined as in Eq. (10)] converges to zero.

IV. SIMULATION AND MEASUREMENT RESULTS

In this section DAMAS2, FFT-NNLS, and RL are examined by means of computer simulations and measurements. The beamforming techniques used prior to the mentioned deconvolution algorithms will be introduced briefly before presenting the results.

A. Beamforming techniques for a UCA

DS beamforming and a more recent technique called CH beamforming, which is especially conceived for UCAs,[5,6] are the techniques selected to test the deconvolution algorithms. DS beamforming is based on delaying the signals captured at each array microphone by a certain amount and adding them up to focus the system to a specific direction in space that depends on the applied delay. Instead CH beamforming is based on decomposing the sound field into a summation of harmonics (as in a Fourier series) and comparing the resulting coefficients with the ones obtained from decomposing the expected sound field in the looking direction of the array. These techniques are implemented to localize the direction of sound sources that lay in the plane of the array, or close to it, but sufficiently far so that the generated waves are regarded as planar at the array position; see Fig. 1. Obviously beamforming procedures with such array geometry for mapping the sound field over 360° provide information about the azimuth of the source, φ', but do not account for its polar angle, θ', which means that those sources with a certain elevation are always projected in the plane of the array. For the present investigation, a UCA with the microphones flush-mounted on a rigid sphere as the one shown in Fig. 3 is assumed. This configuration provides better results than a UCA in which the microphones are suspended in free space in terms of both width of the main beam (resolution) and level of the largest secondary lobe (the so-called maximum side lobe level).[6]

FIG. 3. (Color online) UCA mounted on a rigid sphere.

Assuming a UCA of radius R and M microphones, the output of a CH beamformer focused toward φ is given in the Fourier transform domain (spatial frequency domain) by

$$b_{\mathrm{CH}}(kR,\,\varphi) = \left| A\sum_{m=1}^{M}\tilde{p}_m(kR)\sum_{n=-N}^{N}\frac{1}{Q_n(kR)}e^{-jn(\varphi_m-\varphi)}\right|^2, \tag{14}$$

where k is the wave number of the frequency of interest, A is a scaling factor, $\tilde{p}_m$ is the sound pressure captured by the mth microphone placed at an angle φ_m, and N is the maximum number of harmonics used for the algorithm. This value should follow $N = \lceil kR \rceil$, where $\lceil\cdot\rceil$ refers to the ceiling function, up to a maximum equal to $M/2 - 1$, to obtain the optimal map (higher orders would amplify the influence of noise dramatically).[5,6] The function $Q_n(kR)$ depends on the geometry of the UCA. For a UCA mounted on the equator of a rigid sphere,

$$Q_n(kR) = \sum_{q=|n|}^{\infty}(2q+1)(-j)^q\left(j_q(kR) - j'_q(kR)\frac{h_q(kR)}{h'_q(kR)}\right) \times \frac{(q-|n|)!}{(q+|n|)!}(P_q^{|n|}(0))^2, \tag{15}$$

where j_q and h_q are spherical Bessel and spherical Hankel functions of order q, j'_q and h'_q are their derivatives with respect to the radial direction r evaluated at $r = R$, and $P_q^{|n|}$ is a Legendre function of degree q and order n.

On the other hand, the output of a DS beamformer is expressed by

Author's complimentary copy

$$b_{\mathrm{DS}}(kR,\,\varphi) = \left| B\sum_{m=1}^{M}\tilde{p}_m(kR)\sum_{n=-N}^{N}Q_n^*(kR)e^{-jn(\varphi_m-\varphi)}\right|^2, \tag{16}$$

where B is a scaling factor and the parameter $Q_n(kR)$ is again given by Eq. (15). The value of N should be in this case at least $N = \lceil kR \rceil + 1$, up to a maximum equal to $M/2-1$ as for CH beamforming.

The scaling factors of CH and DS beamforming can be chosen such as the maximum value of the beamformer output is equal to one when a plane wave with amplitude unity is detected. To accomplish this A and B need to be $A = 1/(M(2N+1))$ and $B = \sum_{m=1}^{M} p_m(kR)p_m(kR)^*$, where p_m is the sound pressure of a plane wave of amplitude unity created at, e.g., 0°.

Regardless of the beamforming technique, it should be kept in mind that because the sound field is sampled at discrete positions with the array microphones, modal aliasing occurs at those frequencies the wavelength of which is less than twice the distance between two consecutive microphones. When aliasing occurs side lobes increase dramatically, becoming replicas of the main lobe in the worst case (the so-called aliased lobes).

From the given beamforming techniques, the PSF corresponding to each of them can be obtained assuming that a plane wave of amplitude unity is captured at the array. A detailed description of the calculation of the PSF can be found in the Appendix.

B. Test case using computer simulations

Let us assume a plane wave with frequency 1.6 kHz and amplitude $a = 2$ captured by a CH beamformer that consists of a UCA with radius 9.75 cm and 16 microphones mounted on the equator of a rigid sphere (corresponding to a microphone at every 22.5°). With this configuration, the array is capable of operating up to about 4.5 kHz without aliasing. The wave is generated by a source placed at an azimuth angle of 60°. The PSF of such beamformer and the beamformer output are shown in Fig. 4. As can be seen, the beamforming process successfully detects the wave because a main beam is visualized around 60°. However, the main beam is rather broad, and the map presents side lobes elsewhere, which can lead to confusion.

The beamformer map is then postprocessed with DAMAS2, FFT-NNLS, and RL. For these processes, a grid of azimuth angles from 0° to 359° with a resolution of 1° has been used. Note that besides the direction of the sources, the retrieved value s gives the information of the squared amplitude of the plane waves at the array position emitted by them because both the beamforming output and the PSF (given in the Appendix) correspond to magnitude squared functions.

The top row of Fig. 5 shows the source distribution recovered with DAMAS2, FFT-NNLS, and RL after 500 iterations. The three algorithms produce a clean map compared to the beamformer response; the direction of the source is pointed out with a narrow main lobe, and the effect of side lobes is practically removed. Theoretically the recovered sources should be represented by a delta function with its maximum being the squared amplitude of the plane wave (a^2), 4 in this case. However, none of the methods provides this result after 500 iterations.

An estimate of the squared amplitude of each impinging wave, $\tilde{a}^2$, can be obtained with an integration method that consists of summing the values $\tilde{s}(\varphi)$ inside the region of interest, G' (Ref. 12),

$$\tilde{a}^2 = \sum_{\varphi\in G'}\tilde{s}(\varphi). \tag{17}$$

The resulting level estimates obtained with DAMAS2, FFT-NNLS, and RL are 4.13, 4.04, and 4.00, respectively, which agree with the value of the squared amplitude of the plane wave under consideration.

The convergence of the algorithms given by the standard deviation of the residual (i.e., the difference between the estimated beamformer output and the actual one) as a function of the number of iterations n is shown in Fig. 6. For all the algorithms, the standard deviation of the residuals converges to a value close to zero when the number of iterations increases as expected. For this particular example, it can be seen that from about 5000 iterations, the standard deviation of the residuals is practically zero. Therefore ideally one

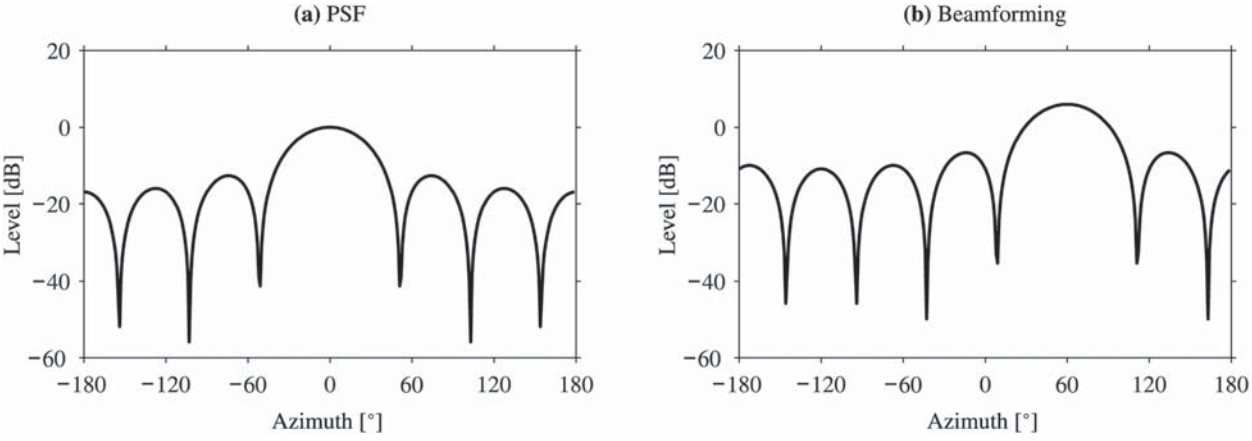

FIG. 4. PSF (left) and output (right) of a CH beamformer that consists of a UCA with 16 microphones mounted on the equator of a rigid sphere with radius of 9.75 cm. A source in the far field at $\varphi' = 60°$ is assumed for the simulations.

Author's complimentary copy

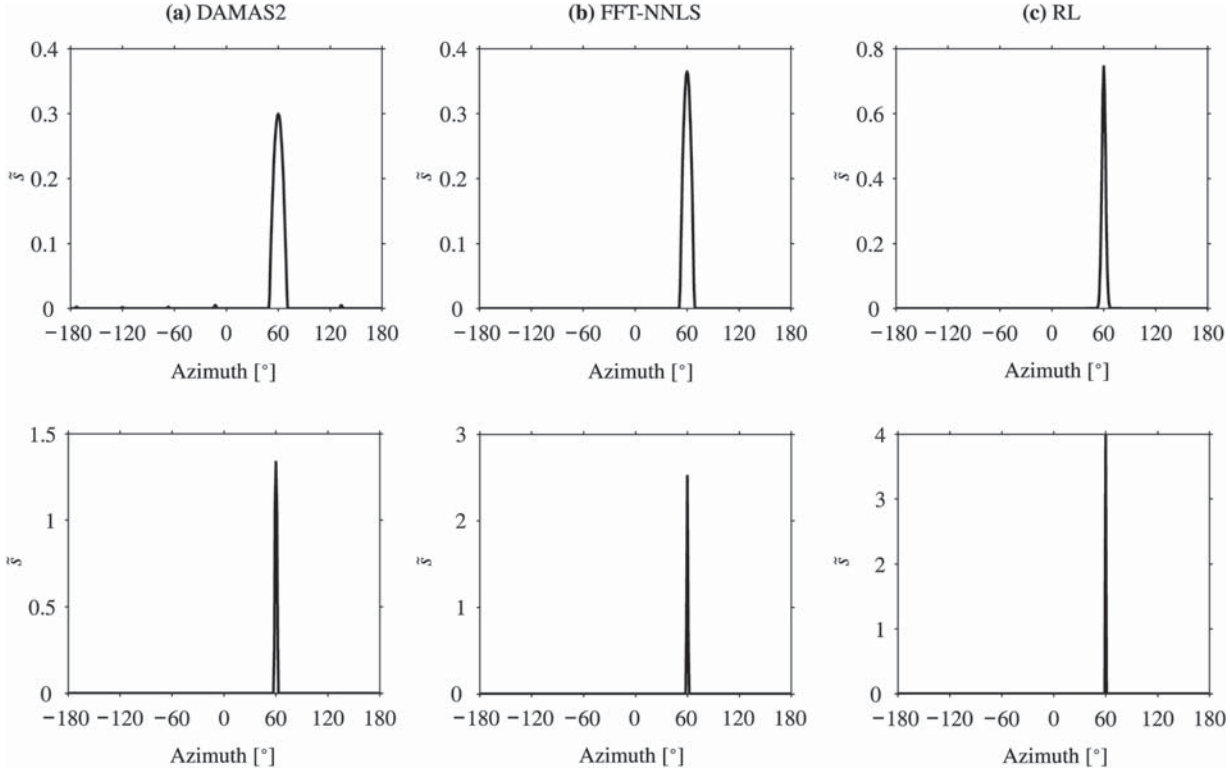

FIG. 5. Maps retrieved with DAMAS2 (left column), FFT-NNLS (middle column), and RL (right column) after 500 iterations (top row), and after 1×10^6 iterations (bottom row). A source in the far field at $\varphi' = 60^\circ$ is considered. CH beamforming is used prior to the deconvolution algorithms.

would expect a recovered source distribution represented by a delta function with a level of 4 at 60°. However, even after 1×10^6 iterations, the retrieved source distribution with DAMAS2 and FFT-NNLS differs from a delta function as can be seen in the bottom row of Fig. 5. In the case of RL, the result is much closer to the ideal response, but a close-up of the figure reveals that there is still some spreading (the peak is not exactly 4 and the neighboring values are not zero). This means that more iterations are needed to get a response as close as possible to the ideal response.

The deconvolution processes are particularly useful when more than one source are present in the sound field because they make it possible to locate the different sources even when they are not visible in the beamformer output. Let us consider that besides the source at 60° responsible for the previous plane wave with frequency 1.6 kHz, there is another source at 90° that creates a plane wave with unity amplitude at the same frequency. The two sources are incoherent. The beamformer map obtained with CH beamforming is shown in Fig. 7. As can be seen, the beamforming map reveals only a source located at about 60° (the maximum is actually at 63°). Although the main beam presents an asymmetric shape that can indicate that there is another source present, it is not possible to state that this is placed at 90° as assumed.

After applying deconvolution the maps shown in Fig. 8 are achieved with 5000 iterations. The three methods reveal

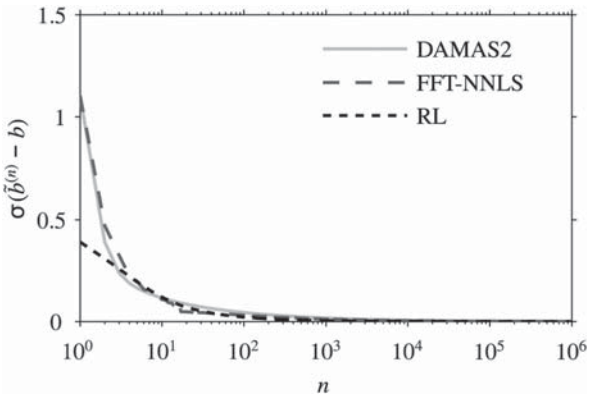

FIG. 6. Standard deviation of the residual as a function of the number of iterations n, for DAMAS2, FFT-NNLS, and RL.

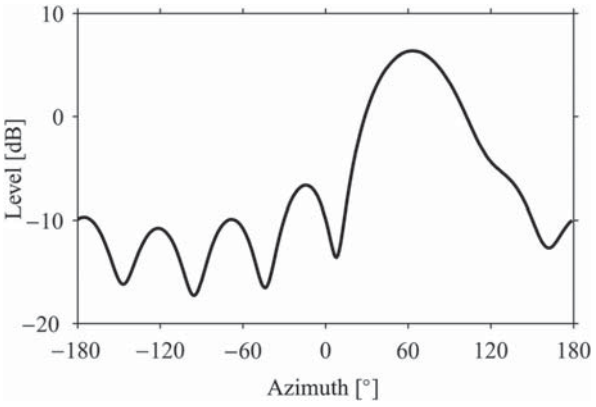

FIG. 7. Map obtained with CH beamforming. Two plane waves are present in the sound field, one with amplitude 2 created at 60° and another one with amplitude 1 created at 90°.

Author's complimentary copy

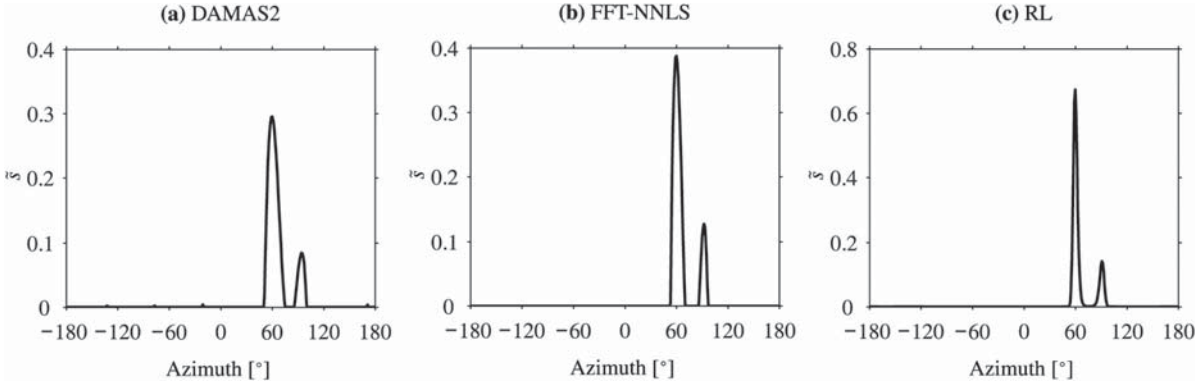

FIG. 8. Maps retrieved with DAMAS2, FFT-NNLS, and RL after 5000 iterations. Two sources in the far field at 60° and 90° are considered. CH beamforming is used prior to the deconvolution algorithms.

two sources, the strongest being located at 60° as expected. However, the other source is not exactly located at 90° but close to it: at 94° with DAMAS2, at 92° with FFT-NNLS, and at 91° with RL. The estimates of the squared amplitude of the sources are very close to the expected level of the two waves (2^2 and 1^2); 4.2 and 0.8 with DAMAS2, 4.1 and 0.9 with FFT-NNLS, and 4.0 and 0.9 with RL. As in the case of having only one source, it can be shown that with the increase of the number of iterations the maps become clearer, and moreover the source with less energy is located at an azimuth angle that tends to the actual value.

Although not shown similar results are obtained with DS beamforming.

C. Simulated and experimental data results

The deconvolution methods DAMAS2, FFT-NNLS, and RL have been tested experimentally and compared to computer simulations. For this purpose, measurements with the UCA shown in Fig. 3 were carried out in an anechoic room with a volume of about 1000 m^3. The array consisted of 16 1/4 in. microphones, Brüel and Kjær (B&K) type 4958, mounted on the equator of a rigid sphere with a radius of 9.75 cm. The array and the source, a loudspeaker, were controlled by a B&K PULSE analyzer. The loudspeaker was placed at 4 m from the array center but at the very same height at an azimuth angle of 180°. It was driven by a signal from the generator, pseudorandom noise of 1 s of period, 6.4 kHz of bandwidth, and 1 Hz of resolution. The signal had a duration of 5 s. The microphone signals were recorded with the analyzer, and after averaging for each channel, they were postprocessed with CH beamforming and DS beamforming in the frequency range from 50 Hz to 5.5 kHz. These procedures scanned directions from 0° to 359° with a resolution of 1°. Subsequently the obtained beamforming maps were processed with DAMAS2, FFT-NNLS, and RL, using 500 iterations.

1. Sound source localization

To analyze the performance of the deconvolution methods in terms of localization of sound sources, the beamforming maps prior to the deconvolution algorithms were normalized for simplicity.

The left side of Fig. 9 shows the normalized output obtained with CH beamforming and the source distribution maps obtained with deconvolution as a function of frequency. The predictions made with computer simulations are also depicted on the right side of the figure.

To account for the background noise present in the measurements, the simulations were carried out with a signal-to-noise ratio (SNR) of 30 dB at the input of each microphone due to uniformly distributed noise.

At first sight, it can be seen that measurements and simulations yield very similar results. The beamformer procedure (top row) reveals the direction of the main source at 180° in all the frequency range, but the main lobe is rather broad, specially at low frequencies, and side lobes appear along the map. However, the map is satisfactorily improved after applying DAMAS2 (second row), FFT-NNLS (third row), and RL (bottom row) because the main lobe becomes more directive and side lobes are reduced significantly. Interestingly, these procedures can still visualize the direction of the source clearly at those frequencies where aliasing in the beamforming map occurs, this is, above 4.5 kHz approximately. This effect could be important for those applications dealing with broadband sources. However, it has been observed that the retrieved map is free of aliasing just when a single source is present.

The results obtained with DS beamforming as well as the recovered maps after deconvolution are shown in Fig. 10. In this case, there is also a very good agreement between measurements and simulations. Similar to the results obtained with CH beamforming, the deconvolution algorithms yield an improved version of the beamforming map. Furthermore, they are capable of unveiling the direction of the source at very low frequencies where the DS beamformer is omnidirectional.

For both techniques, it can be seen that in the case under analysis 500 iterations are sufficient to demonstrate a clear improvement of the maps after deconvolution. However, the width of the main beam is not constant after the deconvolution processes; it becomes narrower with increasing frequency. This implies that to obtain better results at the lower frequencies, the deconvolution algorithms should include more iterations.

Although a comparison of the three techniques could be done at this point, this is out of the scope of the present study

Author's complimentary copy

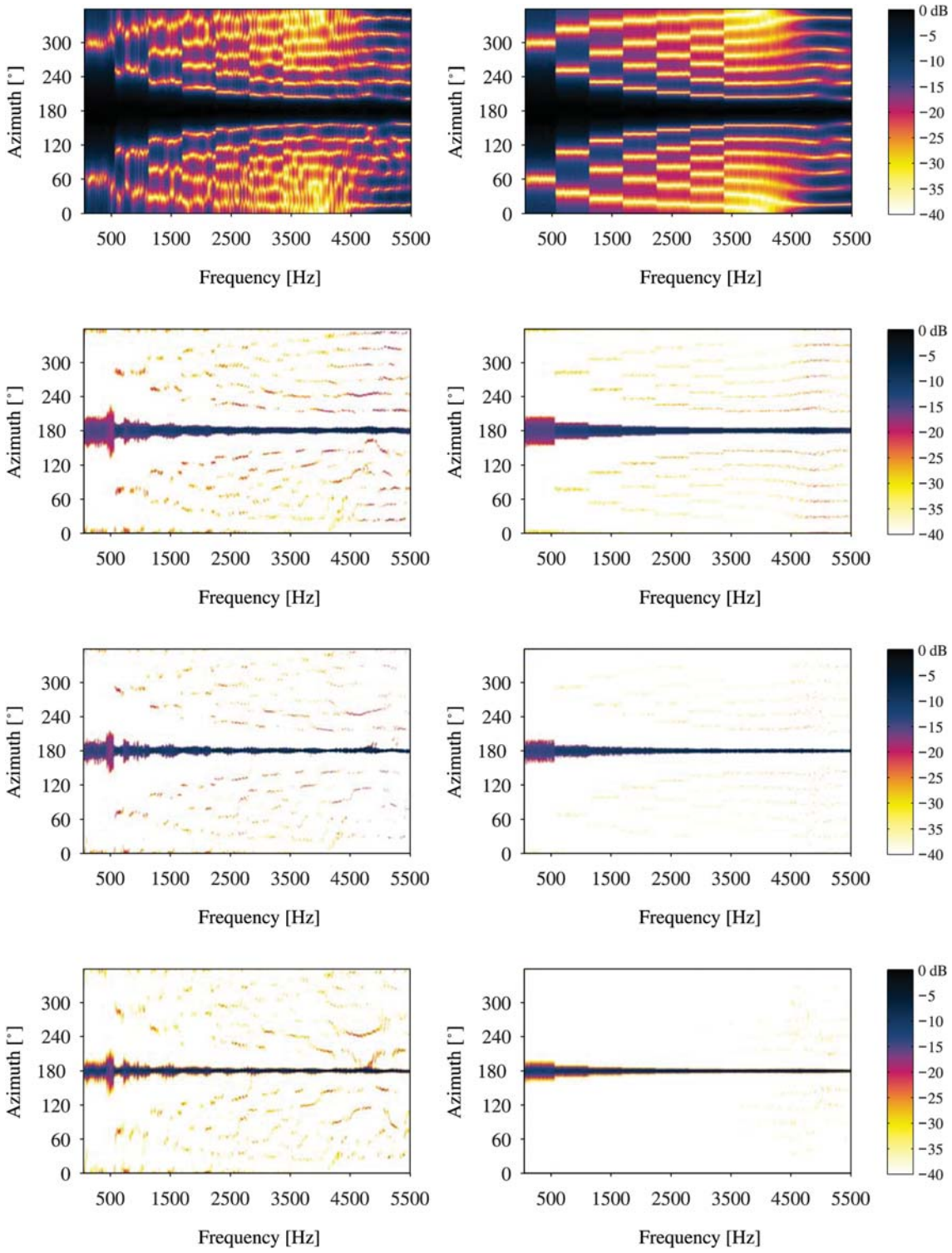

FIG. 9. (Color online) Normalized output obtained with CH beamforming (top row) and resulting maps after applying DAMAS2 (second row), FFT-NNLS (third row), and RL (bottom row). The left column shows experimental results and the right column computer simulations.

because it has been observed that their performance depends strongly on the case under analysis.

2. Estimated sound pressure level

The sound pressure level of the impinging waves at the array can be estimated after deconvolution by means of the estimated squared amplitude, see Eq. (17). As mentioned in Sec. II, the level of the sources cannot be estimated because these are assumed to be in the far field of the array, and therefore the wave fronts at the array position are practically planar.

The estimated sound pressure level obtained after deconvolution is similar to the sound pressure level captured

Author's complimentary copy

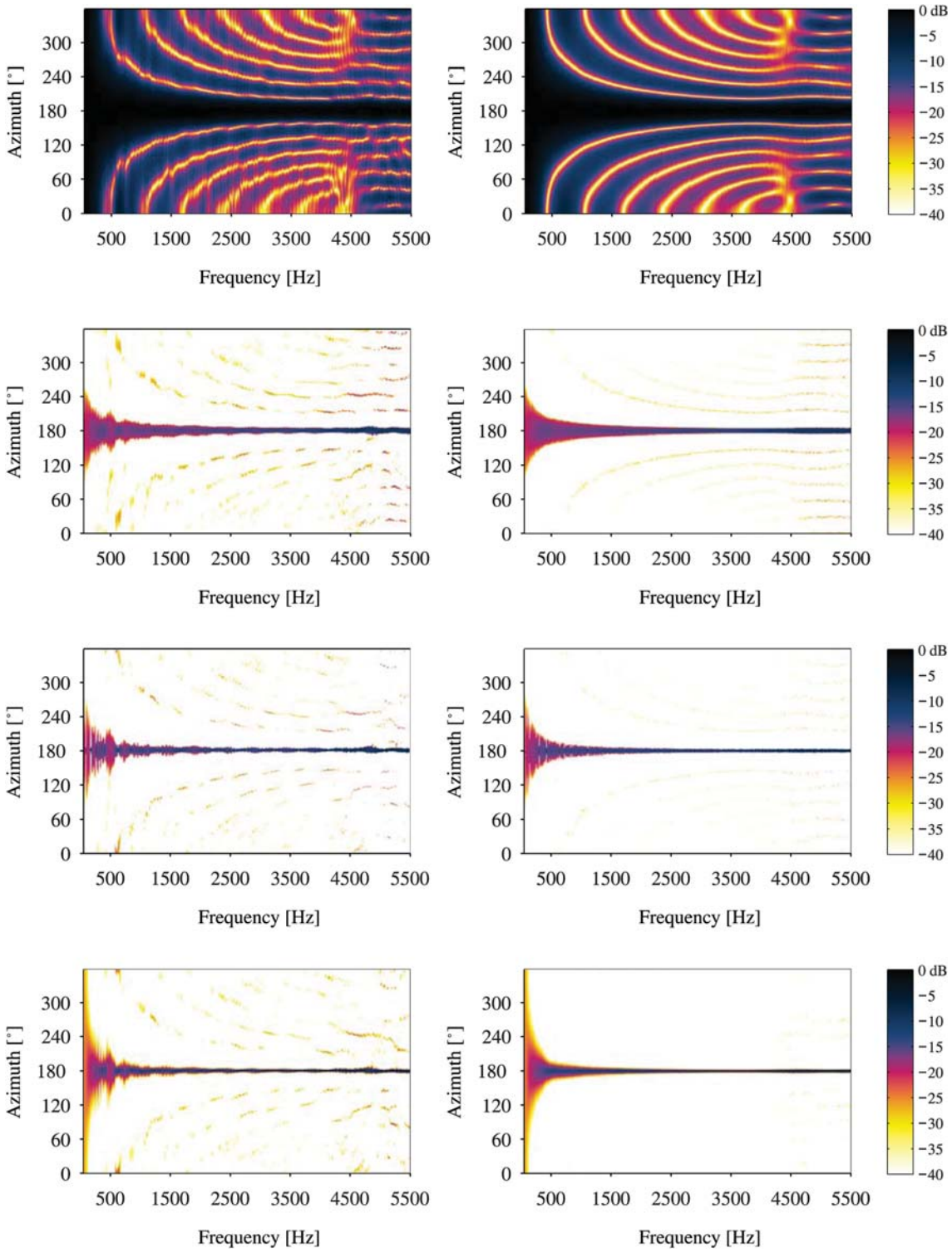

FIG. 10. (Color online) Normalized output obtained with DS beamforming (top row) and resulting maps after applying DAMAS2 (second row), FFT-NNLS (third row), and RL (bottom row). The left column shows experimental results and the right column computer simulations.

by the array microphones. To show this, in Fig. 11 the sound pressure level averaged across the array microphone signals is plotted together with the estimated sound pressure level retrieved with DAMAS2 when CH and DS beamforming are used prior to the deconvolution process. Note that for this analysis, the beamforming maps were not normalized, so that the recovered sound pressure level is comparable to the averaged sound pressure level captured by microphones.

The agreement between the estimated sound pressure level obtained after deconvolution and the averaged sound pressure level of the microphone signals is particularly good at lower frequencies. In fact, the curves are totally overlapped at these frequencies in the case of DS beamforming

Author's complimentary copy

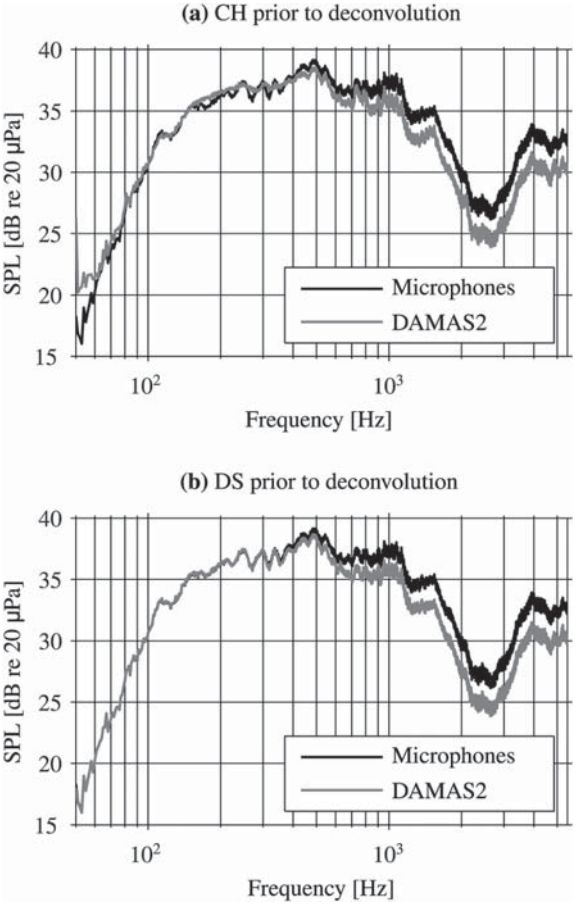

FIG. 11. Averaged sound pressure level captured by the array microphones and estimated sound pressure level obtained with DAMAS2. Maps with CH beamforming (top) and DS beamforming (bottom) are obtained prior to deconvolution.

prior to the deconvolution process, probably due to the robustness of this technique. With increasing frequency, the retrieved level with deconvolution becomes lower than the mean level of the microphones. The difference between low and high frequencies is given by the fact that at low frequencies, the rigid sphere does not affect the sound field, whereas at high frequencies, it acts as a scatterer. The averaged pressure at the microphones is amplified due to the scattering effect at these frequencies. However, with deconvolution, the effect of the scatterer is removed because this is accounted for in the beamforming algorithms given in Eqs. (14) and (16).

Although not shown, very similar results were obtained with FFT-NNLS and RL.

V. CONCLUSIONS

A UCA can be used for scanning the sound field over 360° to detect sound sources located in the array plane. By means of beamforming procedures, the direction of the existing incoherent sound sources can be found, but these procedures give rise to a blurred map. An investigation for improving the visualization of the beamforming map has been carried out by applying deconvolution procedures, which are capable of recovering the location of the actual sources with improved precision. The resulting maps present better resolution and are practically free from effects of side lobes. The deconvolution methods methods initially suggested for planar sparse arrays have been adapted to the circular geometry, which has the advantage that beamforming maps can be deblurred very efficiently with those deconvolution methods based on spectral procedures, namely, DAMAS2, FFT-NNLS, and RL. The performance of these methods has been examined for two beamforming techniques, DS and CH beamforming, with computer simulations and experimental results. For the three deconvolution methods, the resulting maps are improved by applying the deconvolution algorithms in comparison with the conventional beamforming maps.

APPENDIX: CALCULATION OF THE BEAMFORMER'S PSF

Consider a plane wave of amplitude a created by a source in the far field of a UCA, $ae^{j\mathbf{k}\cdot\mathbf{r}'}$. When the array is mounted on a sphere, the pressure captured at the surface of the sphere, at a point with spherical coordinates $[R,\ \theta,\ \varphi]$, is[23,24]

$$p(kR,\ \theta,\ \varphi,\ \theta',\ \varphi') = 4\pi a \sum_{q=0}^{\infty} b_q(kR) \sum_{v=-q}^{q} Y_q^v(\theta,\ \varphi) Y_q^v(\theta',\ \varphi')^*, \tag{A1}$$

where

$$b_q(kR) = (-j)^q \left(j_q(kR) - \frac{j_q'(kR)}{h_q'(kR)} h_q(kR) \right), \tag{A2}$$

$$Y_q^v(\theta,\ \varphi) \equiv \sqrt{\frac{(2q+1)}{4\pi} \frac{(q-v)!}{(q+v)!}} P_q^v(\cos\theta) e^{jv\varphi}. \tag{A3}$$

Note that in Eq. (A1), the temporal term $e^{-j\omega t}$ is omitted; and the angles of the position of the source $[\theta',\ \varphi']$ are used instead of the angles of the incident wave $[\theta_k,\ \varphi_k]$; these being related by $\theta' = \pi - \theta_k$ and $\varphi' = \varphi_k + \pi$ because the unit vector of the incident wave $\hat{\mathbf{k}}$ is opposite to the unit vector of the position of the source $\hat{\mathbf{r}}'$, $\hat{\mathbf{k}} = -\hat{\mathbf{r}}'$.

At the position of each microphone, $[R,\ \pi/2,\ \varphi_m]$, the pressure is

$$\tilde{p}_m(kR) = p(kR,\ \pi/2,\ \varphi_m,\ \theta', \varphi'). \tag{A4}$$

In the present study, the PSF is defined as the beamformer response to a plane wave of unit amplitude created by a source placed in the far field of the array, but at its very same plane, i.e., at an inclination angle $\theta' = \pi/2$ and azimuth angle φ'. The PSF is then obtained when the expression given in Eq. (A4) for a plane wave with amplitude $a = 1$ is inserted into the beamformers output given in Eqs. (14) and (16) for CH and DS beamforming, respectively. It should be emphasized that the PSF considered in the deconvolution methods presented in Sec. III requires that the source used for its calculation is placed at an angle $\varphi' = 0$; see Eq. (5). With these considerations the expressions of the PSF for CH and DS beamforming result in

Author's complimentary copy

$$H_{\mathrm{CH}}(kR,\varphi) = \left| \frac{4\pi}{M(2N+1)} \sum_{m=1}^{M} \sum_{q=0}^{C} b_q(kR) \times \sum_{v=-q}^{q} Y_q^v(\pi/2,\varphi_m) Y_q^v(\pi/2,0)^* \times \sum_{n=-N}^{N} \frac{1}{Q_n(kR)} e^{-jn(\varphi_m-\varphi)} \right|^2, \quad \text{(A5)}$$

and

$$H_{\mathrm{DS}}(kR,\varphi) = \left| \frac{4\pi}{M} \sum_{m=1}^{M} \sum_{q=0}^{C} b_q(kR) \times \sum_{v=-q}^{q} Y_q^v(\pi/2,\varphi_m) Y_q^v(\pi/2,0)^* \times \sum_{n=-N}^{N} Q_n^*(kR) e^{-jn(\varphi_m-\varphi)} \right|^2, \quad \text{(A6)}$$

where the coefficients Q_n are given in Eq. (15). Although the upper limit of the second summation operator of each technique, C, should be ideally infinity, it has to be truncated for implementation purposes. In the present study, the value used for C followed $\lceil kR \rceil + 5$ because this guaranteed that all the coefficients b_q that were left out of the summation had a value very close to zero.

[1]D. H. Johnson and D. E. Dudgeon, *Array Signal Processing Concepts and Techniques* (Prentice Hall, Englewood Cliffs, NJ, 1993), pp. 112–119.
[2]J. Meyer, "Beamforming for a circular microphone array mounted on spherically shaped objects," J. Acoust. Soc. Am. **109**(1), 185–193 (2001).
[3]G. Daigle, M. Stinson, and J. Ryan, "Beamforming with air-coupled surface waves around a sphere and circular cylinder (L)," J. Acoust. Soc. Am. **117**(6), 3373–3376 (2005).
[4]H. Teutsch and W. Kellermann, "Acoustic source detection and localization based on wavefield decomposition using circular microphone arrays," J. Acoust. Soc. Am. **120**(5), 2724–2736 (2006).
[5]E. Tiana-Roig, F. Jacobsen, and E. Fernandez-Grande, "Beamforming with a circular microphone array for localization of environmental noise sources," J. Acoust. Soc. Am. **128**(6), 3535–3542 (2010).
[6]E. Tiana-Roig, F. Jacobsen, and E. Fernandez-Grande, "Beamforming with a circular array of microphones mounted on a rigid sphere (L)," J. Acoust. Soc. Am. **130**(3), 1095–1098 (2011).
[7]A. Parthy, N. Epain, A. van Schaik, and A. T. Jin, "Comparison of the measured and theoretical performance of a broadband circular microphone array," J. Acoust. Soc. Am. **130**(6), 3827–3837 (2011).
[8]A. M. Torres, M. Cobos, B. Pueo, and J. J. Lopez, "Robust acoustic source localization based on modal beamforming and time-frequency processing using circular microphone arrays," J. Acoust. Soc. Am. **132**(3), 1511–1520 (2012).
[9]P. Sijtsma, "Circular Harmonics Beamforming with multiple rings of microphones," in *18th AIAA/CEAS Aeroacoustics Conference*, Colorado Springs, CO (June 4–6, 2012), AIAA Paper 2012–2224.
[10]R. P. Dougherty, "Extension of DAMAS and benefits and limitations of deconvolution in beamforming," in *11th AIAA/CEAS Aeroacoustics Conference*, Monterey, CA (May 23–25, 2005), AIAA Paper 2005–2961.
[11]K. Ehrenfried and L. Koop, "Comparison of iterative deconvolution algorithms for the mapping of acoustic sources," AAIA J. **45**, 1584–1595 (2007).
[12]T. F. Brooks and W. M. Humphreys, "A deconvolution approach for the mapping of acoustic sources (DAMAS) determined from phased microphone arrays," J. Sound Vib. **294**, 856–879 (2006).
[13]T. F. Brooks and W. M. Humphreys, "Extension of DAMAS phased array processing for spatial coherence determination (DAMAS-C)," in *12th AIAA/CEAS Aeroacoustics Conference*, Cambridge, MA (May 8–10, 2006), AIAA Paper 2006–2654.
[14]T. Yardibi, J. Li, P. Stoica, and L. Cattafesta III, "Sparsity constrained deconvolution approaches for acoustic source mapping," J. Acoust. Soc. Am. **123**(5), 2631–2642 (2008).
[15]T. Yardibi, J. Li, P. Stoica, N. Zawodny, and L. Cattafesta III, "A covariance fitting approach for correlated acoustic source mapping," J. Acoust. Soc. Am. **127**(5), 2920–2930 (2010).
[16]V. Fleury and J. Bulté, "Extension of deconvolution algorithms for the mapping of moving acoustic sources," J. Acoust. Soc. Am. **129**(3), 1417–1428 (2011).
[17]A. Xenaki, F. Jacobsen, E. Tiana-Roig, and E. Fernandez-Grande, "Improving the resolution of beamforming measurements on wind turbines," in *Proceedings of the 20th International Congress of Acoustics, Sidney, Australia* (2010), pp. 1–8.
[18]A. Xenaki, F. Jacobsen, and E. Fernandez-Grande, "Improving the resolution of three-dimensional acoustic imaging with planar phased arrays," J. Sound Vib. **331**, 1939–1950 (2012).
[19]J. J. Fuchs, "On the application of the global matched filter to DOA estimation with uniform circular arrays," IEEE Trans. Signal Process. **49**(4), 702–709 (2001).
[20]C. L. Lawson and R. J. Hanson, *Solving Least Squares Problems* (SIAM, Philadelphia, 1995), 351 pp.
[21]W. H. Richardson, "Bayesian-based iterative method of image restoration," J. Opt. Soc. Am. **62**, 55–59 (1972).
[22]L. B. Lucy, "An iterative technique for the rectification of observed distributions," Astronom. J. **79**, 745–754 (1974).
[23]E. G. Williams, *Fourier Acoustics: Sound Radiation and Nearfield Acoustic Holography* (Academic Press, London, 1999), pp. 4–5, 224–230.
[24]B. Rafaely, "Plane-wave decomposition of the sound field on a sphere by spherical convolution," J. Acoust. Soc. Am. **116**(4), 2149–2157 (2004).

Author's complimentary copy

Paper D

Towards an enhanced performance of uniform circular arrays at low frequencies

Elisabet Tiana-Roig [1], Antoni Torras-Rosell [2], Efren Fernandez-Grande [3], Cheol-Ho Jeong [4], and Finn T. Agerkvist [5]

[1, 3, 4, 5]Acoustic Technology, Dep. Electrical Engineering,

Technical University of Denmark, Ørsteds Plads 352, 2800 Kgs. Lyngby, Denmark

[2]DFM, Danish National Metrology Institute,

Matematiktorvet 307, 2800 Kgs. Lyngby, Denmark

ABSTRACT

Beamforming using uniform circular arrays of microphones can be used, e.g., for localization of environmental noise sources and for conferencing. The performance depends strongly on the characteristics of the array, for instance the number of transducers, the radius and whether the microphones are mounted on a scatterer such as a rigid cylinder or a sphere. The beamforming output improves with increasing frequency, up to a certain frequency where spatial aliasing occurs. At low frequencies the performance is limited by the radius of the array; in other words, given a certain number of microphones, an array with a larger radius will perform better than a smaller array. The aim of this study is to improve the performance of the array at low frequencies without modifying its physical characteristics. This is done by predicting the sound pressure at a virtual and larger concentric array. The propagation of the acoustic information captured by the microphones to the virtual array is based on acoustic holography. The predicted pressure is then used as input of the beamforming procedure. The combination of holography and beamforming for enhancing the beamforming output at low frequencies is examined with computer simulations and experimental results.
Keywords: Uniform circular array, Beamforming, Holography

1. INTRODUCTION

Beamforming based on a uniform circular array of microphones (UCA) is a well-known method to localize sound sources around the array from 0 to 360°. In the present paper, the main concern is the improvement of the performance at low frequencies. In the recent years, various strategies have been suggested

[1] etr@elektro.dtu.dk
[2] atr@dfm.dk
[3] efr@elektro.dtu.dk
[4] chj@elektro.dtu.dk
[5] fa@elektro.dtu.dk

in this matter, such as the design of beamforming techniques other than delay-and-sum. For instance, circular harmonics beamforming is a clear example of how a beamforming technique can be designed to suit a particular geometry, in this case, the circular geometry. This technique is based on the decomposition of the sound field in a series of coefficients by means of a Fourier series.[1] With this technique most of the frequency range is improved. Another possibility is to flush-mount the microphones on a rigid baffle, such as a rigid sphere or a spherical cylinder. The effect of the scatterer has proved to be beneficial compared to the case where the array microphones are suspended in the free space.[2–4] Yet another alternative is the use of deconvolution methods, which clean the beamforming map by means of iterative algorithms to finally recover the distribution of the sources present in the sound field. These methods are very effective, but require high computational effort, in particular at low frequencies. Methods such as the Deconvolution Approach for the Mapping of Acoustic Sources 2 (DAMAS2), the Fourier-based Non-Negative Least Squares (FFT-NNLS) and the Richardson-Lucy (RL) have already been adapted to the circular geometry.[5,6]

In all cases the performance improves with increasing frequency, up to a frequency where spatial aliasing occurs. The poor performance at the lowest frequencies is especially of concern with delay-and-sum because this presents an omnidirectional pattern, and therefore sources in this frequency range cannot be localized. Although the use of a scatterer improves its performance, it does not completely eliminate this problem. With deconvolution methods the low frequency problems can be resolved, even with beamforming patterns obtained originally with delay-and-sum. However if the same resolution is to be achieved in the entire frequency range, the lower the frequency the more the iterations needed. Or in other words, the deconvolution methods are less efficient at low frequencies.

In this article we suggest a simple method to improve the performance of UCAs at low frequencies, which does not imply the design of new beamforming techniques or a modification of the geometry of the array. The basic idea is that for a specific number of microphones, a UCA with a larger radius will perform better at low frequencies than an array with a smaller radius, because the distance between the microphones will be larger, and the wavelengths corresponding to the low frequencies will be better captured. Inspired by this concept, one could measure the sound field with a UCA, and by means of acoustic holography predict the sound pressure at a larger and virtual radius. The estimated pressure could be then used as input to the beamforming algorithm. A sketch of the procedure can be seen in Fig. 1.

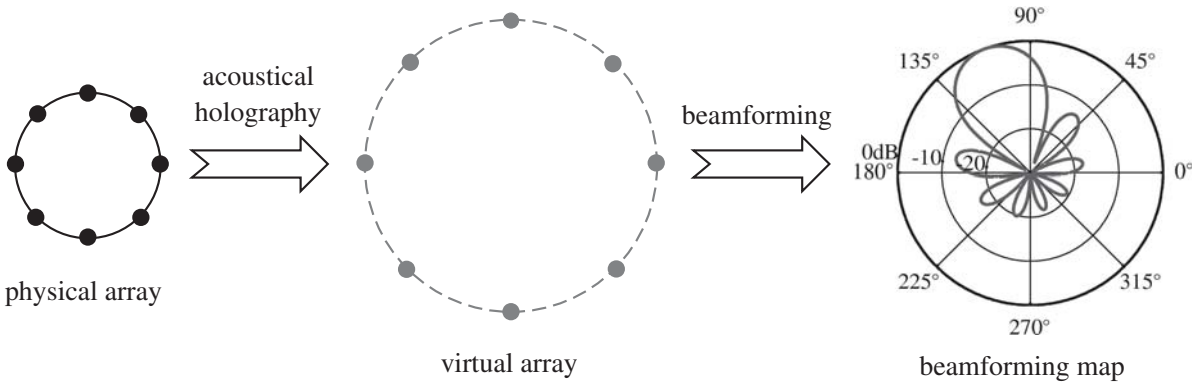

Fig. 1 – Sketch of the procedure for the calculation of the beamforming map. The pressure captured by a UCA is used for the prediction of the pressure at a larger and virtual array by means of acoustical holography. The predicted pressure is used as input of the beamforming procedure.

The combination of holography and beamforming for the improvement of the performance at low frequencies is the subject of study in the present work, and this is examined by means of computer simulations and experiments.

2. BACKGROUND THEORY

2.1. Acoustic Holography

Acoustic holography is a sound visualization technique that makes it possible to reconstruct the sound field over a three-dimensional space based on a two dimensional measurement. Often, the measurement is performed close to the source, as in near-field acoustic holography (NAH) to capture the evanescent waves for an enhanced spatial resolution.[7,8] However, in the present study we are concerned with the reconstruction of the sound field in the far field, prior to the beamforming processing.

In acoustic holography, the measured sound field is typically expanded into a series of basis functions from which the entire acoustic field can be reconstructed. In this paper we focus on a circular space, making use of the fact that the sound field can be predicted on different radii by means of the Bessel functions that account for the propagation in the radial direction. This approach is in a sense analogous to the one commonly used for NAH in spherical coordinates,[9–11] but in this case the radial functions are conventional Bessel functions, and the angular dependency is reduced to the azimuth only, as it follows from a circular harmonic expansion. It is worth noting that the inverse holographic reconstruction, i.e., when propagating towards the source, is an ill-posed problem that requires regularization. It has been shown that in the case of spherical NAH, truncation is an appropriate regularization procedure.[12] Similarly, truncation is adequate for the circular geometry.

Let us consider that a plane wave that travels perpendicularly to the z-axis (i.e., the wavefronts are parallel to the z-axis) is captured by a UCA of radius R placed at the xy-plane, at $z = 0$. The sound pressure at the array can be represented in terms of solutions of the Helmholtz equation in a cylindrical coordinate system with origin at the center of the UCA. After applying the boundary conditions (basically that the sound field at the origin must be finite), the pressure can be expressed as[7]

$$p(kr, \varphi) = \sum_{n=-\infty}^{\infty} A_n J_n(kr) e^{jn\varphi}, \tag{1}$$

where k is the wavenumber and A_n is the coefficient of the n'th term. As can be seen the angular dependency of the pressure is given by the circular harmonics $e^{jn\varphi}$, whereas the radial dependency is given by the Bessel functions J_n. Note that the time dependency $e^{-j\omega t}$ is omitted. The previous expression can be ideally used to determine a particular sound field at any point by means of acoustic holography. For this purpose we need to determine the values of the coefficients A_n. The pressure at the UCA, at $r = R$ is

$$p(kR, \varphi) = \sum_{n=-\infty}^{\infty} A_n J_n(kR) e^{jn\varphi}. \tag{2}$$

Making use of the orthogonality of the circular harmonics,

$$\frac{1}{2\pi} \int_0^{2\pi} e^{jn\varphi} e^{-jm\varphi} d\varphi = \delta_{mn}, \tag{3}$$

the coefficients A_n can be retrieved by multiplying each side of Eq. (2) by a complex conjugated circular harmonic and integrating over the entire circle, from 0 to 2π. The resulting expression follows

$$A_n = \frac{\frac{1}{2\pi} \int_0^{2\pi} p(kR, \varphi) e^{-jn\varphi} d\varphi}{J_n(kR)}. \tag{4}$$

This expression implies a continuous integral of the sound pressure. However the pressure is known at discrete positions, because the sound field is sampled with M microphones. Therefore, the integral must be approximated by means of a finite summation:

$$\int_0^{2\pi} p(kR, \varphi) e^{-jn\varphi} d\varphi \quad \Rightarrow \quad \sum_{i=1}^{M} \alpha_i p(kR, \varphi_i) e^{-jn\varphi_i}, \tag{5}$$

where the coefficients α_i must equal $2\pi/M$ to keep the orthogonality properties of the circular harmonics given in Eq. (3) in discrete notation. Finally the coefficients A_n are calculated as

$$\hat{A}_n = \frac{\frac{1}{M} \sum_{i=1}^{M} p(kR, \varphi_i) e^{-jn\varphi_i}}{J_n(kR)}. \tag{6}$$

By inserting this expression into Eq. (1), the sound pressure can be, in principle, predicted anywhere. As mentioned earlier, regularization is needed in practice. This is done by truncating the limits of the summation presented in Eq. (2) to certain values $-N$ and N,

$$p(kr, \varphi) = \sum_{n=-N}^{N} \hat{A}_n J_n(kr) e^{jn\varphi}. \tag{7}$$

It can be shown that a reasonable value of N follows $N = \lceil kr \rceil + 1$, where $\lceil \cdot \rceil$ is the ceiling function, up to a maximum value $M/2 - 1$.

2.2. Beamforming

Beamforming is a signal processing technique commonly used in acoustics to localize sound sources. The beamforming technique used in the present study is the classical delay-and-sum beamforming, which is a very simple, but robust, method. It is based on delaying the signals of each array microphone by a certain amount and adding them together, to reinforce the resulting signal. Depending on the delay applied to the different microphones the array is steered to a particular direction.[13] Expressed in the spatial frequency domain the beamforming output follows

$$b(kR,\varphi) = A\sum_{m=1}^{M} w_i \tilde{p}(kR,\varphi_m)p^*(kR,\varphi_m), \tag{8}$$

where w_m is the weighting coefficient of the m'th microphone, $\tilde{p}(kR,\varphi_m)$ is the pressure measured at the m'th microphone, and $p^*(kR,\varphi_m)$ is the theoretical complex conjugated pressure due to a plane wave with origin at φ. In the presence of a single source, when the beamformer is focused to the direction of the actual source, the maximum output is achieved. Ideally the beamformer would present a peak at the direction of the source and zeros elsewhere, but this is not the case due to the fact that the sound field is captured at discrete positions with the microphones. This implies that the beamforming map presents a main lobe around the direction of the source and side lobes elsewhere.

In case of an unbaffled UCA, the theoretical pressure is simply the closed form for a plane wave, $e^{j\boldsymbol{k}\cdot\boldsymbol{r}}$, at the array microphones, so the beamformer output is

$$b(kR,\varphi) = \frac{1}{M}\sum_{m=1}^{M} \tilde{p}(kR,\varphi_m)e^{jkR\cos(\varphi_m-\varphi)}. \tag{9}$$

Note that the weights w_m have been set to 1 and $A = 1/M$, in order to have a maximum beamformer output equal to one when a plane wave of amplitude unity is present.

Although the focus of the current study is the improvement of the performance at low frequencies, it should be mentioned that the operation of a beamformer is limited at high frequencies when the Nyquist sampling criterion is not fulfilled, i.e., at those frequencies whose corresponding wavelengths are less than twice the distance between two adjacent microphones. When aliasing occurs side lobes increase dramatically, becoming replicas of the main lobe in the worst case (the so-called aliased lobes).

2.3. Combining acoustic holography with beamforming

The aim of this study is to combine acoustic holography and beamforming to improve the beamforming output at low frequencies. As shown in Fig. 1 the pressure is measured with a UCA of radius R and M microphones placed at φ_i. By means of holography the pressure is predicted at a larger and virtual array of radius R_v. In the present study the number of virtual microphones and their azimuth angles are the same as for the actual array. In fact, by means of simulations it has been observed that the position of the microphones is not that relevant as long as the distance between microphones remains constant. This makes sense since UCAs are practically shift-invariant, i.e., the beamforming pattern is the same regardless the focusing direction.[14]

The pressure predicted with acoustic holography, which follows from evaluating Eq. (1) at (R_v,φ_i), is then used as input of the beamforming procedure. The coefficients $\hat{A}_n$ given in Eq. (6) are obtained with the pressure measured with the actual array microphones. Then the beamforming algorithm follows from inserting Eqs. (6) and (7) into Eq. (9),

$$b(kR_v,\varphi) = \frac{1}{M^2}\sum_{m=1}^{M}\sum_{n=-N}^{N}\sum_{i=1}^{M} \tilde{p}(kR,\varphi_i)\frac{J_n(kR_v)}{J_n(kR)}e^{j(n(\varphi_m-\varphi_i)+kR_v\cos(\varphi_m-\varphi))}, \tag{10}$$

where $N = \lceil kR_v \rceil + 1$, up to a maximum value $M/2-1$.

3. RESULTS AND DISCUSSION

3.1. Computer simulations

The effect of combining beamforming and holography is analyzed in this section by means of computer simulations. A UCA like the one shown in Fig. 2 has been assumed. The array radius is $R = 11.9$ cm and it has 12 microphones. The array used for the simulations coincides with the array used for the measurements

Fig. 2 – Prototype UCA of radius 11.9 cm and 12 microphones used for the measurements.

presented in the next section. Following from the Nyquist sampling theorem, this array will present spatial aliasing from ca. 2.8 kHz.

A plane wave generated at $180°$ is considered. The frequency range of interest is from 50 Hz to 2 kHz. A signal-to-noise ratio (SNR) of 30 dB at each array microphone due to uniformly distributed noise is assumed for the simulations to account for background noise.

Beamforming has been performed in the usual way with the pressure at the array microphones following from Sec. 2.2. Besides this, by means of holography, the simulated pressure has been used to predict the pressure at a larger and virtual radius, twice the size of the actual array radius ($2R$) at the same azimuth angles. The predicted pressure at the virtual array has been used for the beamforming procedure as indicated in Sec. 2.3. In parallel, beamforming has been performed in ideal conditions (in absence of noise) with a UCA of radius $2R$ and 12 microphones. Note that for this case, as well as for the case of the virtual array, aliasing is expected from about 1.4 kHz; i.e., the operating frequency range is half the range of the array of radius R.

For ease of understanding the resulting normalized beamforming outputs for a single frequency, in this case 400 Hz, are shown in Fig. 3. It can be seen that in all cases a main lobe around $180°$ is present, which

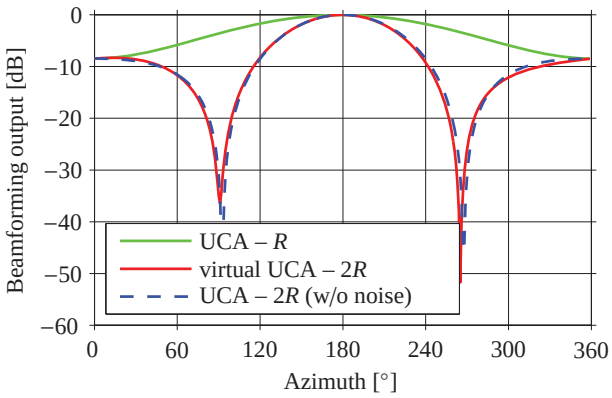

Fig. 3 – Normalized beamforming outputs at 400 Hz obtained with three UCAs with 12 microphones: a real array of radius $R = 11.9$ cm, a virtual array of radius $2R$ and a real array of radius $2R$.

indicates that there is a source in this direction, as expected. However the main lobe obtained with the array with radius R is very wide, which can lead to confusion, whereas the virtual array and the array with radius $2R$ present a narrower main lobe, which makes the interpretation of the map clearer.

The maps obtained for all frequencies are shown in Fig. 4. Note that Fig. 3 corresponds to a vertical cut

of the beamforming maps at 400 Hz.

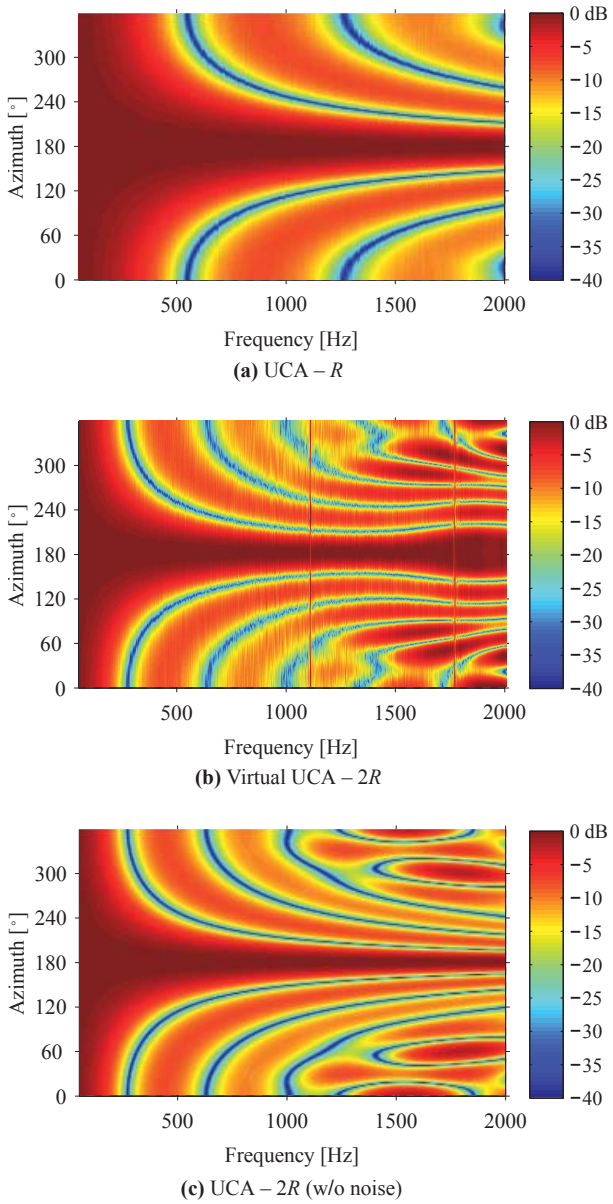

(a) UCA – R

(b) Virtual UCA – $2R$

(c) UCA – $2R$ (w/o noise)

Fig. 4 – Normalized beamforming maps obtained with three UCAs with 12 microphones. (Top) map obtained with an array of radius $R = 11.9$ cm, (middle) map obtained with a virtual array of radius $2R$ by means of combining holography and beamforming, and (bottom) ideal map obtained with an array of radius $2R$. A source at $180°$ is assumed. For the small and the virtual array a SNR of 30 dB is accounted for.

In all the cases the maps are omnidirectional at the lowest frequencies. With increasing frequency the patterns become more directive, unveiling a source at $180°$. For the virtual array and the array of radius $2R$ aliasing is observed at about 1.4 kHz as expected.

The virtual array is more directive at low frequencies compared to the actual array of radius R as expected from the theory. In fact the virtual array is omnidirectional in a narrower frequency range (half the range of the actual array) and from the upper frequency limit of the omnidirectional range it becomes more and more directive. Regarding the level of the side lobes, it can be seen that in both cases the levels are similar.

The performance of the virtual array is very similar to the ideal performance of the array of radius $2R$, up to the Nyquist sampling frequency where differences are observed. This shows that the virtual array behaves in this range as a real array with the same radius. The most apparent difference is the vertical line at 1103 Hz, which shows that for that frequency the beamforming is rather omnidirectional. This is caused by the fact

that the Bessel function in the denominator of Eq. (10) is zero for $n = 0$ at that frequency.

Alternatively to the beamforming maps, the performance of the array can be analyzed by means of two measures: the resolution and the maximum side lobe level (MSL). The resolution is the -3 dB width of the main lobe, whereas the MSL is the difference between the highest secondary lobe and the main lobe. In both cases, the smaller the values, the better. The resolution and the MSL are shown in Fig. 5.

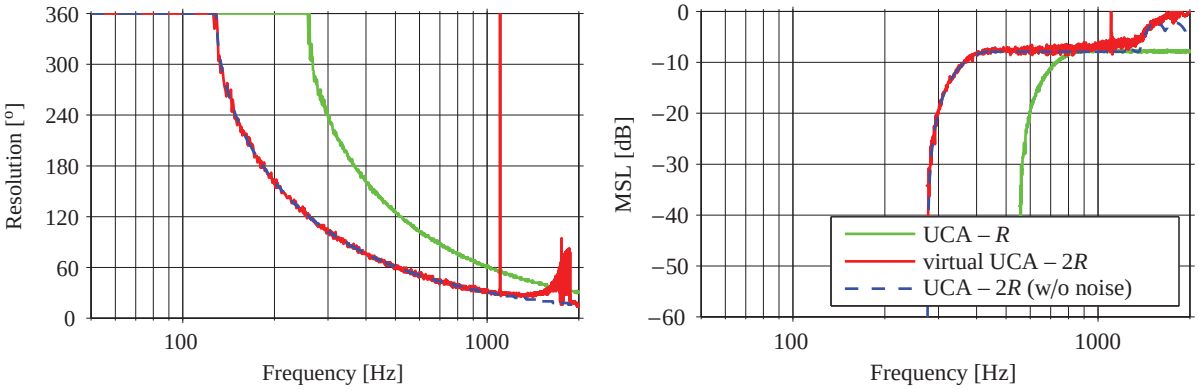

Fig. 5 – Resolution (left) and MSL (right) obtained with UCA of radius $R = 11.9$ cm and 12 microphones, a virtual UCA with radius $2R$, and an ideal UCA of radius $2R$. A plane wave created by a source at $180°$ is assumed. For the small array and the virtual array a SNR of 30 dB is considered.

These two measures confirm that the virtual array behaves like a real array with the same dimensions, especially in terms of resolution, up to the frequencies where sampling error occurs. However, in terms of MSL the levels are slightly higher for the virtual array from about 800 Hz. The peak at 1103 Hz seen in both the resolution and MSL with the virtual array corresponds to the singularity observed previously in the beamforming map.

3.2. Experimental results

Measurements with the prototype array with radius 11.9 cm and 12 microphones shown in Fig. 2 were carried out in an anechoic room of dimensions 12.1 m $\times$ 9.7 m $\times$ 8.5 m. The array microphones were 1/4 in. microphones Brüel & Kjær (B&K) Type 4935.

A picture of the set-up is shown in Fig. 6. The array and the source placed in the far-field of the array were controlled by a B&K PULSE analyzer. The loudspeaker was driven with a signal from the generator, pseudorandom noise of 1 s of period, 3.2 kHz of bandwidth, and 1 Hz of resolution. Each microphone signal was recorded with the analyzer, and after Fourier transforming they were postprocessed with beamforming. The resulting map can be seen in the top panel of Fig. 7.

The data from the microphones were used to predict the pressure by means of acoustical holography at a virtual UCA with twice the radius of the array used for the measurements. With the predicted pressure used as input of the beamforming algorithm, the normalized map shown in the bottom of Fig. 7 was obtained. As can be seen the beamforming maps are very similar to the maps obtained with simulations in the previous section, although they appear slightly more blurry.

The resolution and the MSL for the actual and the virtual arrays can be seen in Fig. 8. These two measures resemble the curves obtained with simulations. In terms of the resolution, the major differences are observed in the peak at 1103 Hz, which is more abrupt, and in the region where aliasing occurs, although this region is not of interest. For the MSL it can be seen that the curves appear slightly shifted towards high frequencies compared with the simulations, and that the MSL of the virtual array is a bit higher than expected in the range between 800 Hz and 1 kHz.

In any case, the results prove that at the low frequencies the actual (and small) array benefits from using holography to predict the pressure at a larger and virtual radius and combine it with beamforming.

4. FINAL REMARKS AND FUTURE WORK

In this article it has been shown that the performance of delay-and-sum beamforming improves at low frequencies by combining acoustic holography with beamforming. The procedure is the following: the pressure captured by a UCA is used to predict the pressure at a virtual array with a larger radius by means of

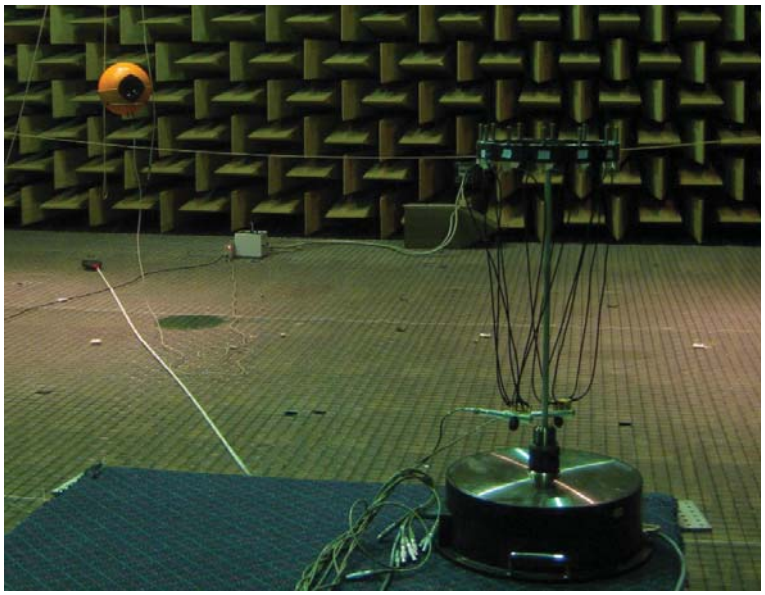

Fig. 6 – Measurement set-up.

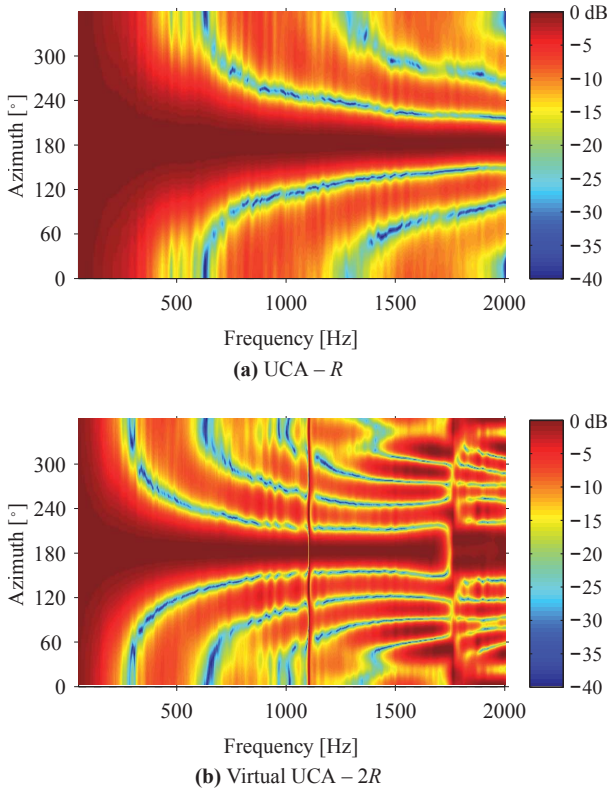

(a) UCA – *R*

(b) Virtual UCA – 2*R*

Fig. 7 – (Top) Normalized beamforming map obtained with a UCA with 12 microphones and radius 11.9 cm. The pressure captured by the array microphones is used to predict the pressure at a virtual UCA with twice the radius of the original array by means of acoustical holography. The predicted pressure is used to compute the normalized beamfroming map (bottom).

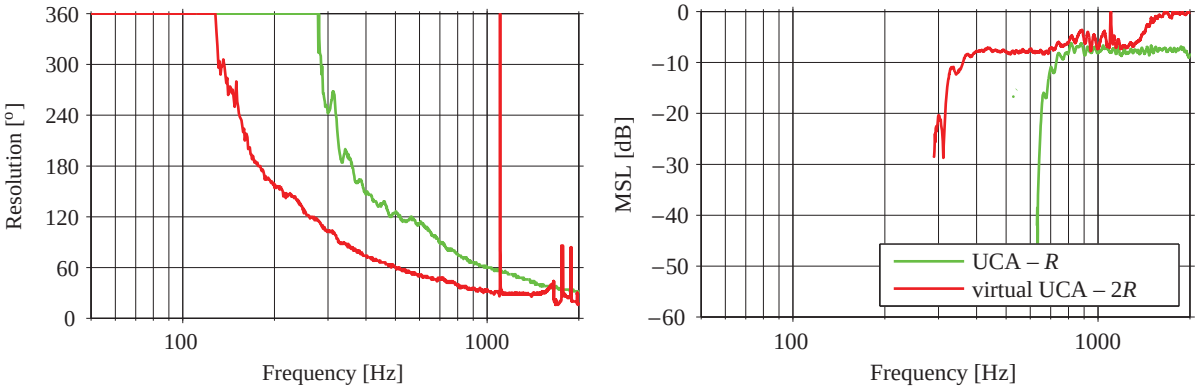

Fig. 8 – Resolution (left) and MSL (right) obtained with UCA of radius $R = 11.9$ cm and 12 microphones and a virtual UCA with radius $2R$. A plane wave was created by a source at $180°$.

acoustical holography. The predicted pressure is then used as input to the delay-and-sum beamforming algorithm. The benefits of using a virtual array have been proven by means of simulations and experimental results.

The combination of holography and beamforming adds new features to UCAs without any additional cost. Specifically the array gains more flexibility, for example at high frequencies the array measurements could be used directly for the beamforming procedure in the usual way, whereas at low frequencies acoustic holography could be used prior to beamforming to enhance the beamforming map at those frequencies.

There are still some questions that need to be examined further, e.g., the effect of using other beamforming techniques different from delay-and-sum beamforming, the applicability of the method in noisier conditions, and how large the virtual array can be. In this sense virtual arrays with radius larger than twice the radius of the actual array have been tested. The results, which are not included in the article, reveal that both resolution and MSL become worse than expected with increasing the radius. However this statement needs additional investigation.

The idea presented in the present study can be applied to other UCAs mounted on a scatterer such as a rigid cylinder, or to spherical arrays to map a three dimensional sound field.

ACKNOWLEDGMENTS

The authors are thankful to Finn Jacobsen who was involved in this study at an early stage.

REFERENCES

[1] E. Tiana-Roig, F. Jacobsen, and E. Fernandez-Grande, “Beamforming with a circular microphone array for localization of environmental noise sources”, J. Acoust. Soc. Am. **128(6)**, 3535–3542 (2010).

[2] G. Daigle, M. Stinson, and J. Ryan, “Beamforming with air-coupled surface waves around a sphere and circular cylinder (L)”, J. Acoust. Soc. Am. **117(6)**, 3373–3376 (2005).

[3] H. Teutsch and W. Kellermann, “Acoustic source detection and localization based on wavefield decomposition using circular microphone arrays”, J. Acoust. Soc. Am. **120(5)**, 2724–2736 (2006).

[4] E. Tiana-Roig, F. Jacobsen, and E. Fernandez-Grande, “Beamforming with a circular array of microphones mounted on a rigid sphere (L)”, J. Acoust. Soc. Am. **130(3)**, 1095–1098 (2011).

[5] E. Tiana-Roig and F. Jacobsen, “Acoustical source mapping based on deconvolution approaches for circular microphone arrays”, in *Proceedings of Inter-noise 2011, Osaka, Japan* (2011).

[6] E. Tiana-Roig and F. Jacobsen, “Deconvolution for the localization of d sources using a circular microphone array,”, J. Acoust. Soc. Am. (To be published).

[7] E. G. Williams, *Fourier Acoustics: Sound radiation and near field acoustic holography* (Academic, London) (1999).

[8] J. D. Maynard, E. G. Williams, and Y. Lee, “Nearfield acoustic holography : I . Theory of generalized holography and the development of NAH”, J. Acoust. Soc. Am. **78(4)**, 1395–1413 (1985).

[9] E. G. Williams, N. Valdivia, and P. C. Herdic, "Volumetric acoustic vector intensity imager", J. Acoust. Soc. Am. **120(4)**, 1887–1897 (2006).

[10] E. G. Williams and K. Takashima, "Vector intensity reconstructions in a volume surrounding a rigid spherical microphone array", J. Acoust. Soc. Am. **127(2)**, 773–783 (2010).

[11] F. Jacobsen, G. M. Pescador, E. Fernandez-Grande, and J. Hald, "Near field acoustic holography with microphones on a rigid sphere (L)", J. Acoust. Soc. Am. **129(6)**, 3461–3464 (2011).

[12] A. Granados, F. Jacobsen, and E. Fernandez-Grande, "Regularized reconstruction of sound fields with a spherical microphone array", in *ICA 2013 Montreal, Montreal, Canada* (2013).

[13] D. Johnson and D. Dudgeon, *Array Signal Processing Concepts and Techniques* (Prentice Hall, Englewood Cliffs, New Jersey) (1993).

[14] J. Meyer, "Beamforming for a circular microphone array mounted on spherically shaped objects", J. Acoust. Soc. Am. **109(1)**, 185–193 (2001).

Paper D

BeBeC-2014-03

ENHANCING THE BEAMFORMING MAP OF SPHERICAL ARRAYS AT LOW FREQUENCIES USING ACOUSTIC HOLOGRAPHY

Elisabet Tiana-Roig[1], Antoni Torras-Rosell[2], Efren Fernandez-Grande[1], Cheol-Ho Jeong[1] and Finn T. Agerkvist[1]

[1]Acoustic Technology, Dep. Electrical Engineering, Technical University of Denmark
Ørsteds Plads 352, 2800 Kgs. Lyngby, Denmark
[2]DFM, Danish National Metrology Institute
Matematiktorvet 307, 2800 Kgs. Lyngby, Denmark

ABSTRACT

Recent studies have shown that the localization of acoustic sources based on circular arrays can be improved at low frequencies by combining beamforming with acoustic holography. This paper extends this technique to the three dimensional case by making use of spherical arrays. The pressure captured by a rigid spherical array under free-field conditions is used to compute the expected pressure on a virtual and larger sphere by means of acoustic holography. Beamforming is then applied with the pressure predicted at the virtual array. Since the virtual array has a larger radius compared to the one of the physical array, the low frequencies (the ones with larger wavelength) are better captured by the virtual array, and therefore, the performance of the resulting beamforming system is expected to improve at these frequencies. The proposed method is examined with simulations based on delay-and-sum beamforming. In addition, the principle is validated with experiments.

1 INTRODUCTION

Spherical arrays of microphones have been of interest in the last decade, because of the ability to measure in a three-dimensional sound field [1, 2]. Typically, these arrays are suitable for sound source localization using beamforming [3–6] and for sound recording in higher order reproduction systems such as Ambisonics [7–9].

Several strategies to improve the performance of beamforming systems have been suggested in the recent years. For example, it has been shown that arrays with flushed-mounted microphones on a rigid sphere perform better compared to open (or transparent) spherical arrays [2, 10, 11]. Besides this, different beamforming techniques have been designed for this geometry [6]. Among them, phase-mode (or spherical harmonics) beamforming is of particular interest, because it exploits the spherical geometry by decomposing the sound field in a series of spherical harmonics. Compared to the classical delay-and-sum beamforming, phase-mode beamforming presents a better directivity, at the expense of being more sensitive to noise [5]. In fact, delay-and-sum beamforming is a very robust technique, but it performs poorly at low frequencies, being omnidirectional in the worse case.

Inspired by an article on uniform circular arrays presented recently in Ref. [12], the present article examines the possibility of enhancing the localization of noise sources with spherical arrays at low frequencies by combining spherical acoustic holography [13–15] and delay-and-sum beamforming. The idea behind this concept is that for a given number of transducers, an array with a larger radius will perform better at low frequencies than a smaller array [2]. However, if one cannot change the geometry of the array, a simple solution to obtain a virtually larger array is illustrated in Fig. 1: the sound pressure is captured with a spherical array (rigid or transparent), and by means of acoustic holography the pressure is predicted at a virtual spherical array with larger radius. Finally the pressure at this virtual array is used for the beamforming process. The theory presented in this work is supplemented with simulations and measurements.

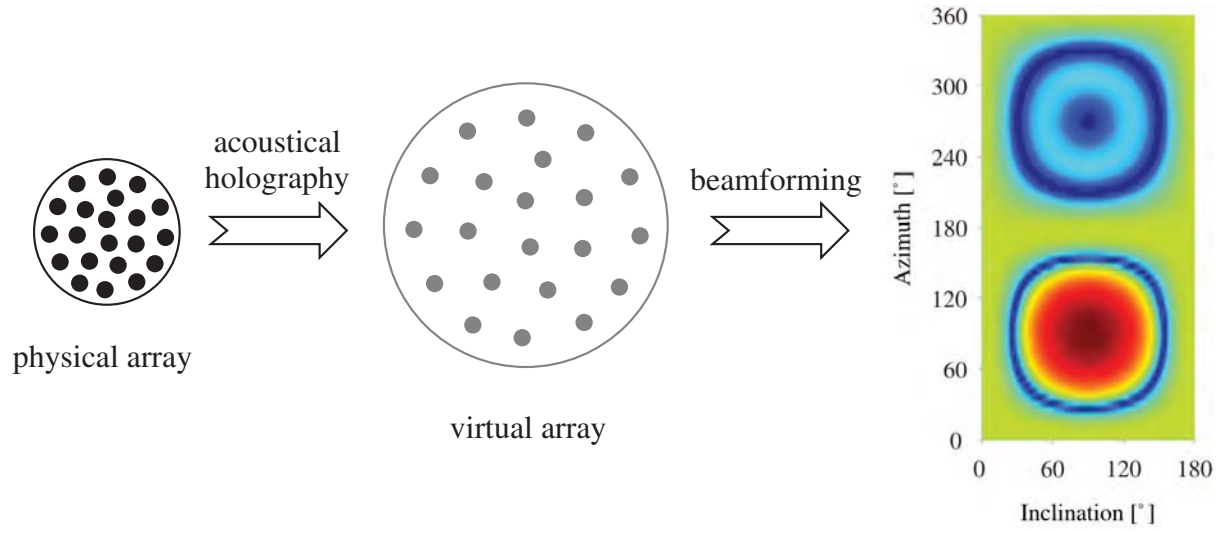

Figure 1: Procedure to obtain the beamforming map: the pressure captured by a spherical array is used to predict the pressure at a larger and virtual array with acoustic holography, and from this beamforming is carried out.

2 ACOUSTIC HOLOGRAPHY AND BEAMFORMING WITH A SPHERICAL ARRAY

2.1 Acoustic holography

Acoustic holography with a spherical array of transducers is a sound visualization technique that enables the reconstruction of a sound field over the three-dimensional space, based only on the sound pressure or particle velocity captured with the array. Acoustic holography measurements are usually performed very close to the source and the reconstruction lies somewhere between the measurement position and the source, as in near-field acoustic holography (NAH). However, in the present study, measurements in the far field of the sound source are of concern.

Let us consider a rigid spherical array with radius R centered at the origin of the coordinate system. The pressure at a point outside the array is given by the sum of the incident sound pressure and the scattered pressure due to the presence of the sphere,

$$p = p_{inc} + p_{sca}. \tag{1}$$

Given the spherical geometry, it makes sense to describe both pressures in terms of solutions of the Helmholtz equation in spherical coordinates (r, θ, φ) (θ being the inclination angle with respect to the $z-$axis and φ being the azimuth). The incident pressure, which is the one that would be measured if the scatterer was not present, must be described by means of spherical Bessel functions, because these are finite (even at the origin) [15, 16],

$$p_{inc}(kr, \theta, \varphi) = \sum_{n=0}^{\infty} \sum_{m=-n}^{n} A_{mn} j_n(kr) Y_n^m(\theta, \varphi), \tag{2}$$

where j_n is the spherical Bessel function of order n, and the terms Y_n^m are the so-called spherical harmonics,

$$Y_n^m(\theta, \varphi) = \sqrt{\frac{2n+1}{4\pi} \frac{(n-m)!}{(n+m)!}} P_n^m(\cos\theta) e^{jm\varphi}, \tag{3}$$

in which P_n^m is the associated Legendre function. Note that the time dependence $e^{-j\omega t}$ is omitted. The scattered pressure must be described as outgoing waves, represented in this case by the spherical Hankel functions of the first kind [17],

$$p_{sca}(kr, \theta, \varphi) = \sum_{n=0}^{\infty} \sum_{m=-n}^{n} B_{mn} h_n^{(1)}(kr) Y_n^m(\theta, \varphi), \tag{4}$$

where $h_n^{(1)}$ is the Hankel function of the first kind and order n.

The relationship between the coefficients A_{mn} and B_{mn} is given by the fact that the total radial velocity at the surface of the rigid sphere ($r = R$) is zero. From this condition it follows that

$$B_{mn} = -A_{mn} \frac{j_n'(kR)}{h_n'^{(1)}(kR)}, \tag{5}$$

where j_n' and $h_n'^{(1)}$ are the radial derivatives of j_n and $h_n^{(1)}$. Therefore, the total pressure is

$$p(kr,\theta,\varphi) = \sum_{n=0}^{\infty}\sum_{m=-n}^{n} A_{mn}\left(j_n(kr) - \frac{j_n'(kR)}{h_n'^{(1)}(kR)}h_n^{(1)}(kr)\right)Y_n^m(\theta,\varphi). \tag{6}$$

Since the pressure at the array is known, the coefficients A_{mn} can be retrieved by making use of the orthogonality relationship of the spherical harmonics,

$$\int_0^{2\pi}\int_0^{\pi} Y_n^m(\theta,\varphi)Y_\nu^\mu(\theta,\varphi)^*\sin\theta d\theta d\varphi = \delta_{n\nu}\delta_{m\mu}, \tag{7}$$

where $\delta_{n\nu}$ is the Kronecker delta function. Then, it can be shown that the coefficients A_{mn} are

$$A_{mn} = \frac{\int_0^{2\pi}\int_0^{\pi} p(kR,\theta,\varphi)Y_n^m(\theta,\varphi)^*\sin\theta d\theta d\varphi}{j_n(kR) - \frac{j_n'(kR)}{h_n'^{(1)}(kR)}h_n^{(1)}(kR)}. \tag{8}$$

To implement this equation in practice, the integrals must be substituted by discrete summations, capable of fulfilling the discrete orthogonality relationship of the spherical harmonics, which has to be accounted for in the design of the array,

$$\sum_{i=0}^{M}\alpha_i Y_n^m(\theta_i,\varphi_i)Y_\nu^\mu(\theta_i,\varphi_i)^* = \delta_{n\nu}\delta_{m\mu} \qquad \text{for} \qquad \nu \le N_{hol}, \qquad n \le N_{hol}, \tag{9}$$

where i represents the ith microphone at position (R,θ_i,φ_i), M is the number of sensors, and α_i is an associated integration weight factor that guarantees orthogonality up to a certain order N_{hol}. Using the discrete orthogonality, the expression for the expansion coefficients A_{mn} results in [15]

$$A_{mn} = \frac{\sum_{i=1}^{M}\alpha_i p(kR,\theta_i,\varphi_i)Y_n^m(\theta_i,\varphi_i)^*}{j_n(kR) - \frac{j_n'(kR)}{h_n'^{(1)}(kR)}h_n^{(1)}(kR)}. \tag{10}$$

This relationship assumes that the highest order of spherical harmonics included in the sound pressure is lower or equal to N_{hol}. This is a reasonable assumption as long as the value kR is about N_{hol}. When this requirement is not met aliasing occurs in the coefficients.

The coefficients A_{mn} can be used to compute the incident pressure and the scattered pressure separately (see Eqs. (2) and (4)) and the total pressure (see Eq. (6)) at a point (r,θ,φ).

2.2 Beamforming

Beamforming is a signal processing technique well used for localization of sound sources. There are several beamforming methods, but in the present study, delay-and-sum beamforming is chosen. Although this method is the oldest one, it is still widely used due to its robustness. It consists of delaying the signals of each array microphone by a certain amount and adding them together, to reinforce the resulting signal. Depending on the delay applied to the different microphones, the array is steered to a particular direction, whereas other directions are totally or partially attenuated [18]. Since in the current study the array is mounted on a rigid sphere,

it is simpler to express the beamforming output in the spatial frequency domain, because this allows us to compensate for the effect of the scatterer. In this domain the output is

$$b(kR,\theta,\varphi) = B\sum_{i=1}^{M} w_i \tilde{p}(kR,\theta_i,\varphi_i)\, p(kR,\theta_i,\varphi_i|\theta,\varphi)^*, \tag{11}$$

where B is a scaling factor, w_i is a weighting factor, $\tilde{p}$ is the measured pressure at the ith microphone, while p corresponds to the theoretical pressure at the ith microphone due to a source in the far-field at (θ,φ). It can be shown that the pressure at (R,θ_i,φ_i) due to a plane wave created by a source at (θ,φ) is [4]

$$p(R,\theta_i,\varphi_i) = \sum_{n=0}^{\infty}\sum_{m=-n}^{n} Q_n(kR) Y_n^m(\theta_i,\varphi_i) Y_n^m(\theta,\varphi)^*, \tag{12}$$

where Q_n is

$$Q_n(kR) = 4\pi(-j)^n \left(j_n(kR) - \frac{j_n'(kR)}{h_n'^{(1)}(kR)} h_n^{(1)}(kR) \right). \tag{13}$$

Making use of this expression the output of the delay-and-sum beamformer is

$$b(kR,\theta,\varphi) = B\sum_{i=1}^{M} w_i \tilde{p}(kR,\theta_i,\varphi_i) \sum_{n=0}^{N} \left(Q_n(kR) \sum_{m=-n}^{n} Y_n^m(\theta_i,\varphi_i) Y_n^m(\theta,\varphi)^* \right)^*. \tag{14}$$

Note that the second summation has to be truncated at N for the real implementation. A reasonable value is $N \approx kR+1$. By making use of the addition theorem [19] that states that

$$P_n(\cos\psi_q) = \frac{4\pi}{2n+1} \sum_{m=-n}^{n} Y_n^m(\theta,\varphi) Y_n^m(\theta_q,\varphi_q)^*, \tag{15}$$

where

$$\cos(\psi_q) = \cos\theta\cos\theta_q + \sin\theta\sin\theta_q\cos(\varphi-\varphi_q), \tag{16}$$

the beamformer output can be simplified:

$$b_N(kR,\theta,\varphi) = B\sum_{i=1}^{M} w_i\, p(kR,\theta_i,\varphi_i) \sum_{n=0}^{N} \frac{2n+1}{4\pi} Q_n(kR)^* P_n(\cos\psi_i). \tag{17}$$

To have an output equal to one when a plane wave with amplitude unity is measured at the array, it is easy to show that the value of B should be

$$B = \frac{1}{\sum_{i=0}^{M} w_i \left| p(kR,\theta_i,\varphi_i|\theta_0,\varphi_0) \right|^2}, \tag{18}$$

where θ_0 and φ_0 can be any angle, because with the spherical array the shape of the beampattern is independent of the steering direction, as it is practically shift-invariant [2].

2.3 Beamforming with a virtual array

As mentioned in the introduction, the goal of this study is to combine acoustic holography together with beamforming to improve the beamforming map at the low frequencies. To do this, the concept of virtual array has been presented; see Fig. 1. The pressure captured with a rigid spherical array is used to predict the pressure at a virtual spherical array with larger radius R_v, with virtual sensors placed at $(R_v, \theta_i, \varphi_i)$. The number of virtual sensors and their azimuth and inclination is kept the same as in the physical array. At this point we can consider two possibilities: 1) A virtual transparent array or 2) a virtual rigid array. For the virtual transparent array the expression is simply the incident pressure given in Eq. (2), evaluated at $r = R_v$. For the case of the virtual rigid array we should create a virtual spherical scatterer at R_v. To do that the incident pressure with coefficients A_{mn} (the ones obtained with the physical array) would impinge on the virtual sphere creating a virtual scattered pressure distributed at the surface of the virtual array. In accordance with Eqs. (4) and (5), the scattered pressure at the virtual transducers would be

$$p_{sca}(R_v, \theta_i, \varphi_i) = -\sum_{n=0}^{\infty} \sum_{m=-n}^{n} A_{mn} \frac{j_n'(kR_v)}{h_n'^{(1)}(kR_v)} h_n^{(1)}(kR_v) Y_n^m(\theta_i, \varphi_i). \tag{19}$$

Then, the total pressure at the virtual rigid array (at $r = R_v$) would be

$$p(R_v, \theta_i, \varphi_i) = \sum_{n=0}^{N_{hol}} \sum_{m=-n}^{n} A_{mn} \left(j_n(kR_v) - \frac{j_n'(kR_v)}{h_n'^{(1)}(kR_v)} h_n^{(1)}(kR_v) \right) Y_n^m(\theta_i, \varphi_i). \tag{20}$$

Since a rigid array has benefits compared to the transparent array, a virtual rigid spherical array is chosen for the current study.

To sum up, the procedure for combining holography and beamforming is the following one:

1. With a rigid spherical array measure the pressure at the microphones, $p(R, \theta_i, \varphi_i)$, where $i = 1, \ldots, M$.

2. Insert $p(R, \theta_i, \varphi_i)$ into Eq. (10) to retrieve the coefficients A_{mn} to be used for acoustic holography.

3. Insert A_{mn} into Eq. (20) to obtain the predicted pressure at the virtual rigid array, $p(R_v, \theta_i, \varphi_i)$.

4. Use $p(R_v, \theta_i, \varphi_i)$ as input of the beamforming process, given in Eq. (17), but substituting R by R_v and using $N = kR_v + 1$. In the present study, the chosen weighting factor, w_i, equals the integration factor of the acoustic holography process, α_i.

3 SIMULATION STUDY

The focus of this section is to analyze the outcome of combining acoustic holography and beamforming by means of simulations. A rigid spherical array with radius $R = 9.75$ cm and 50 flush-mounted microphones has been assumed. The characteristics of the array used for the simulations are the same of that used for the measurements (which will be presented in Sec. 4).

A picture of the array can be seen in Fig. 2. The location of the microphones and their associated integration weights result from an optimization procedure inspired by Ref. [20]. This procedure guarantees that the discrete orthogonality relation across microphone positions given in Eq (9) is valid up to order $N_{hol} = 5$, if $kR \leq N_{hol}$. When this condition is not met, that is, above 2.8 kHz, aliasing occurs.

Figure 2: Prototype of spherical array used in the measurements.

The simulations assume a plane wave created at coordinates $(\theta, \varphi) = (90°, 90°)$. However, the origin of the plane wave is not important because the array is practically shift-invariant. The frequency range of analysis contains the low frequencies up to 2 kHz. To account for the background noise, a signal-to-noise ratio (SNR) of 30 dB at each microphone due to uniformly distributed noise is considered.

Following the procedure described in the previous section, acoustic holography is performed prior to beamforming, considering a virtual array with a radius 4 times larger than the radius of the physical array used to measure the actual sound field. The normalized beamformer output obtained with the physical array using conventional beamforming and the output of the virtual array are shown in Fig. 3 for a frequency of 210 Hz. For ease of reference, the ideal beamformer output that would be obtained in absence of noise with a physical array of the same radius is also shown.

As can be seen in the leftmost subfigure in Fig. 3, the output for the physical array is rather omnidirectional (the level is quite uniform). However the map is significantly improved when using the pressures at the virtual array as the source located at $(90°, 90°)$ is successfully identified. Moreover, the beamformer map resembles the map of the physical array of the same radius under ideal conditions to a high extent. The discrepancies are caused by the noise assumed for the virtual array simulation.

The performance is also quantified by two measures: the resolution and the maximum side lobe level (MSL). The resolution is the -3 dB width of the main lobe, whereas the MSL is the difference between the highest secondary lobe and the main lobe. For both measures, the smaller the values, the better. The resulting resolution for the azimuth and inclination angles, as well as the MSL, can be seen in Fig. 4, along the entire frequency range of interest. This figure includes the results with the physical array with radius R (black curve) and the ones obtained at four virtual arrays with radii $2R$ (continuous blue curve), $3R$ (continuous green curve), $4R$ (continuous red curve), and $5R$ (continuous cyan curve). The ideal curves obtained with arrays

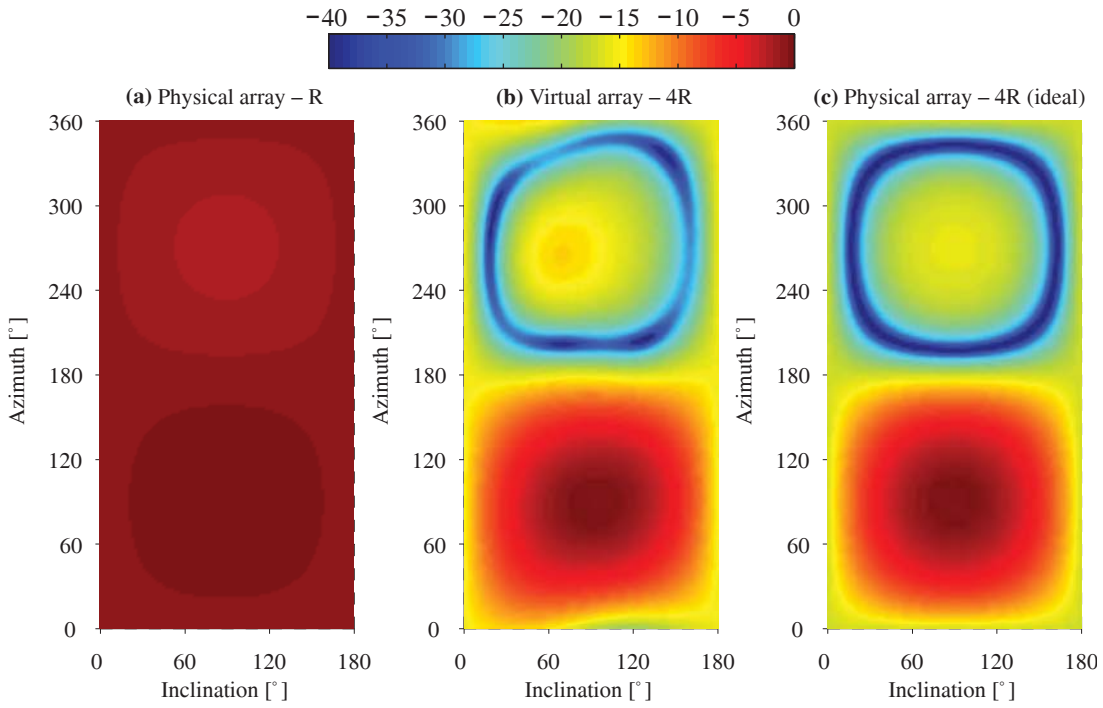

Figure 3: Normalized beamforming outputs at 210 Hz obtained with three rigid spherical arrays: one with radius $R = 9.75$ cm (left), a virtual array with radius $4R$ (middle) that results from the pressure at the physical array with radius R via acoustic holography, and an array of radius $4R$ with absence of noise (right). A SNR of 30 dB was assumed at each microphone of the physical array with radius R.

with radii $2R$ (dashed blue curve), $3R$ (dashed green curve), $4R$ (dashed red), and $5R$ (dashed cyan) for a SNR of infinity are also depicted.

In all cases it can be seen that both the resolution and the MSL are non-existent at low frequencies, meaning that the beamforming map is omnidirectional. From a particular frequency that depends on the array characteristics, the resolution improves, and sidelobes arise resulting in a certain MSL.

The resolution for both azimuth and inclination angles is improved towards the low frequencies with increasing radius of the virtual array, in comparison with the physical array of radius R used to capture the signals. Interestingly the curves of the virtual arrays are very similar to the ones of the arrays with the same radius under ideal conditions, although some deviations that become stronger with increasing virtual radius are observed for the virtual arrays of radii $3R$, $4R$ and $5R$.

On the other hand, the MSL of the virtual arrays is progressively shifted towards the low frequencies with increasing virtual radius. However, the MSL is more sensitive to noise than the resolution, as this measure worsens towards the high frequencies with increasing virtual radius, and the differences with the ideal MSL obtained with the physical arrays of the same radii in absence of noise (dashed curves) become larger. This is a consequence of the holography process itself, as the noise captured with the physical array is amplified with increasing distance to the reconstruction points, specifically for $r > R$. Therefore the reconstructed pressure deviates

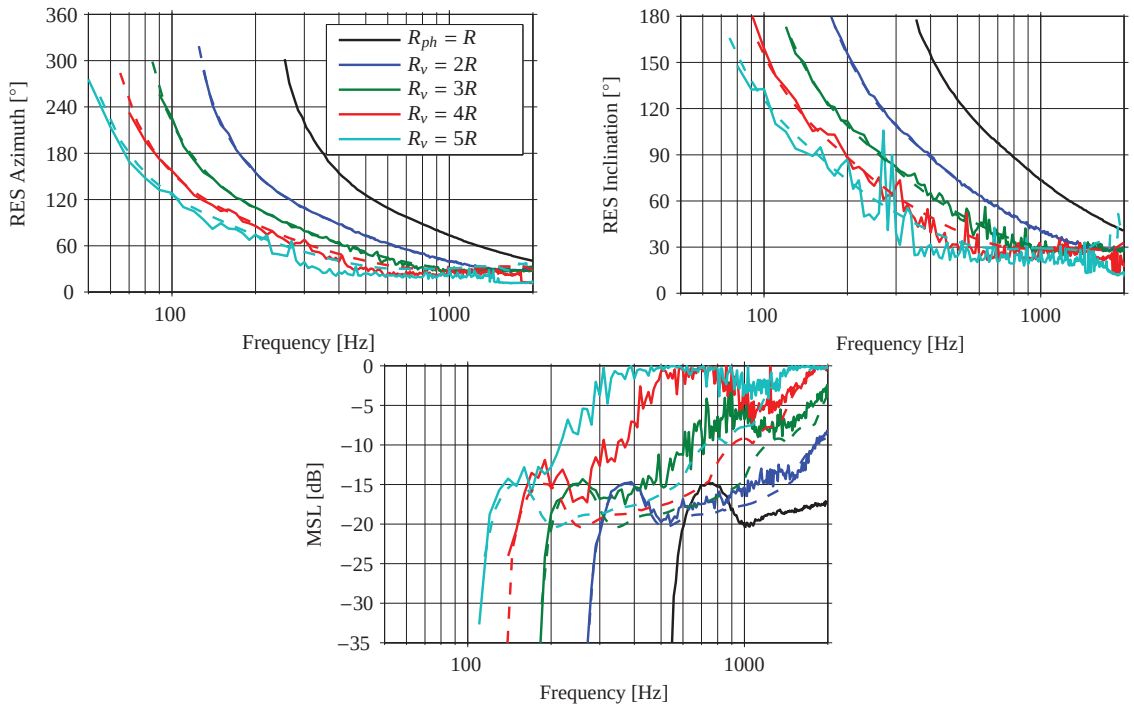

Figure 4: Resolution along the azimuth angle (top left), along the inclination angle (top right) and MSL (bottom) obtained by means of simulations with a physical array of radius $R = 9.75$ cm and 50 microphones (black continuous curve), as well as with four virtual arrays with radii $2R$, $3R$, $4R$ and $5R$ (blue, green, red and cyan continuous curves), that result from the pressure at the physical array with radius R via acoustic holography. The colored dashed lines show the results with arrays of the same radii as the virtual arrays, but with a SNR of infinity. A plane wave was created at $(\theta, \varphi) = (90°, 90°)$, and a SNR of 30 dB was assumed for the physical array with radius R.

from the ideal one [15], having a direct impact on the beamforming map, particularly on the sidelobes. Although not shown here, simulations reveal that the amplification of noise with an virtual array of radius $6R$ has dramatic influence on the beamforming map.

In conclusion, the results from the simulations show that one could take advantage of virtual arrays using the appropriate radius for each frequency, determined by the MSL. For example, in the case of study, a virtual array with radius $5R$ is suitable up to 170 Hz, from this frequency to about 280 Hz, one with radius $4R$ would be preferable, from 280 Hz to 400 Hz, $3R$ is more adequate, whereas from 400 Hz to 800 Hz a virtual array with radius $2R$ seems better. Above 800 Hz the physical array should be used as it is.

4 MEASUREMENT RESULTS

Measurements with a Brüel & Kjær (B&K) prototype array were carried out in a large anechoic chamber of about 1000 m^3. The array, which can be seen in Fig. 2, had 50 1/4 in. microphones

B&K Type 4935 flush-mounted on a rigid sphere and 11 video cameras. Its radius, R, was 9.75 cm.

The set-up, shown in Fig. 5, consisted of a loudspeaker placed in the far field, at 5.8 m from the array. The loudspeaker height was 1 m and the array height 1.30 m. The array was placed such as the loudspeaker was detected at about $(\theta, \varphi) = (90°, 90°)$.

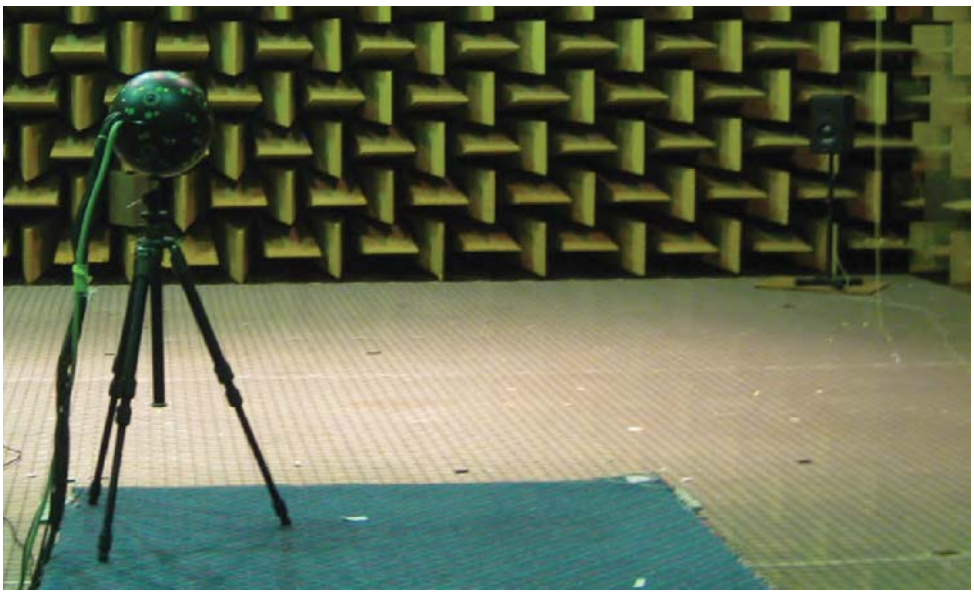

Figure 5: Measurement set-up.

The loudspeaker was fed with white noise. The signal level was adjusted so that the SNR at the array microphones was about 30 dB for most of the frequency range, although the SNR at the low frequencies was lower. The signal at each microphone was recorded with a B&K Pulse analyzer for 10 s. The data was segmented in blocks of 1 s using a Hanning window and a 50% overlapping. For each block, the crosspectra between each microphone and a reference, which was chosen to be microphone number one, was computed. The averaged crosspectra were used as input to conventional delay-and-sum beamforming. Besides, the data were used to predict the pressure at several virtual radii R_v, at $2R$, $3R$, $4R$ and $5R$, before applying beamforming, following the procedure indicated in Sec. 2.3. The resulting resolution for the azimuth and inclination angles, and the MSL with the physical and virtual arrays are shown in Fig. 6.

Both performance indicators follow the same trend observed in the simulations shown in Fig. 4: the resolution improves towards the low frequencies with increasing virtual radius, and the MSL is shifted towards the low frequencies, although its level increases with increasing virtual radius. The reader should keep in mind that the simulations were carried out assuming a SNR of 30 dB, which was not exactly the case for the measurements, especially after postprocessing the data, and therefore, some deviations between simulations and results are expected. In this regard, the MSL curves obtained with the virtual arrays are slightly better than the simulated ones.

These results confirm that the concept of virtual array can be used to enhance the performance of the beamforming system at low frequencies, with an appropriate virtual radius depending on the frequency. In this study, this makes it possible to extend the lower frequency of the physical

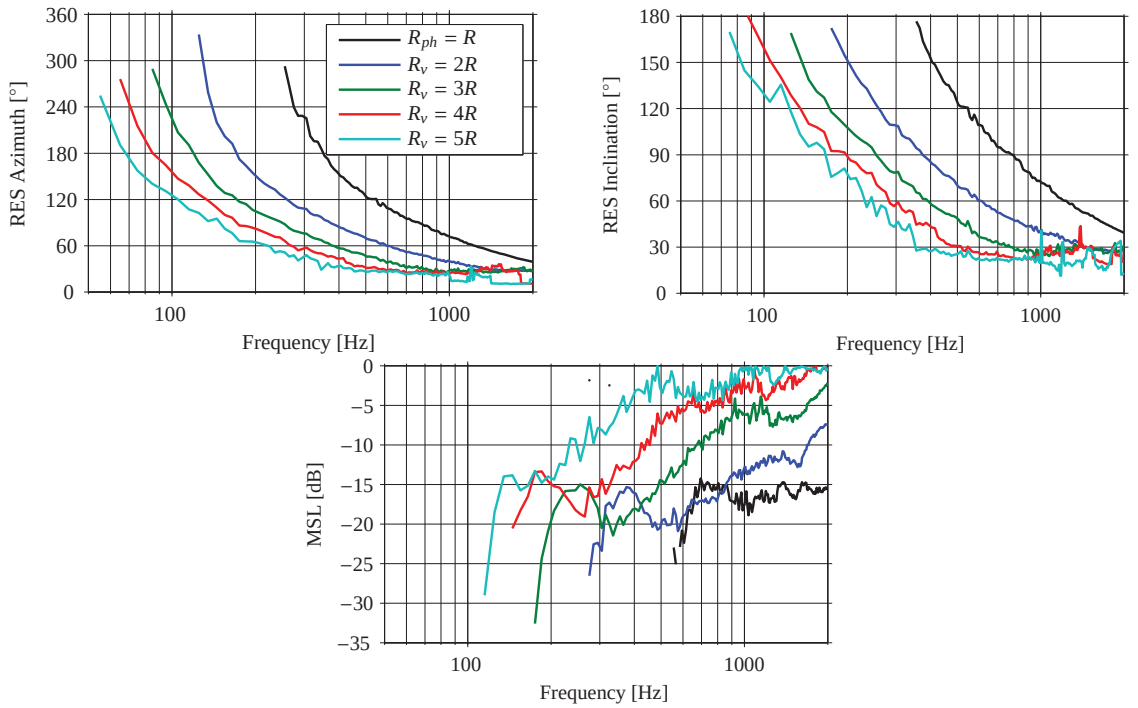

Figure 6: Resolution along the azimuth angle (top left), resolution along the inclination angle (top right) and MSL (bottom) obtained by means of measurements with a rigid spherical array of radius $R = 9.75$ cm and 50 microphones (black continuous curve), as well as the resulting resolution and MSL when considering four virtual spherical arrays with radii $2R$, $3R$, $4R$ and $5R$ (blue, green, red and cyan continuous curves), that result from the pressure at the physical array with radius R via acoustic holography. A plane wave was created at about $(\theta, \varphi) = (90°, 90°)$.

array down to about 55 Hz and 75 Hz in terms of resolution for the azimuth and the inclination angles, respectively, and 110 Hz in terms of MSL, in comparison with the original 250 Hz, 350 Hz and 550 Hz.

The advantage of combining acoustic holography and beamforming is further illustrated in Fig. 7, where the beamforming map obtained with the physical array at 210 Hz is shown, together with the maps obtained with virtual arrays with radii $2R$, $3R$ and $4R$. The larger the virtual radius, the clearer the map becomes, making it possible to localize better the sound source at its actual position, $(90°, 90°)$.

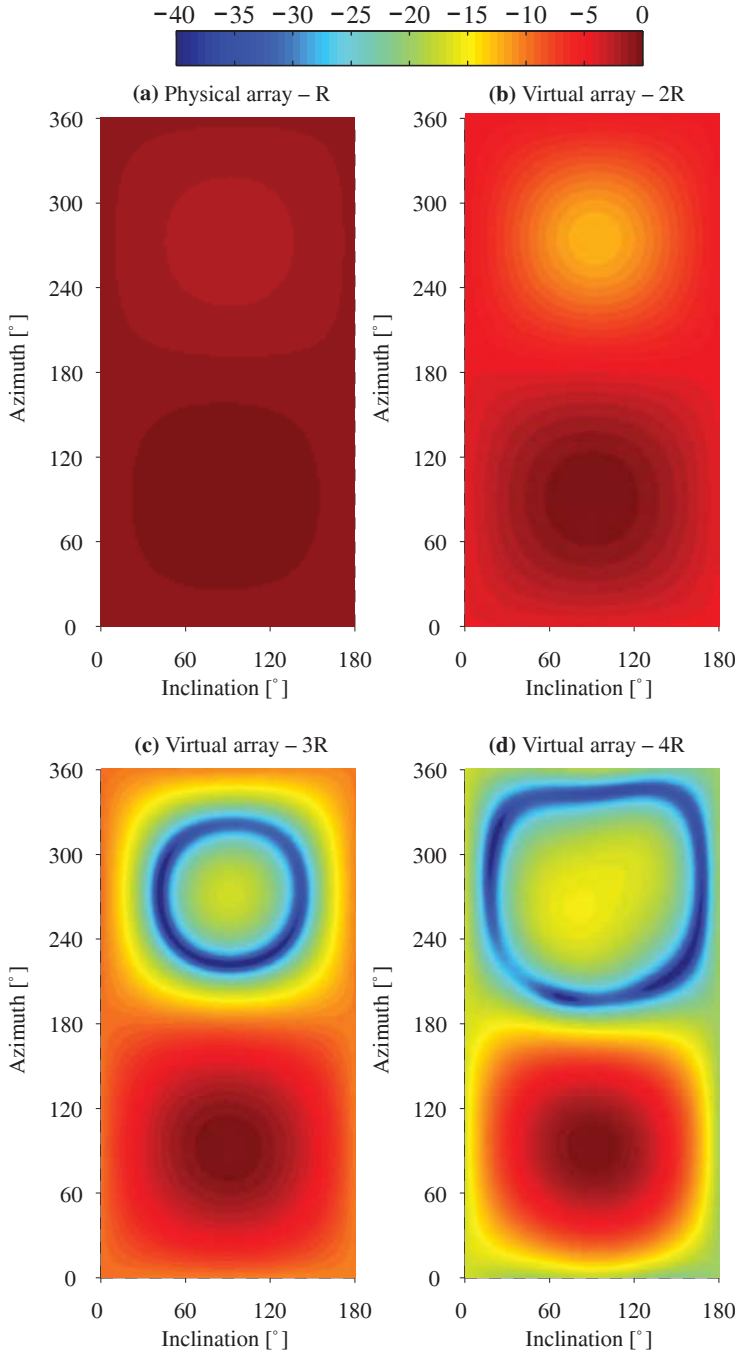

Figure 7: Normalized beamforming outputs at 210 Hz measured with a rigid spherical array with 50 microphones and radius $R = 9.75$ cm (top left), and three virtual rigid spherical arrays of radii $2R$ (top right), $3R$ (bottom left), and $4R$ (bottom middle), that result from the pressure at the physical array with radius R via acoustic holography.

5 CONCLUSIONS

Beamforming with spherical arrays is a powerful tool to localize and identify sound sources in a three-dimensional sound field. However, the resulting maps are difficult to interpret at low frequencies because such frequencies imply poor directivity, in particular with delay-and-sum beamforming. Inspired by the fact that the performance of the array would improve at low frequencies if a larger array was used, the present paper has presented a simple method that consists of predicting the pressure at a larger and virtual array by means of acoustic holography, and using it as input to the delay-and-sum beamforming procedure.

The performance of this combined approach has been assessed with two performance indicators, namely the resolution and the MSL. Both simulations and experimental results show that the resolution improves with increasing virtual radius, at the cost of the MSL, which is more sensitive to noise. This implies that the maximum virtual radius appropriate for each frequency is mainly determined by the MSL.

The use of holography prior to delay-and-sum beamforming offers new possibilities without any additional cost. At low frequencies the concept of virtual array can be used to improve the maps at such frequencies, while conventional beamforming can be applied directly at high frequencies.

ACKNOWLEDGMENTS

The authors would like to thank Karim Haddad, Brüel & Kjær, for lending us the spherical array used in the measurements.

REFERENCES

[1] T. Abhayapala and Darren B. Ward. “Theory and design of high order sound field microphones using spherical microphone arrays.” *IEEE ICASSP*, II, 1949–1952, 2002.

[2] J. Meyer and G. Elko. “A highly scalable spherical microphone array based on an orthonormal decomposition of the soundfield.” *IEEE ICASSP*, II, 1781–1784, 2002.

[3] M. Park and B. Rafaely. “Sound-field analysis by plane-wave decomposition using spherical microphone array.” *J. Acoust. Soc. Am.*, 118(5), 3094–3103, 2005.

[4] B. Rafaely. “Plane-wave decomposition of the sound field on a sphere by spherical convolution.” *J. Acoust. Soc. Am.*, 116 (4), 2149–2157, 2004.

[5] B. Rafaely. “Phase-mode versus delay-and-sum spherical microphone array processing.” *IEEE Signal Processing Letters*, 12(10), 2005.

[6] B. Rafaely. “Spatial sampling and beamforming for spherical mircrophone arrays.” *IEEE HSCMA*, 2008.

[7] S. Favrot and M. Marschall. “Metrics for performance assessment of mixed-order ambisonics spherical microphone arrays.” *Proceedings of the AES 25th UK Conference*, 2012.

[8] M. Marschall, S. Favrot, and J. Buchholz. "Robustness of a mixed-order Ambisonics microphone array for sound field reproduction." *Proceedings of the AES 132nd Convention, Budapest, Hungary*, 2012.

[9] S. Moreau, J. Daniel, and S. Bertet. "3D sound field recording with higher order Ambisonics - objective measurements and validation of a 4th order spherical microphone." *Proceedings of the AES 120th Convention, Paris, France*, 2006.

[10] B. Rafaely. "Analysis and design of spherical microphone arrays." *IEEE Transactions on Speech and Audio Processing*, 13(1), 2005.

[11] B. Rafaely and B. Weiss. "Spatial aliasing in spherical microphone arrays." *IEEE Transactions on Signal Processing*, 55(3), 2007.

[12] E. Tiana-Roig, A. Torras-Rosell, E. Fernandez-Grande, C.-H. Jeong, and F. Agerkvist. "Towards an enhanced performance of uniform circular arrays at low frequencies." *Internoise 2013, Innsbruck, Austria*, 2013.

[13] E.G. Williams, N. Valdivia, P.C. Herdic and J. Klos. "Volumetric acoustic vector intensity imager." *J. Acoust. Soc. Am.*, 120(4), 1887–1897, 2006.

[14] E.G. Williams and K. Takashima. "Vector intensity reconstructions in a volume surrounding a rigid spherical microphone array." *J. Acoust. Soc. Am.*, 127(2), 773–783, 2010.

[15] F. Jacobsen, G. Moreno-Pescador, E. Fernandez-Grande, and J. Hald. "Near field acoustic holography with microphones on a rigid sphere (L)." *J. Acoust. Soc. Am.*, 126(6), 3461–3464, 2011.

[16] F. Jacobsen and P. Juhl. *Fundamentals of general linear acoustics*. Wiley, 2013.

[17] F. Jacobsen, J. Hald, E. Fernandez-Grande, and G. Moreno. "Spherical near field acoustic holography with microphones on a rigid sphere." *Acoustics'08, Paris*, 2008.

[18] D. Johnson and D. Dudgeon. *Array Signal Processing Concepts and Techniques*. Prentice Hall, 1993.

[19] G. Arfken and H. Weber. *Mathematical methods for physicists*. Elsevier Academic Press, Burlington, MA, 2005.

[20] I. Sloan and R. Womersley. "External systems of points and numerical integration on the sphere." *Advances in Computational Mathematics*, 21, 107–125, 2004.

www.elektro.dtu.dk
Department of Electrical Engineering
Acoustic Technology
Technical University of Denmark
Ørsteds Plads
Building 348
DK-2800 Kgs. Lyngby
Denmark
Tel: (+45) 45 25 38 00
Fax: (+45) 45 93 16 34
Email: info@elektro.dtu.dk